Hà Thị Hải Yến M.Sc.

Electrochemical Investigations of the Diffusion Coefficients and the Heterogeneous Electron Transfer Rates of Organic Redox Couples measured in Ionic Liquids

DISSERTATION

Zur Erlangung des akademischen Grades

Doktorin der Naturwissenschaften

eingereicht an der

Technischen Universität Graz

Betreuer

O. Univ.-Prof. Dipl.-Ing. Dr. rer. nat. Günter Grampp

Institut für Physikalische und Theoretische Chemie

Technische Universität Graz

Graz, September 2014

EIDESSTATTLICHE ERKLÄRUNG

AFFIDAVIT

Ich erkläre an Eides statt, dass ich die vorliegende Arbeit selbstständig verfasst, andere als die angegebenen Quellen/Hilfsmittel nicht benutzt, und die den benutzten Quellen wörtlich und inhaltlich entnommenen Stellen als solche kenntlich gemacht habe. Das in TUGRAZonline hochgeladene Textdokument ist mit der vorliegenden Dissertation identisch.

I declare that I have authored this thesis independently, that I have not used other than the declared sources/resources, and that I have explicitly indicated all material which has been quoted either literally or by content from the sources used. The text document uploaded to TUGRAZonline is identical to the present doctoral dissertation.

…….. ……..

Datum / Date Unterschrift / Signature

ABSTRACT

The diffusion properties and the heterogeneous electron transfer rate constant of tetracyanoethylene (TCNE), tetrathiafulvalene (TTF) and its radical cation ($TTF^{\cdot+}$), 2,2,6,6-tetramethylpiperidine-1-oxyl (TEMPO) and 4-hydroxy-2,2,6,6-tetramethylpiperidine-1-oxyl (TEMPOL) have been studied in organic solvents and in eight imidazolium-based ionic liquids (ILs).

The values of the diffusion coefficients are obtained by using cyclic and steady-state voltammetry (for TTF, TEMPO only) over a range of 293 - 343 K. Diffusion of all the investigated compounds was analysed then with respect to concentration, temperature, viscosity, nature of substances. Diffusion coefficients are found to be independent on concentration. The temperature-dependence of the diffusion coefficients is well described by an Arrhenius-type relation. The diffusional activation energies of all compounds in ILs are similar and fit well to the activation energies of viscous flow for the corresponding ILs. The significant point of this work is that the diffusion of $TTF^{\cdot+}$ radical cation in ILs was slower compared with the neutral TTF which is not the case in acetonitrile. The ratio of the diffusion coefficients of $TTF^{\cdot+}$ and TTF at 293 K was observed to be 0.43 - 0.62 in five different ILs, as compared to 0.90 in acetonitrile. The diffusion coefficients of $TTF^{\cdot+}$ and TTF also were measured in a viscous organic solvent, sulfolane, which gave the ratio of 0.67 of those diffusion coefficients. The diffusion of TTF and $TTF^{\cdot+}$ was described using the Stokes-Einstein and Sutherland models. For TCNE, TEMPO and TEMPOL, hole theory was used to explain the observed diffusion coefficients.

Heterogeneous electron transfer rate constants (k_{het}) were determined using cyclic voltammetry. It was found that k_{het} depends on viscosity. k_{het} is 2 - 3 order of magnitudes smaller than that in organic solvents. A correlation between activation energy of electron transfer process and activation energy of viscosity is performed. The result also suggested the inapplicability of Marcus theory in explaining the outer-sphere reorganization energy of electron transfer reaction in ILs.

ZUSAMMENFASSUNG

Von Tetracyanoethylen (TCNE), Tetrathiafulvalen (TTF) und seinem Radikal Kation, 2,2,6,6,-Tetramethylpiperidin-N-oxid (TEMPO) und 4-Hydroxy-2,2,6,6,-tetramethylpiperidin-N-oxid (TEMPOL) wurden die Diffusionseigenschaften sowohl in organischen Lösungsmitteln, als auch in acht Ionischen Flüssigkeiten (ILs) untersucht. Die Anionen aller verwendeten ILs sind auf einem Imidazolring aufgebaut. Zusätzlich wurden die Geschwindigkeitskonstanten des heterogenen Elektronentransfers bestimmt.

Diffusionskoeffizienten wurden mittels zyklischer Voltammetrie und Steady-State Voltammetrie (nur für TTF, TEMPO) im Temperaturbereich von 293-343 K ermittelt. Die Abhängigkeit der Diffusion von Konzentration, Temperatur, Viskosität und Art der Substanz wurde analysiert. Es zeigte sich keine Abhängigkeit der Diffusionskoeffizienten von den Konzentrationen. Die Temperaturabhängigkeit folgt einem Arrhenius-ähnlichen Zusammenhang und die daraus ermittelten Aktivierungsenergien passen zu jenen für Diffusion in den entsprechenden ILs. Eine wichtige Beobachtung im Rahmen dieser Arbeit ist, dass das Radikal Kation von TTF in den ILs wesentlich langsamer diffundiert als die Neutralsubstanz, was jedoch in Acetonitril nicht der Fall ist. Bei 293 K wurde in fünf ILs ein Verhältnis der Diffusionskoeffizienten von $TTF^{\cdot+}$: TTF von 0,43-0,62 bestimmt. In Acetonitril beträgt das Verhältnis 0,9. In Sulfolan, ein hochviskoses organisches Lösungsmittel, wurde dieses Verhältnis mit 0,67 bestimmt. Um die Diffusion zu beschreiben wurden für TTF und $TTF^{\cdot+}$ die Modelle nach Stokes Einstein und Sutherland verwendet, für die anderen Systeme die sogenannte "hole theory".

Die Geschwindigkeitskonstanten des heterogenen Elektronentransfer (k_{het}) wurden mittels zyklischer Voltammetrie bestimmt. Es wurde für k_{het} eine entscheidende Abhängigkeit von der Viskosität festgestellt. Die Werte sind in ILs 2 - 3 Größenordnungen kleiner als in organischen Lösungsmitteln. Durch einen Vergleich der Aktivierungsenergien des Elektronentransfers mit der für Diffusion wurden große Abweichungen gefunden, was nahe legt, dass Marcus Theorie nicht zur Beschreibung der äußeren Reorganisationsenergie in ILs verwendet werden kann.

CONTENTS

LIST OF TABLES

LIST OF FIGURES

ACKNOWLEDGEMENTS

It would not be possible to finish my dissertation without the guidance and support that I have received over the whole period of my Ph.D study. I would therefore like to express my deep gratitude to:

First and foremost, I am really thankful to my supervisor, Prof. Günter Grampp who gave me an opportunity to work as a PhD student in his group. Thank for allowing me to grow as a scientist and giving me the freedom to pursue targets. I appreciate all his contributions of time, ideas and his encouragements on my research whenever the things went wrong. He has provided a good example as an enthusiastic, optimistic, generous, humorous and knowledgeable supervisor. He remains my best teacher who brings the physical chemistry to students in a simple way. I am also grateful to his wife, Jutta for her caring, kindness, willingness and enthusiasm. She always welcomes with a warm heart of an angel. I feel very comfortable when I am in their house. Watering the plants, visiting the garden make me feel like at home. Thank for spending time on teaching me swimming, German and cooking so delicious German and Austrian food for me and the other colleagues.

I would like to acknowledge Prof. Stephan Landgraf for constructing electrochemical cells using ionic liquids. It would not have been possible to run the measurements properly without those cells. Thank for correcting my paper, listening and answering my questions about electrochemistry.

I am also grateful to all the colleagues: Kenneth Rasmussen (very kind, helpful and knowledgeable. Thanks for an invaluable help, discussing about progress of my work, correcting my paper, and creating such a friendly atmosphere); Daniel Kattnig (a nice and knowledgeable expert who gave me helpful assistance), Noureen (thank for electrochemical guidance at the beginning); Helmut Eisenkölbl (a kind technician who supported me not only for the technical lab but also for my electronic things); Joshua (has been enthusiastically in translating the abstract into German and inspired me by his enthusiasm). I would also like to express my thanks to Hilde Freiβmuth, Marion Hofmeister, Herbert Lang, Ines Gössler for their technical support and invaluable assistance in making my life easier. I especially acknowledge Vân and Hảo who are not only my good colleagues but also my good friends sharing feelings with me every day no matter if I am in good or bad time. Thank to other

colleagues Boryana, Beate, Alexander, Pat for their helpful discussion, fruitful cooperation and creating a warm group. Thank to Brigitte, Kraiwan, Anne Marie for helping me with my life here at the beginning.

My time was made unforgettable in Graz with many friends who became a part of my life. I thank Romina for her kindness, caring and encourage. I will never forget the wonderful time we were together, cooking, hiking, dancing salsa. I know that when we are getting older, Romina still be there as my good friend. Thanks to Pawel for helping me proofread, photo-making lesson and many nice hiking mountain trips, giving suggestions. I also grateful for times spent with my flatmates in B4/Studentenheim Leechgasse 1. Thanks to Paula, Ahmed, Daria, Anil, Roja, Stella, Catia, Miki, Andrea, Joanna, Kia, Joseph for a warm atmosphere, for the discussion about life, for the nice parties together.

My time was also enriched by the Vietnamese and other friends by their kindnesses. Thanks to Annilise, Bảo, Hoàng, Hương, Việt, Vinh, Long, Thắng, Thắng, Trường, Huyền, Tùng, Hà for the joyful gatherings and discussing about science and politics.

I am sincerely grateful to the financial supports of ÖAD during my Ph.D study.

Last but not least I would like to thank my family for all their unconditional love and support. To my mom who sacrificed her life to raise me, my brother and my sister, I cannot thank enough for all of her love and support during my bad and good times. To my dad in the Heaven, thank for being with me even in short time and believing in me so that I could achieve all I wanted. I wish you could see me trying to fullfill your dream. To my sister and brother, thanks for encouraging and giving me the confidence to know that I can succeed. To my parents - in law, thanks for being so supportive throughout my three years of Ph.D study. Thanks to my grandparents, aunts and uncle Vinh, who are always encouraging me with their best wishes. And above all, for my loving, encouraging and patient husband Thịnh. Dear my beloved husband, without your understanding and encouragements I could not have finished this work. Thank you for being by my side whenever I need you and give me the confidence and courage to make the choices I have. Thank you for looking after our family during my study abroad and for your unconditional and constant love through all the ups and downs.

PUBLICATIONS

Poster presentations

1. Cyclic voltammetric study of diffusion coefficients of radical ions and the corresponding neutral molecules in room temperature ionic liquids. Yen Ha Thi Hai , G. Grampp and S. Landgraf. 4th EUCHEMS Congress, August 26-30th 2012, Prague, Czech Republic.

2. Electrochemical studies on the electron transfer rate constants of organic redox-couples in room temperature ionic liquids. Günter Grampp, Noureen Siraj, Stephan Landgraf, Thi Hai Yen Ha. Conference of electrochemistry 2012 Fundamental and Engineering Needs for Sustainable Development, September 17 – 19th 2012, Technische Universität München, Munich, Germany.

3. Electrochemical and ESR-Studies on the electron transfer rate constants of organic redox-couples in room temperature ionic liquids. Günter Grampp, Noureen Siraj, Stephan Landgraf, Thi Hai Yen Ha, Boryana Mladenova-Kattnig and Daniel Kattnig. Bunsentagung (Conference of German Society for Physical Chemistry) May 17 – 19th 2012, Universität Leipzig, Leipzig, Germany.

4. Electrochemical study of diffusion coefficients of organic molecules in ionic liquids. Thi Hai Yen Ha , Günter Grampp, Stephan Landgraf. 15th Austrian Chemistry Days, September 23 – 26th 2013. Graz University of Technology, Graz, Austria.

Papers

Diffusion of tetrathiafulvalene and its radical cation in ionic liquids in comparison to conventional solvents. Thi Hai Yen Ha, Kenneth Rasmussen, Stephan Landgraf, Günter Grampp. Electrochimica Acta 141, 2014, 72-81.

1. Introduction

Ionic liquids (ILs) possess many novel physicochemical properties such as a large electrochemical window, low-pressure volatilization, high thermal stability, etc. Therefore, ILs have been applied extensively in theoretical and experimental studies, for example as solvents without adding any supporting electrolyte, batteries, electro-deposition, fuel cells, and photo-electrochemical cells, etc. [1–3]. However many ILs have high viscosity in comparison with conventional solvents and the complex structure of ILs lead to unusual results in mass and charge-transfer dynamics.

Recent publications indicate that diffusion coefficients of redox species and heterogeneous electron transfer rate constants are usually quite smaller in ILs compared with traditional solvents [4]. Recently, it was found that the diffusion coefficients are independent on the concentration of Fc and cobaltocenium cation in eight ILs [5–8]. In classical organic solvents, the values of diffusion coefficients of the initial redox species and its electro-generated form are almost similar with the ratio is in a range of 0.8 – 1.0 [4,9]. However, in ILs, diffusion coefficients of neutral species are larger than those of the corresponding ionic forms [4,6,7,10]. Arrhenius type-relations has been used to check the temperature-dependence of diffusion coefficients in ILs [4,7,11,12]. The Stokes-Einstein behaviour also holds very well in many cases [13]. In contrast, non-Stokesian diffusion was observed for triiodide in binary mixtures of two ILs [14]. Recently, Abbott et al. applied a hole theory in interpretation of diffusion in ILs [15,16].

Electron transfer reaction kinetics in conventional solvents have been investigated in detail giving a good agreements between experimental results and current electron transfer theories. Heterogeneous rate constant (k_{het}) in organic solvents depends on solvent, supporting electrolyte and electrode material. Solvent dynamic effects have been found as contributions to the pre-exponential factor. A good linear relationship between k_{het} and the longitudinal relaxation time of solvent, τ_L, is observed. However, this is not the case for ILs. The re-organization energy in Marcus theory is based on the relaxation of solvent dipoles surrounding the transition complex during electron transfer. This is not

relevant to ILs containing charged ions. It is reported that outer-sphere electron transfer, described in the sense of Marcus theory for a conventional polar solvent, behaves differently in the case of ILs. There is no correlation between k_{het} and hydrodynamic radius in ILs [17,18] which is expected in organic solvents.

Also, different pictures of electrical double layer structures have been proposed because ILs are composed of bulky ions which are attached directly to the surface of electrode [19].

All the investigations above lead to the question whether current theories conceived for conventional solvent are applicable for ILs, too. This has motivated a detailed investigation of the diffusion and electron transfer rate constants of several organic molecules in different imidazolium-based ionic liquids: containing imidazolium cations: 1-ethyl-3-methylimidazolium [emim], 1-butyl-3-methylimidazolium [bmim], and 1-hexyl-3-methylimidazolium [hmim] coupled with the different anions: bis(trifluoromethylsulfonyl)imide [NTf_2], tetrafluoroborate [BF_4], hexafluorophosphate [PF_6], trifluoromethanesulfonate [OTf] and dicyanamine [dca] at different temperatures. Tetracyanoethylene (TCNE), tetrathiafulvalene (TTF) and its radical cation ($TTF^{\cdot+}$), 2,2,6,6-tetramethylpiperidine-1-oxyl (TEMPO) and 4-hydroxy-2,2,6,6-tetramethylpiperidine-1-oxyl (TEMPOL) were used as electrochemical probes. Investigated here are: the first oxidation of TTF, the reduction of $TTF^{\cdot+}$ and the first reduction of TCNE.

$$TTF \rightarrow TTF^{\cdot+} + 1e^-$$

$$TTF^{\cdot+} + 1e^- \rightarrow TTF$$

$$TCNE + 1e \rightarrow TCNE^{\cdot-}$$

$$TEMPO^{\cdot} \rightarrow TEMPO^{+} + 1e^-$$

$$TEMPOL^{\cdot} \rightarrow TEMPOL^{+} + 1e$$

This thesis is constructed in the following way. Theory of electron transfer will be discussed in chapter 2. In addition, this chapter also includes an introduction of

diffusion and the experimental methods for measuring diffusion coefficient, as well as factors effects on diffusion. Chapter 3 gives an overview of ILs from history and their physical and electro-chemical properties. Move on chapter 4 describes the experiments details. Before doing any electrochemical measurements, the characteristic of substances as well as ILs were investigated using UV-Vis and NIR spectroscopy. Then, the diffusion coefficients of all compounds were determined by cyclic voltammetry and steady-state voltammetry (for TTF, TEMPO only). Two different temperature-controlled cells for millimeter - and micrometer working electrodes were newly built for measuring small volumes of solution. Cyclic voltammograms were then utilised in order to get the values of k_{het}. The results of D and k_{het} are presented in chapter 5. Analysis of diffusion was carried out under the effects of temperature, viscosity and structure of compounds. The results are compared to those in organic solvents with low viscosity, like acetonitrile and high viscosity, such as sulfolane. In addition, D was investigated in terms of classical models and the hole model to get a picture of diffusion of molecules in ionic liquids. The second part of the discussion in chapter 5 focuses on the rate constants k_{het} of electrochemical electron transfer reactions. The results of k_{het} in ILs are considered under the present theories of electron transfer to understand how the outer-sphere activation energy is different in ILs compared with conventional solvents. From the results obtained a conclusions and outlooks are given chapter 6.

2. Theoretical considerations

This chapter focuses on the theory of electron transfer which was used in the present work. The theoretical values of activation energy were later compared to experimental results in ionic liquids. Due to the important role of diffusion in calculate heterogeneous electron transfer rate constant, the second part supplies the brief consideration of diffusion. It includes diffusion mechanism, electrochemical methods of measuring diffusion coefficient (D) and the factors effect on D.

2.1. Theory of electron transfer

An often used electron transfer theory was suggested by Marcus who got the idea based on Libby´s paper [20]. In 1992, Marcus got the Nobel prize for his theory [21–28]. Many other chemists have been contributed in developing the theory in the fields of reorganization energy, dynamic solvent effect, etc. [26,29–31]

2.1.1. Mechanism of electron transfer

The basic of this theory is that electron transfer (ET) is an activated process. The distance must be less than 20 Å in the case of intermolecular ET. The scheme of homogeneous ET reaction can be described:

$$A + D \underset{k_{-d}}{\overset{k_d}{\rightleftharpoons}} \underbrace{[A.....D]}_{\text{Precursor (P)}} \xrightarrow{k_{ex}} \underbrace{[A^-.....D^+]}_{\text{Successor (S)}} \xrightarrow{k_{diss}} A^- + D^+ \qquad (2.1)$$

Where (1) is forming precursor complex [A…D] and (2) electron transfer process to from successor complex [A^-…D^+] and (3) diffusing to [A^-] and [D^+].

Heterogeneous electron transfer is the simple electrochemical reduction or oxidation at the working electrode:

$$A + e^- \xrightarrow{k_{het}} A^- \quad (2.2)$$

$$D \xrightarrow{k_{het}} D^+ + e^- \quad (2.3)$$

Electron transfer happens at very short time scale (10^{-15} s) in comparison with the nuclear motion (10^{-13} – 10^{-14} s) (Fig. 2.1). This means that during electron jumping, the nucleus is frozen. Reactants reach the energy which is corresponding to the energy of transition state during thermal collision with surrounding solvent. The structures of reactants change. Electron is transferred. Finally, energy is transferred from the excited state to the environment via thermal collisions to form successor.

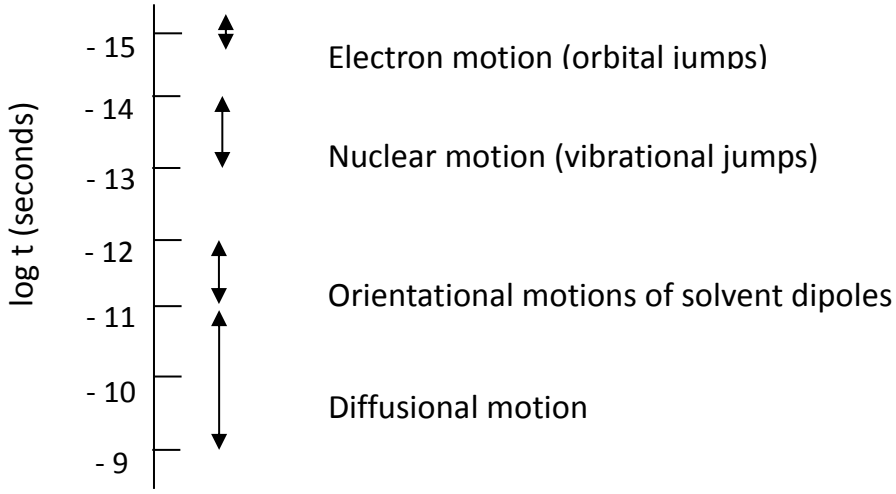

Figure 2.1. Timescales of chemical events during electron transfer. Adapted from [32].

2.1.2. Inner-sphere and outer-sphere electron transfer

i) Homogeneous process:

- Inner-sphere (bonded) electron transfer: electron transfer happens between two metal redox centres in two reactants through a sharing ligand. The electronic interaction between two reactants is strong with the energy higher than 20 kJ/mol.
- Outer-sphere (bonded) electron transfer: during electron transfer, there is no bridge connecting donor and acceptor. The energy of electronic interaction is small, 4-16 kJ/mol.

ii) Heterogeneous process [33–35]

- Outer-sphere electrode mechanism (Fig. 2.2a): the interaction between reactant and electrode is weak. Electron transfer occurs at outer Helmholtz plane (OHP) where reactant and electrode is far away at least one layer of solvents. All the theoretical calculation for this case is similar to the case of homogeneous of self-exchange electron transfer.
- Inner-sphere electrode mechanism (Fig. 2.2b): The atoms on the surface of metal electrode are bound with the electrochemically active complex (precursor in homogeneous) via ligand (bridge inner sphere mechanism) or via metal ion (non-bridge inner sphere mechanism). Electron is transferred through this ligand or metal ion which is at inner Helmholtz plane. Therefore, transition state is formed at inner-Helmholtz plane. This happens if the reactant adsorbs strongly on the surface of electrode cause the strongly dependent of electron transfer on electrode material.

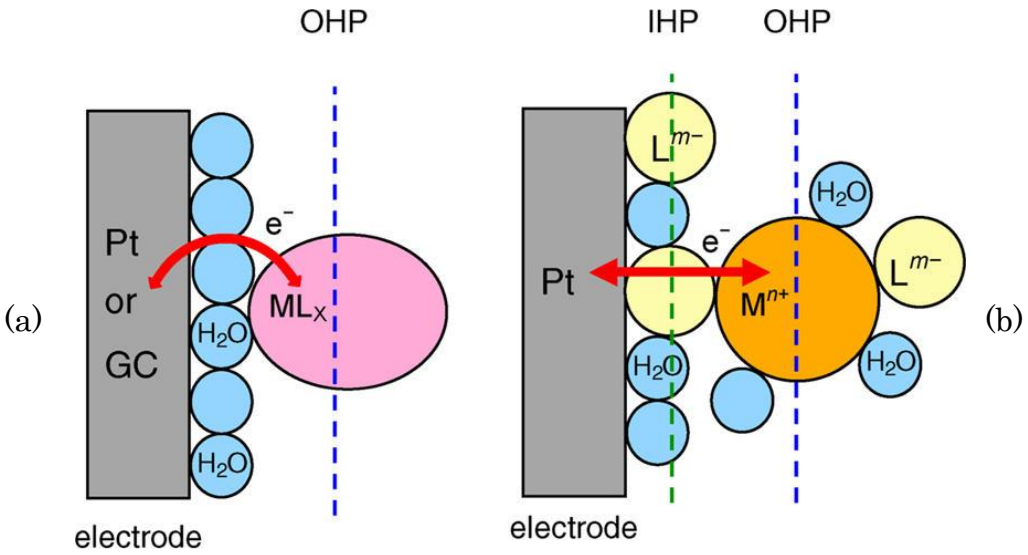

Figure 2.2. Inner- and outer-sphere electron transfers at electrode. Adapted from [16].

2.1.3. Activation energy

Electron transfer only happens if the precursor can overcome the free-energy barrier. This activation energy includes bond changes and the orientation of surrounding molecules. In other word, the total activation energy is:

$$\Delta G^* = \Delta G^*_{in} + \Delta G^*_{out} \tag{2.4}$$

Where ΔG^*_{in} denotes the inner-reorganization and ΔG^*_{out} is the outer-sphere reorganization.

In Marcus theory, activation energy is related to the driving force of the reaction:

$$\Delta G^* = \frac{\lambda}{4}\left(1+\frac{\Delta G^0}{\lambda}\right)^2 \tag{2.5}$$

Where λ is the total reorganization energy.

$$\lambda = \lambda_{in} + \lambda_{out} \tag{2.6}$$

λ_{in} is inner-sphere and λ_{out} outer-sphere reorganization energy. λ_{in} is the energy change in bond length and bond angles during electron-transfer process. λ_{out} is the energy for the rearrangement of solvent shell surround donor and acceptor.

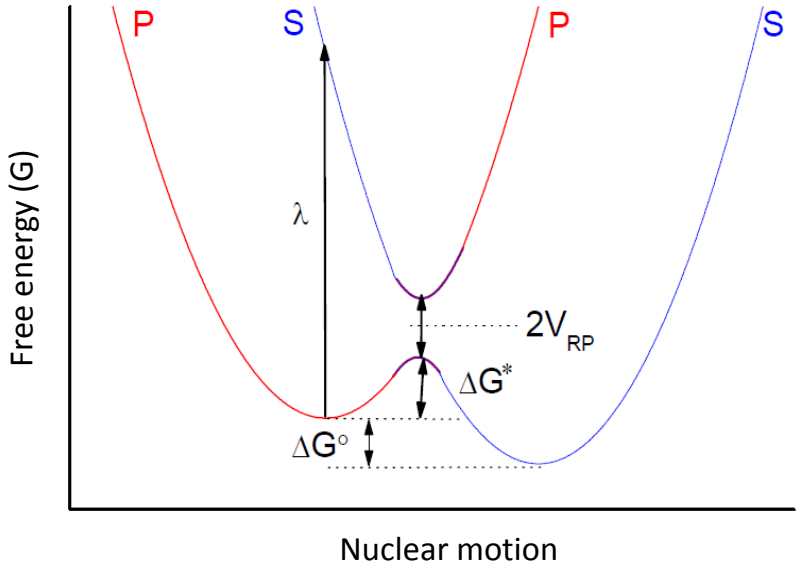

Figure 2.3. Potential energy surfaces of electron transfer reaction with driving force ΔG^o; activation energy ΔG^* and resonance splitting energy V_{RP}.

ΔG^* can be calculated from electron transfer rate constant (k_{et}) at different temperatures using Arrhenius –type equation:

$$k_{et} = \kappa_{el}\, \nu_n \exp\left(\frac{-\Delta G^*}{RT}\right) \qquad (2.7)$$

With $\kappa_{el}\ \nu_n$ is pre-exponential factor which includes ν_n, the nuclear frequency factor and κ_{el} is the transmission coefficient (as shown in 2.1.5.2).

For electron self-exchange reaction:

$$X \;+\; X^{-/+} \overset{k_{et}}{\rightleftharpoons} X^{-/+} \;+\; X \qquad (2.8)$$

The driving force, $\Delta G^o = 0$ (the energy of reactant and product are the same), therefore

$$\Delta G^* = \frac{\lambda}{4} = \frac{\lambda_{in} + \lambda_{out}}{4} \qquad (2.9)$$

$$\text{with} \quad \Delta G^*_{in} = \frac{\lambda_{in}}{4} \quad (2.10) \quad \text{and} \quad \Delta G^*_{out} = \frac{\lambda_{out}}{4} \quad (2.11)$$

2. 1.4. Reorganization energy

2.1.4.1. Inner-sphere reorganization energy

The first approach to calculate inner-sphere reorganization energy is:

$$\lambda_{in} = \sum_j^n \frac{f_j^R + f_j^P}{f_j^R f_j^P} \left(\Delta q_j\right)^2 \qquad (2.12)$$

With f_j^R, f_j^P are the force constants for the j^{th} vibration for the reactant and product, respectively. Δq_j is the change in equilibrium bonds and/or angles between the reactant and the product. However, it is not easy to determine all the contributing vibrations.

Another approach based on vertical electron affinity and ionisation potential was proposed by Nelson [33,36]. This method does not need the knowledge of changes in bond-lengths and force constants like the method above.

$$\lambda_{in} = E\,(D,q_D^+) - E\,(D,q_D) + E\,(A,q_A^-) - E\,(A,q_A) \qquad (2.13)$$

E (D,q_D), E (D,q_D^+), are the energy of donor in neutral and cation geometry, respectively. It is similar for acceptor, E (A,q_A), E (A,q_A^-).

2.1.4.2. Outer-sphere reorganization energy

The reorganisation of solvent during electron transfer includes two components. The fast process is electronic polarization which relates to the instant change of electron in solvent due to the change in electric field. This contributions are given by the optical dielectric constant, ε_∞, equals to n_D^2 with n_D is refractive index. The second component is the arrangement of the solvent dipole moments. This is associated to the nuclear mode and addressed to the static dielectric constant, ε_s. The picture of reorganisation of surrounding molecules can be described as following: when the precursor reaches transition state, electronic polarization reacts immediately, but the dipole reorientation is only completely achieved when successor is formed.

Outer-sphere reorganization energy also depends on the radius of reactants (r_A, r_D) and the distance (d) between them during electron transfer.

The reorganisation energy can be calculated for a homogeneous system using the continuum model:

$$\lambda_{out} = \frac{e_0^2}{4\pi\varepsilon_0}\left(\frac{1}{2r_D} + \frac{1}{2r_A} - \frac{1}{d}\right)\left(\frac{1}{n_D^2} - \frac{1}{\varepsilon_s}\right) \qquad (2.14)$$

With $\gamma = \frac{1}{n_D^2} - \frac{1}{\varepsilon_s}$ is Pekar's factor is the difference of the inverse of dielectric constant of the solvent at infinite frequency and at zero frequency (ε_s).

For heterogeneous system, the following equation is used because in an electrochemical reaction only one molecule must be activated.

$$\lambda = \frac{e_0^2}{8\pi\varepsilon_0}\left(\frac{1}{r} - \frac{1}{d_{het}}\right)\left(\frac{1}{n_D^2} - \frac{1}{\varepsilon_s}\right) \quad (2.15)$$

The reaction distance can be calculated using Marcus or Hush model:

- Marcus model: $d_{het} = 2r$ or the reaction distance is equal to the distance of two reactants in the case of homogeneous system in solution.
- Hush model [26]: $1/d_{het} \approx 0$ the reaction distance is large due to the electron transfer at the outer Helmholtz plane.

2.1.5. Pre-exponential factor

2.1.5.1. Nuclear frequency factor v_n

In Marcus theory [27], v_n is the collision factor of two uncharged species in solution (homogeneous process) or of a uncharged species with an area of electrode (heterogeneous process).

$$v_n\,(\text{hom}) = d^2\sqrt{\frac{16\pi kT}{M}} \quad (2.16)$$

$$v_n\,(\text{het}) = \sqrt{\frac{kT}{2\pi M}} \quad (2.17)$$

With d is the collision diameter and M is molar mass.

If the formation of precursor is considered, the frequency factor of both solvent v_i and reactant v_o must be added to the total frequency factor.

$$v_n = \sqrt{\left(\frac{v_i^2\lambda_i + v_o^2\lambda_o}{\lambda}\right)} \quad (2.18)$$

However, the Eq. 2.18 is only used for rapid dielectric relaxation.

As shown before in section 2.1.4.2 the solvent polarity has a large effect on the outer-sphere reorganization energy. In addition, if the friction between reactants ad solvents is taken into account, the frequency factor is therefore influenced by dynamic solvent effect [30,31,37–40]. The orientation of solvent molecule is addressed in longitudinal relaxation time τ_L.

$$\tau_L = \frac{\varepsilon_\infty}{\varepsilon_s}\,\tau_D \tag{2.19}$$

With τ_D is dielectric relaxation time which is the rotational diffusion time of a single molecule. τ_D is an order of magnitude larger than $\tau_L$and can be calculated by Debye equation (Eq. 2.20).

$$\tau_D = \frac{3V_M\eta}{RT} \tag{2.20}$$

With V_M is the molar volume of the reactant.

In the case of adiabatic electron transfer, dynamic solvent motions play an important role and the frequency factor can be represented in equation below.

$$\nu_n = \frac{1}{\tau_L}\sqrt{\frac{\lambda_o}{4\pi RT}} \tag{2.21}$$

2.1.5.2. The transmission coefficient, κ_{el} - Adiabatic and diabatic electron transfer reaction

To describe electron transfer process, potential energy surfaces of the reactant and the product are used. When resonance splitting energy (V_{RP}) is so small that interaction of R and P surfaces is weak. As a result, the potential energy surfaces of reactant and product still remain and intersect. This is so-called non-adiabatic or diabatic. In this case, the probability of electron transfer $\kappa_{el} \ll 1$.

On contrary, if the interaction between the reactants is large enough, a quantum mechanical splitting happen at the intersection point of the reactant and product curves. The merge of these two curves at the transition state to from one curve leads to the electron transfer takes place smoothly along this lower surface. The

probability of electron transfer in this case is close to 1. It is called adiabatic system. Adiabatic reactions usually occur when the two reactants are close in terms of Van der Waals contact or close coupling in an intramolecular.

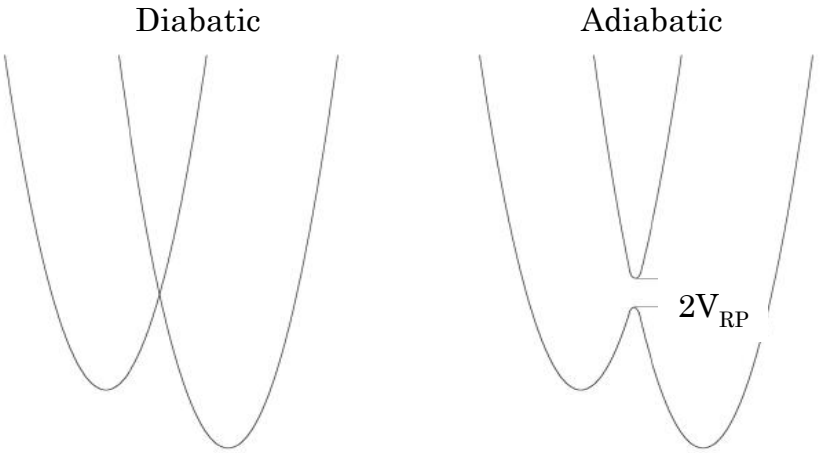

Figure 2.4. Non-adiabatic and adiabatic electron transfer reactions

2.1.6. Inverted Marcus region

Activation energy relate to driving force in a quadratic equation (Eq. 2.5). Therefore, there are three situation can happen (Fig. 2.5).

+ The normal region: $-\Delta G^o < \lambda$; ΔG^* decreases together with the decrease of λ. ΔG_o becomes more negative leading to the increase in k_{et}.

+ $\Delta G^o = -\lambda$, ΔG^* reaches 0 and the rate reaches the maximum.

+ The Marcus inverted region: $-\Delta G^o > \lambda$; ΔG^o becomes even more negative, λ decreases but ΔG^* increases result in decreasing rate constant.

The experiment are evidence for Marcus inverted region was first observed by John Miller and Gerhard Closs when investigating the intramolecular electron transfer in steroids [41,42].

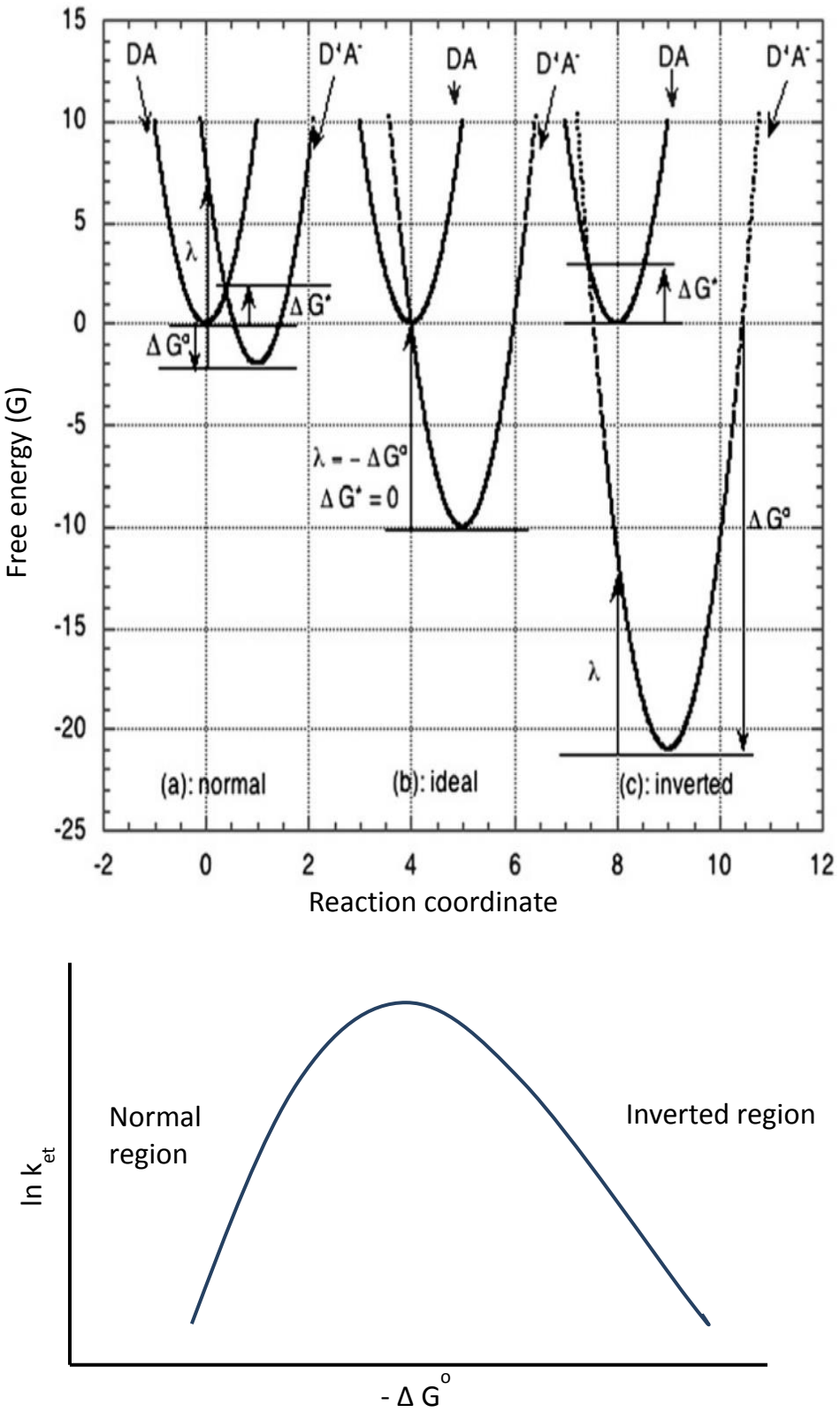

Figure 2.5. Three cases of electron transfer reaction according to Marcus theory. Adapted from [43].

2.2. Diffusion

Diffusion plays an important role in mass transport. A rigorous study of diffusion coefficients brings a better understanding of electrochemical systems related to mass transfer.

Molecules can diffuse toward a disk working electrode in two different ways including planar and convergent diffusions (Fig. 2.6).

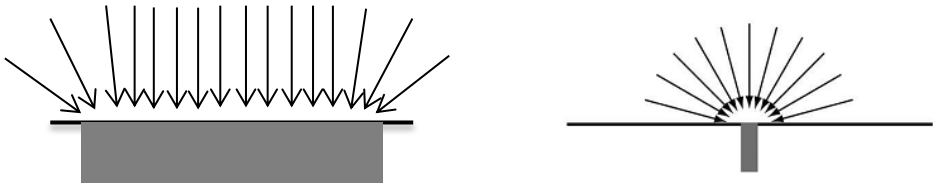

(a) (b)

Figure 2.6. Diffusion mechanisms at disk-macroelectrode (a) and -microlectrode (b).

For a disk-macroelectrode (normally mm-size electrode) planar diffusion is dominant compared with radial diffusion. For a disk-microelectrode, diffusion regime is different. At short time, the diffusion of planar prevails due to the thin diffusion layer corresponding to dimensions of the electrode. As a result, microelectrodes work as a conventional electrode in short measuring time. In contrast, at longer time the diffusion layer becomes larger causing hemispherical diffusion regime. In this situation, the current is independent on time resulting in a steady-state at microelectrodes.

2.2.1. Experimental methods in determining diffusion coefficient

Diffusion coefficients can be measured by different electrochemical methods including: potential step methods (chronoamperometry) at macroelectrode [15] and microelectrode [4,10,14,44], potential sweep method (cyclic voltammetry) at macroelectrode [5,8,15,16,44] and microelectrode [14,45], scanning electrochemical microscopy (SECM) techniques [46]. Beside the above-mentioned methods, diffusion coefficients can be obtained by using other measurements, albeit with less precision, such as impedance spectroscopy and polarization measurement [14].

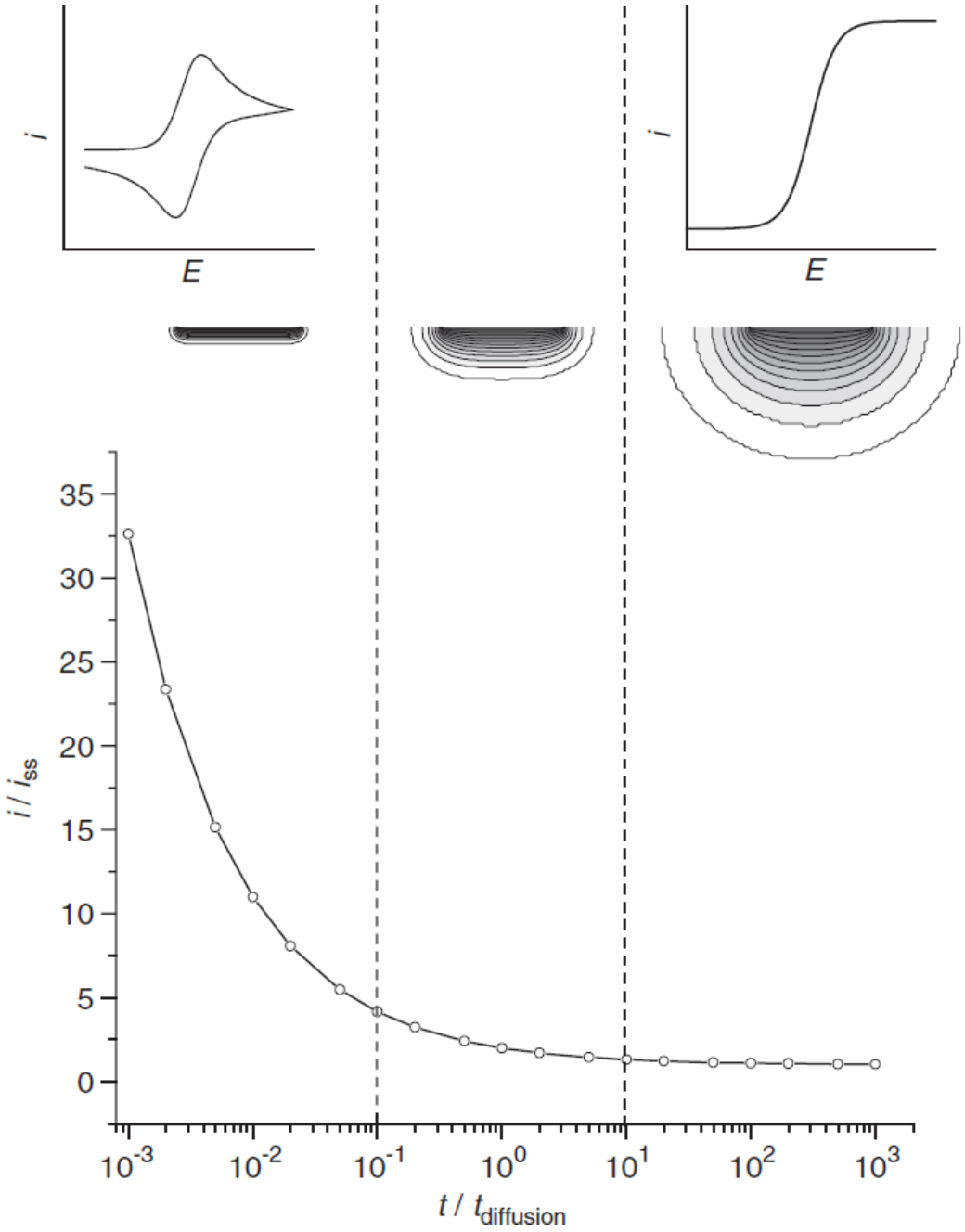

Figure 2.7. Evaluation of diffusion patterns from plannar to hemispherical diffusion at different time-scale at ultramicroelectrode. The diffusion layer for each pattern was described by the grey contour line. Adapted from [47].

Values reported for diffusion coefficients of a specific substance in RTILs provide a wide variation in data. Hence, it is required to use reliable electrochemical methods in determining diffusion coefficients. Herein, only several methods used to determine diffusion coefficients in ionic liquids are listed.

2.2.1.1. Chronoamperometry at microelectrodes

Chronoamperometry at microelectrodes has been largely used especially for systems with slow heterogeneous kinetics and for solvents showing low conductivity. In this technique, the potential is stepped suddenly from a value E_1 where the initial species is electrochemically stable, to a value E_2 where only this species is oxidized or reduced. The diffusion- controlled current is recorded in respect with time (Fig. 2.8a).

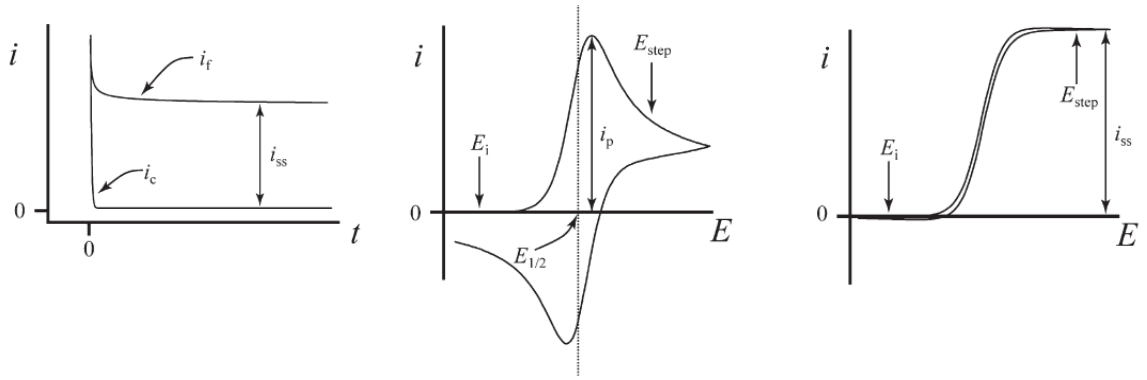

(a) (b) (c)

Figure 2.8. (a) Chronoamperomogram transient (i_f: Faraday current; i_c: charging current); (b) cyclic voltammogram; (c) Steady-state voltammogram. Adapted from [48].

At disk-microelectrode, the transient current is given by:

$$I = 4\ nFcDa\ f(\tau) \tag{2.22}$$

With a is radius of working electrode, c is concentration of species and $f(\tau)$ is a function which can be expressed empirically by using Shoup and Szabo equation:

$$f(\tau) = 0.7854 + 0.8862\ \tau^{-1/2} + 0.2146 \exp(-0.7823\tau^{-1/2}) \tag{2.23}$$

$$\tau = 4Dt/a^2 \tag{2.24}$$

Fitting the chronoamperometric transients to Eq. 2.23 not only supplies the value of the diffusion coefficient but also the concentration of the diffusing species [13]. In addition, double potential step chronoamperometry gives an simple access to the value of diffusion coefficient of oxidized form parallel to that of reduced form by using only one chronoamperometric transient [4].

Choosing an optimal measuring time scale to avoid convection and charging current is the most significant when using this method. τ equals to 2000 give a 1% error (the spherical diffusion is 100 times the planar contribution). From a given diffusion coefficient and diameter of microelectrode, time is easily calculated. It is suggested that the first 100-300 μs should be avoided as well as long transient time due to the charging current of double layer and convection current, respectively. The measuring time in the range of 1 ms to 10 s depends on each experiment. For ILs, it is more difficult to determine the optimal measuring time. Compton et al. [49] have found that reliable values of diffusion coefficient may not be obtained by short transient times due to the large double layer capacitance of ILs.

2.2.1.2. Cyclic voltammetry at macro-electrode

The second method addressed in many papers is cyclic voltammetry at macro-electrodes. The current is recorded as a function of scanning potential (from an initial potential E_1 to a step potential E_2 and often back to the initial value) (Fig. 2.8b).

For a planar diffusion-controlled system, Randles–Sevčik equation (Eq. 2.25) is used to determine the diffusion coefficients of redox species [50,51].

$$I_p = 0.4463nFAc\left(\frac{nF}{RT}\right)^{1/2} v^{1/2}D^{1/2} \qquad (2.25)$$

In Eq. 2.25, I_p denotes the peak current, A the surface area of the working electrode, and c the concentration of the redox species. From the slopes of plots of I_{p_a} vs. $v^{1/2}$ (Fig. 2.8b), D is easily calculated by use of Eq. 2.25.

The conditions to use Eq. 2.25 are: (i) the redox system should be reversible which means that the value of ΔE_p and $\Delta E_{p_a/2}$ are around 56 mV at 293 K and they are independent on scan rates; (ii) the reaction is planar-diffusion controlled what can be checked by a linear dependence between of I_p vs. sqrt (v) with an intercept of 0. However, it should be noted that the proportionality of I_p and

sqrt(v) is also given for irreversible processes. Therefore, two conditions above must be fulfilled when using Eq. 2.25.

For an irreversible redox processes, diffusion coefficients are calculated using the Eq. 2.26 [51,52]:

$$I_p = 0.496nFAc\left(\frac{nF}{RT}\right)^{1/2}\alpha^{1/2}v^{1/2}D^{1/2} \quad (2.26)$$

With α is the transfer coefficient.

A mentioned above, the peak current is proportional to sqrt (v) for irreversible system. However, ΔE_p and $\Delta E_{p_a/2}$ are increasing with the increase in scan rate.

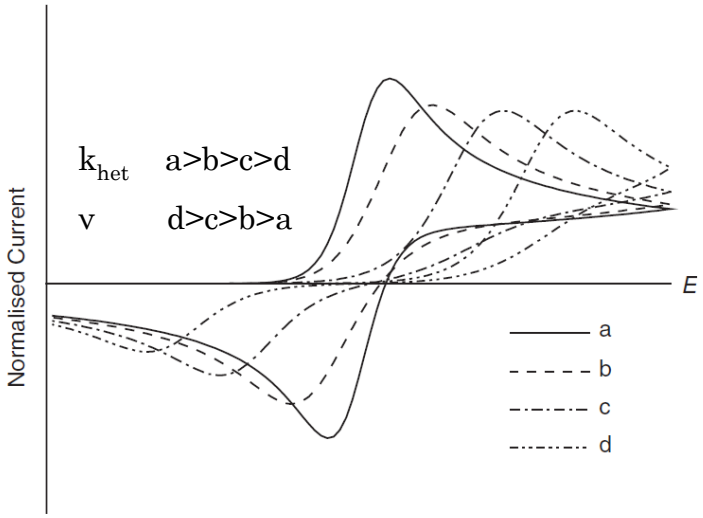

Figure 2.9. Shapes of cyclic voltammograms under kinetic control: (a) the diffusion coefficient is smaller than k_{het} , (b, c, d) k_{het} is increasingly smaller than the diffusion coefficient. Adapted from [47].

The quasi-reversible process is considered to be the most complicated case where the diffusion coefficient may not be obtained due to the requirement of the value of heterogeneous rate constant [51]. In this case, the peak current is not proportional to sqrt (v).

For a redox process, the shape of cyclic voltammogram can be distorted due to the unequal variation of diffusion coefficient in comparison with heterogeneous rate constant (Fig. 2.9).

From practical considerations, there are some important points must be noticed when using CV. E_2 must be adequately negative (reduction) or positive (oxidation) in order to avoid the dependence of the reverse current on E_2. The second issue is using only the first scan.

2.2.1.3. Steady –state voltammetry

Steady-state voltammetry at microelectrode has been also applied to measure diffusion coefficients in ionic liquids (Fig. 2.8c). It is important to determine a scan rate (v) to reach steady-state conditions [52]:

$$v \ll RTD/nFa^2 \quad (2.27)$$

Where R is the gas constant, D is the diffusion coefficient of the species, T denotes the temperature, n is the number of electron transferred and F is Faraday constant and a the radius of working electrode.

When using this method in ILs, one must note that the true steady state can only be achieved at very slow scan rates due to the slow diffusion in these solvents.

From the limiting current, diffusion coefficients were calculated using the following equation [52]:

$$I_{ss} = 4nFaDC \quad (2.28)$$

Where I_{ss} is steady-state current and a the radius of microelectrode

2.2.2. Effects on diffusion coefficient of redox species in ILs

There are many factors that effects on diffusion coefficient such as: impurities, substances, charge and neutral form, viscosity and temperature.

2.2.2.1. Temperature

Diffusion coefficients increase with the increase of temperature. Arrhenius-type equation is commonly used to test the dependence of D on temperature.

$$D = D_o\, e^{-E_{a,D}/RT} \quad (2.29)$$

where $E_{a,D}$ is the activation energies of diffusion of redox species or of viscous flow of solvents, respectively; D_o, are hypothetical values of D, at infinite T. The good conformity of temperature-dependence of diffusion coefficients to Arrhenius type-relations has been reported in ionic liquids [4,7,11,12].

The Vogel-Fulcher-Tamman (VFT) equation was also used to describe the relation of self-diffusion coefficient and temperature in some cases [53][54][55]:

$$D = D_o \times \exp\left[-B/(T-T_o)\right] \quad (2.30)$$

Where D_o (cm^2/s), B (K) and T_o (K) are constants. D_o, B, T_o can be obtained by fitting the experimental value of D at different temp using equation above. The D at a certain temperature can be easily found if the values of D_o, B, T_o are known. The self-diffusion coefficient is larger in the case of cation in compared with the anion of imidazolium-based ILs. Many other factors effect self-diffusion including size of ions, shape and interaction between cation and anion.

2.2.2.2. Viscosity

The diffusion of a molecule in a conventional solvent can be described using Stoke-Einstein equation [56]:

$$D = \frac{kT}{6\pi\eta r} \quad (2.31)$$

With η is viscosity of solvent and r the hydrodynamic radius of the species.

The Stoke-Einstein behaviour hold well in many cases [13]. However, the Stoke-Einstein equation has been reported to be broken down for the diffusion of triiodide in [bmim][BF_4] [14].Moreover, the fractional Stoke-Einstein relations have been used to describe the relation between diffusion coefficient and temperature in some cases [57,58]:

$$D \propto (T/\eta)^m \quad (2.32)$$

Where η is viscosity and m is an exponent with m < 1.

2.2.2.3. Charge and neutral redox species

In organic solvents, equal values of diffusion coefficients of initial redox species and its electro-generated forms in an electron-transfer process are usually assumed. Indeed, the ratio of these values ($D^{+/-}$ / D^{o} with $D^{+/-}$ is diffusion coefficient of charged molecule, D^{o} is that of uncharged molecule) was observed experimentally to be in the range of 0.8 - 1.0 in traditional solvents [9,59–61]. But this is not the case for ILs. Diffusion in ionic liquids of neutral species were found to be faster than the ionic forms [4,6,7,10]. The biggest ratio has been reported in the case of oxygen/superoxide to be 30 in ionic liquids [10]. Therefore, when dealing with ionic liquids, one must be careful when using the assumption of equal diffusion coefficients for both redox states. Especially, several calculations can be influenced by that fact.

2.2.2.4. Concentration

The dependence of diffusion coefficients on concentration has been reported for Fc in some ionic liquids [44,62,63]. Brooks and Doherty investigated the dependence of concentration on diffusion of Fc in [bmim][NTf_2] using chronoamperometry and steady-state measurements. The current increased exponentially at concentration of Fc (> 0.005 % Fc). Nagy showed a plateau of diffusion of Fc at concentration higher than 2.5 mM in [bmim][PF_6]. Later, Speiser et al. also reported the significant increase in diffusion coefficient Fc in [bmim][BF_4] with the concentration of Fc above 15 mM.

Recently, it was found [6–8] that the diffusion coefficients are independent on the concentration of ferrocene and cobaltocenium cation in eight ionic liquids. Vorotyntsev found no concentration dependence of D for Fc in [bmim][NTf_2]. This group found it difficult to determine the real concentration of Fc in solution because of the tiny volume of solution, volatility of Fc and the presence of impurities in Fc. The conclusion was that the above concentration-dependence of

diffusion coefficient in literature was due to the different value of prepared concentration and the real concentration in solution. The independence of diffusion coefficient on concentration has been reported by Bond et al. [5] for Fc, Cc^+ in [bmim][BF_4] and [bmim][PF_6] and by Compton et al. [7] for Fc and Cc^+ in eight ILs.

It has been suggested that the concentration of the redox species needs to be higher than 5 mM in order to obtain an acceptable signal to noise ratio [64].

2.2.2.5. Impurities in solution

Bond et al. observed the significance change in voltammetry Fc in aprotic ILs [bmim][BF_4] and [bmim][PF_6] and in several ILs in the presence of small concentrations of cobaltocenium (Cc^+) and/ or tretrabutylamomnium cation [5,6] lead to the non-additivity of Faradaic current in ILs, not for organic solvents. As a consequence, measuring a blank curve for calibration seem to be unnecessary when measuring CV of redox species in ILs. Diffusion coefficients of Fc, which increase from 8.81×10^{-8} to 10.7×10^{-8} cm^2/s, with the increase of concentration of Cc^+ from 0.13 - 1.0 mM and become constant at higher concentration of Cc^+. The similar behaviour was obtained for D of Fc in the presence of $TBAPF_6$. The explanation is based on the different structures of the ionic order at the interface between IL- electrode due to the solute-solute and solute-IL interactions.

Compton et al. also reported the influence of gases dissolved on diffusion of Fc in [emim][NTf_2] [65]. Ar and CO_2 increase the value of D of Fc in ILs in comparison to the value of D under vacuum or N_2 atmosphere.

2.2.3. Diffusion of molecular in liquids

2.2.3.1. Classical model

Einstein was known as the first person who suggested the famous Stoke-Einstein equation. In fact, a the same time in 1905, William Sutherland separately reported the relation between viscosity and diffusion [66]:

$$D = \frac{kT}{b\pi\eta r} \tag{2.33}$$

With k is the Boltzmann constant, $4 \leq b \leq 6$, a constant which depends on the manner of the diffusion, and r the hydrodynamic radius of the species.

For a 'sticking condition', when the movement of a molecule is hindered by the frictional forces occurring at the interfaces of the fluid layer and the spherical particle, b equals 6 and Eq. 2.33 becomes the Stokes-Einstein equation (Eq. 2.31). In this situation, the frictional forces include two types: one is in front of the particle ($4\pi\eta r$) and the other one parallel to its surface ($2\pi\eta r$). In contrast, for a 'slipping condition', b, or the 'so-called' Sutherland coefficient, is equal to 4 [66]. In this case, there is no interaction between the boundary of diffusing molecule and surface of fluid, the particle then slip moving among the solvent. The slipping case has been found in the diffusion of Fc in viscous ILs while the sticking case in low viscous ILs [67].

Beside the classical model above, there are many empirical equation which predict the diffusion in literature [68–71].

2.2.3.2. Hole theory

The classical model above does not work in some cases in ILs [4,15,16]. The simplicity of the model based on a spherical diffusing particle does not hold well in ILs due to the bulk structure of ILs, a strong interaction between solute-ILs and high viscosity. In fact, in the classical theory, all the equation were derived from the assumptions of a big diffusing molecule compared with the small solvent and of diluted solution of the innocent media of solvents. Abott et al. suggested the application of a hole theory in explaining the abnormal hydrodynamic radius calculated from Stoke-Einstein equation [15,16]. The picture of diffusion of species in ionic liquids was described by hopping between holes in liquid which are form by accidental fluctuations. The size of the hole is calculated using surface tension:

$$r_H = \sqrt{\frac{3.5kT}{4\pi\gamma}} \tag{2.34}$$

with r_H: radius of the hole in liquids, k is Boltzmann constant, γ surface tension.

The size of hole was then compared with the hydrodynamic radius from Eq.2.31 for Fc-MeOH in ILs gave a good agreement in low-viscous ILs [16]. Other disagreement may be contributed to the smaller hole radius (from Eq 2.34) than the real one.

3. Introduction of ionic liquids

Ionic liquids are salts with melting point lower than 100°C and composed completely of ions. ILs are also called room/low/ambient temperature molten salts, fused salts, ionic fluids, liquid organic salts, non-aqueous ionic liquids, or neoteric solvents. The word neoteric solvent has been used recently to indicate that ILs were discovered long time ago and has been applying as new solvents. ILs, possessing many novel physicochemical properties, have been investigated extensively in both theoretical and experimental chemistry. Over the past 10 years, there were more than 6000 papers published related to ionic liquids while only a few hundreds before 2000.

ILs are considered to be green solvents due to non-volatility compared to organic solvents. There is no solvent which has such a low volatility like ionic liquids (except for molten polymer) [72]. With low-pressure volatilization, ILs can be used under high vacuum systems without respiratory protection. In particular, ILs have high electrochemical stability with large electrochemical windows, high thermal stability as well as good conductivity. Therefore, ILs have been used as solvents without adding any supporting electrolyte for some redox reactions which otherwise may not be carried out in organic solvent [73]. Especially, ILs are suitable for exothermic reactions which exploit the property of non-flammable at normal condition. ILs also have been utilised successfully for other applications, including batteries, electro-deposition, fuel cells, and photo-electrochemical cells [1–3] (Fig. 3.1).

However, there are still many challenges one must face with when using ILs. The tunable properties of ILs, such as viscosity, conductivity, and potential window can be affected strongly by the presence of impurities from starting material and particularly by water [74–76]. Other challenges are the high viscosity in comparison with conventional solvents as well as the complex structure of ILs leading to abnormal results in mass and charge-transfer dynamics.

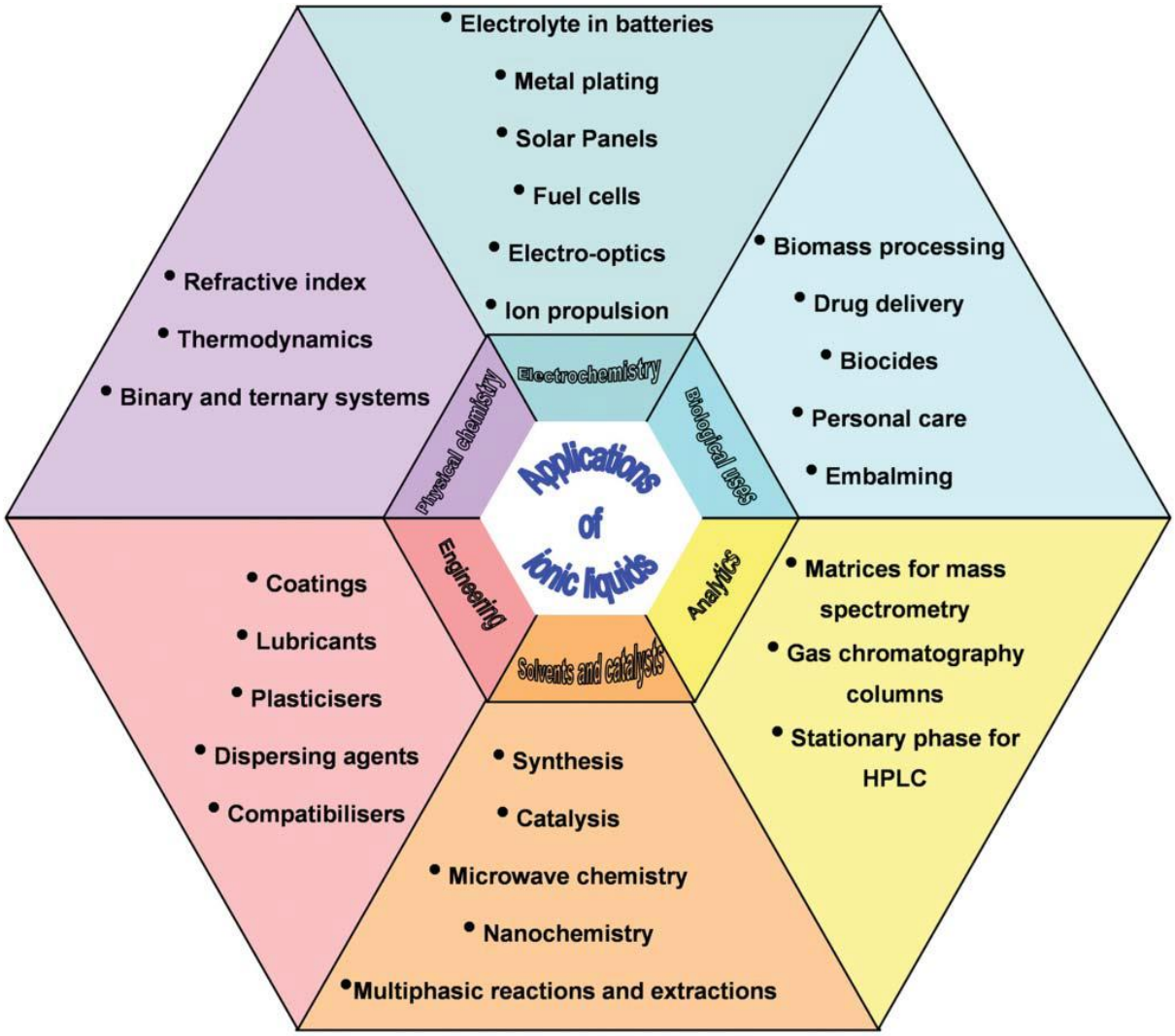

Figure 3.1. Applications of ionic liquids. Adapted from [2].

3.1. History

The first ionic liquids, 'red oil' was observed during a Friedel-Crafts alkylation. The reaction occurs by the substitution of methyl group (from an electrophie chloromethane) to hydrogen of an aromatic ring (benzene) using a strong Lewis acids catalyst $AlCl_3$. Red oil was formed during the reaction and was characterised later when NMR spectroscopy had been applied. In 1888 Gabriel reported ionic liquids ethanolammonium nitrate (colourless crystal, hygroscopic, melting point 52-55^{o}C. In 1914 Paul Walden prepared ethylammominum nitrate (melting point 12^{o}C). Other alkylammomium nitrates were synthesized for liquid propellants in naval guns. In 1963, John Yoke discovered that ionic liquids based on chlorocuprate were formed when mixing solid copper(I) chloride CuCl and

solid tetraalkylammonium chloride [77]. At this time chloroaluminates ionic liquids-based were used intensively as solvents, electrolyte in batteries. Due to the moisture-sensitivity of chloroaluminate salts the imidazolium-based chloroaluminate ILs must be handled under a glove box. In 1992 the first water stable ILs were synthesized by metathesis reactions including [emim] and anions: [BF_4^-], [PF_6^-], [NO_3^-], [CH_3COO^-], [SO_4^{2-}].

Nowadays, many ionic liquids have been prepared and developed widely for many specific purposes.

3.2. Classification

ILs are classified in two big groups: aprotic and protic ILs. In the structure of ILs, a big organic anion is neutralized by the addition of protons, these are so-called protic ILs (PILs). In the other case, organic cation R^+ is added to form aprotic ILs (APILs). The permanence of positive charge in cation is the key to differentiate APILs and PILs. In APILs, the positive charge is lasting and the neutral part is not in equilibrium with the cation. In constrast, in PILs, the proton –donor and –acceptor site are exsited to form a network of H-bond.

In addition, there are based-chloroaluminates ILs which were popular before and replaced by other class of ILs due to their instability under oxygen and moisture.

3.2.1. Aprotic or conventional ionic liquids

Aprotic ILs has been used widely because they have negligible vapour pressure compare to PILs. Fig. 3.2 shows structures of cations and anions in aprotic ionic liquids. ILs are composed of bulky organic cations contain nitrogen, phosphorus, sulphur such as imidazolium, pyridinium, ammonium, phosphonium together with inorganic or organic anions: [BF_4], [OTf], [NTf_2], [PF_6]and [FAP].

In this class, ILs are divided in two sub-groups: immiscible and miscible ILs. Immiscible ILs usually contains [PF_6], especially [NTf_2], and [FAP] which are

prefer to use due to their less sensitivity with moisture. Miscible ILs are based on X-, [BF_4], [OTf], [NO_3] anions.

3.2.2. Protic ionic liquids

Recently, many chemists pay their attention in protic ionic liquids which have been investigated in wide applications such as organic synthesis, biological applications, catalysis, proton conducting electrolytes, etc.

Protic Ils are prepared by proton transfer between a Bronsted acid and a Bronsted base. Due to neutral species in protic ILs, MacFarlane and Seddon suggested that 'pure ionic liquids' may contain less than 1 % of neutral species [78]. Bronsted bases include: amine (primary, secondary, tertiary amide) like: alkylamine (methyl, ethyl, propyl, butyl, pentyl, etc.), N-ethylbutylamine, diethanolammnie, di-n-propylamine, triethylamine, N,N-dimethylethylamine, etc. Bronsted acids are organic acids like: acetic acid, formic acid, glycolic acid, lactic acid, methylsulfonic acid, or inorganic acids: nitric acid, phosphoric acid, sulphuric acid, etc.

3.3. Physical and chemical properties of imidazolium –based ionic liquids

In this chapter, the physical and chemical properties of imidazolium –based of ILs include: density, viscosity, conductivity, surface tension, electrochemical window, thermal and chemical stability will be discussed.

3.3.1. Density

Densities of ionic liquids are usually around 1 to 1.6 g/cm^3. With the same anion, the viscosity decrease when the length of alkyl group increases (Table 3.1). ILs based on bulky anion such as [NTf_2] tends to have high density. With the same cation, densities of ionic liquids increase with the increase of molar mass of anion and follow the trend [BF_4] < [OTf] < [PF_6] < [NTf_2].

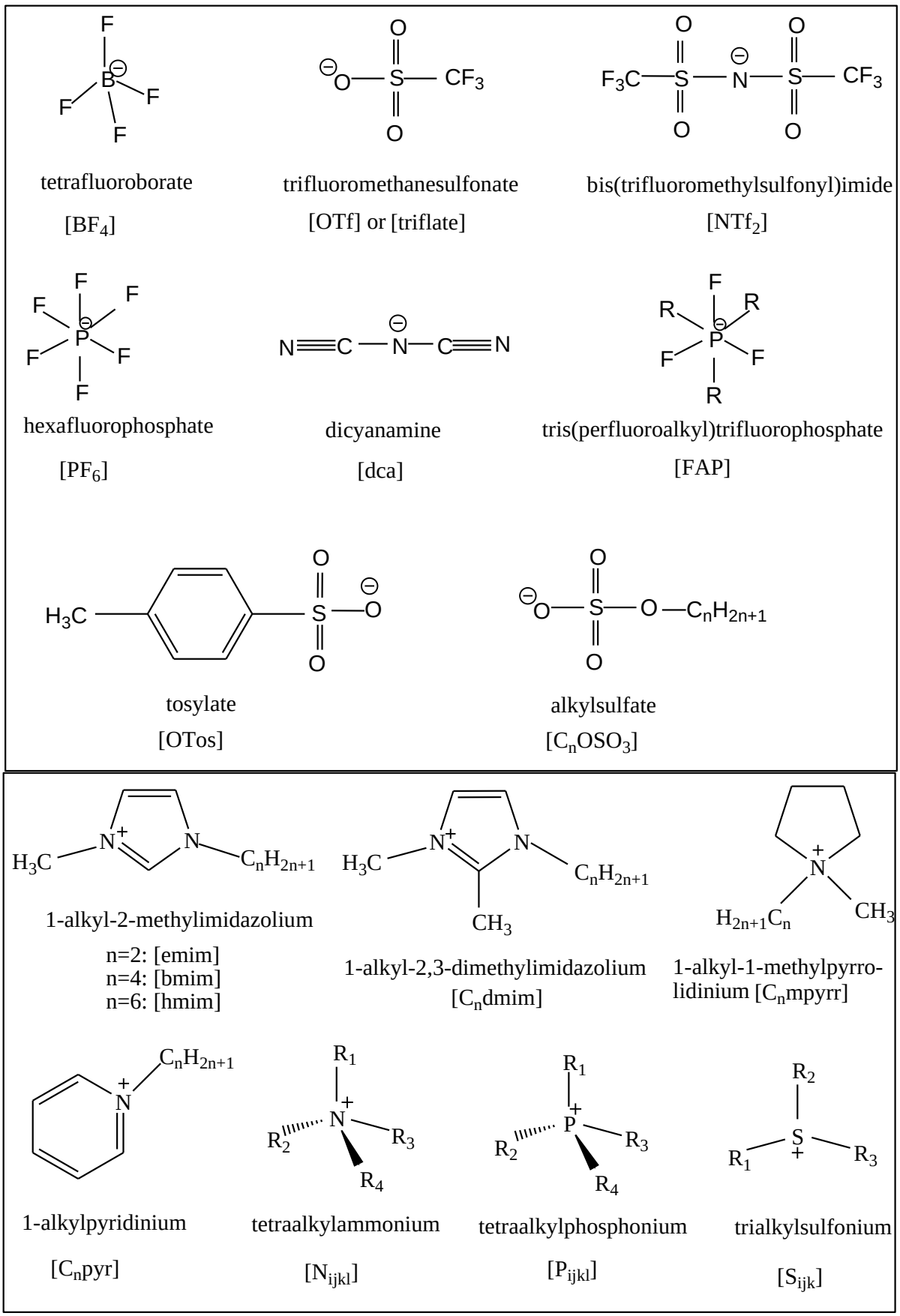

Figure 3. 2. Structures of anions and cations composing aprotic ILs.

3.3.2. Viscosity

ILs are viscous like oil what can cause difficulties when using these solvents. High viscosity leads to the slow diffusion.

The viscosity of IL is two or three orders of magnitude higher than the viscosity of organic solvent. There are low viscous ILs, 30-50 cP or high viscous ILs, 300-500 cP (Table 3.1). For example, the viscosity of the lowest-viscous ILs, [emim][NTf_2], is 39 cP compared with water 0.89 cP.

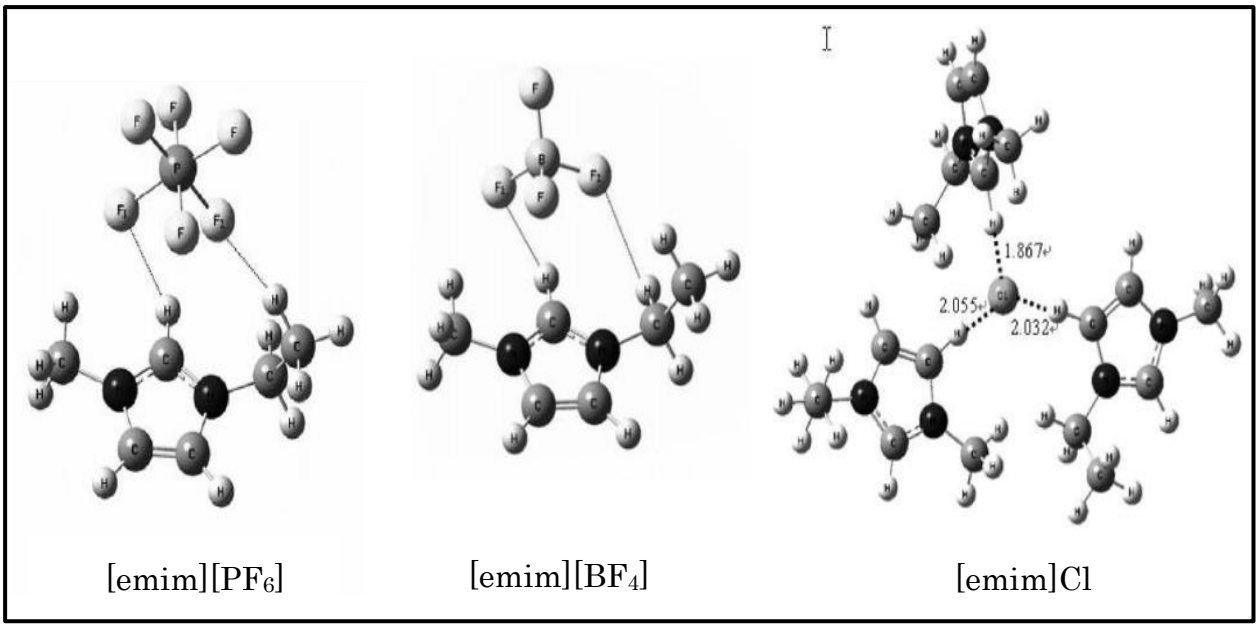

Figure 3.3. Hydrogen bond in ILs. Adapted from [79].

It is known that the viscosity of ILs is influenced strongly by the van der Waals interactions and H-bonding [80]. Viscosities of ILs with the same anion increase with increasing the length of the alkyl group due to the increase in van der Waals interaction. Structure of anion effects dramatically on the viscosity. Small anions which have delocalized negative charge and no hydrogen bonding like [NTf_2] lead to low viscosity of ILs. The amides and methanides-ILs have low viscosity which attributed to the decrease in H- bonding as a result of fluorination of anion [81]. From [emim][NTf_2] (η = 34 cP) to [emim][BF_4] (η = 37,7 cP), H-bond is dominant in cases of small anion [BF_4]. Although van der Waals interaction increase from [emim][NTf_2] to [emim][OTf] (η = 45 cP). In this case H- bond is dominant, [NTf_2]

is the least basic which forms a weak H-bond in compared with [OTf]. ILs containing [CF_3COO], [NTf_2], [dca] and [SCN] have low viscosity.

The temperature dependence of viscosity can be described by an Arrhenius –type equation:

$$\eta = \eta_0 \times \exp(E_\eta/T) \quad (3.1)$$

Where E_η is the activation energy of diffusion of viscous flow of solvents, respectively; η_o are hypothetical values η at infinite T. The higher values of E_η make it difficult for the ions to diffuse cross each other. These values depend on size of anion and interactions in ILs. In general, E_η is larger in the case of higher viscosity ILs.

For glass forming ILs, the dependence of viscosity on temperature can also be described using Vogel-Fulcher-Tamman (VFT) equation.

$$\eta = \eta_0 \times \exp[B/(T-T_o)] \quad (3.2)$$

Where T_o is glass transition temperature, η_0 and B are constant.

Vandernoot et al. reported that Arrhenius equations fit well in the case of ILs contain cations which are less symmetric and lack of functional groups. In contrast, for small ILs composed of symmetric and lighter cations, VFT model fit well. Viscosities of ILs having less symmetric, functional heavy cations are not described well with either Arrhenius or VFT equation.

3.3.3 Melting point

Melting point (T_m) is not easy to predict from the structure of ILs. There is no clear relationship between T_m and hydrogen bonding [80]. ILs containing symmetric inorganic cations ([emim], [mmim]) have higher melting points. When the length of alkyl chain increase (3-5 atoms), the melting points decrease [82]. ILs based on amides and methanides usually have low melting points. T_m of [emim][NTf_2] is lower than [emim][OTf] due to inability of H - bonding of [NTf_2] [80]. When cooling ILs some do not crystalline and form glass. The glass transition temperature in the range of -104 ÷ -75^{o}C [83].

Table 3.1. Data of density, ρ, viscosity, η at 20°C, melting point, T_m, glass trasition temperature, T_g, decomposing temperature, T_d of ILs.

Ionic liquids	ρ (g/cm^3)	η (cP)	T_m (°C)	T_g (°C)	T_d (°C)
[emim][BF_4]	1.297 [84]	38.2 [84]	11 [82]		450[82]
[bmim][BF_4]	1.21	129	-17 [85]	-85 [85]	425[86]
[emim][PF_6]	-	-	62 [82]	-	375[82]
[bmim][PF_6]	1.36	387	11[85]	-76 [85]	373 [85]
[emim][OTf]	1.39 [80]	45 [80]	-9 [80]	-	440[80]
[bmim][OTf]	1.302[87]	90 [80]	13 [85]	-	392[85]
[emim][NTf_2]	1.52	39	-17 [82]	-92 [82]	439[54]
[bmim][NTf_2]	1.44	61	-2[85]	-86 [85]	422 [85]
[hmim][NTf_2]	1.38	90	-6[54]	-81[54]	428[54]
[emim][dca]	1.104[86]	17.54[86]	-	-	-
[bmim][dca]	1.064[86]	33.5[86]	-6[85]	-90 [85]	300 [85]
[emim][CF_3COO]	1.285[80]	35 [80]	-14[80]		150[80]
[bmim][CF_3COO]	1.209[80]	73 [80]	-	-78[53]	176[53]
[emim][SCN]	1.117(25°C)[88]	22(25°C)[88]	-12[89]	-98.5[88]	240[89]
[bmim][SCN]	1.06[89]	29.3[89]	-10[89]	-94[89]	220[89]

3.3.4. Conductivity

ILs composed completely from ions lead to the assumption of high conductivity. But this is not the case for many ILs (Table 3.2). Compared to organic solvents with supporting electrolyte, conductivity of ILs is equal or sometimes lower due to the high viscosity of ILs. Electrical conductivities, σ, of ILs decrease with the increase of alkyl chain length. The longer alkyl chains results in stronger van der Waals interactions that make higher viscosity and lower ionic mobility [90–93] σ decrease about half its value when the alkyl chain increase 2 carbon atoms [93]. In contrast, there is no correlation of conductivity with variation of the anion of the [bmim]- ILs [90,93]. The conductivity increase in the order [bmim][PF_6] < [bmim][OTf] < [bmimTA] (trifuoroacetate)< [bmim][dca]. Other investigations show that conductivities increase in the order [$EtSO_4$] < [OTf] < [NTf_2] [6]. The

reasons are: (i) [NTf_2] has six electronegative fluorine atoms in two large electron withdrawing perflourosulfonyl groups, [OTf] has three fluoros and [$EtSO_4$] has no fluoro atom. As a results, negative charge in [NTf_2] is spread out on the S-N-S moiety lead to better conductivity; (ii) stronger cation – anion interactions in the order [$C_n$mim][$EtSO_4$] > [$C_n$mim][OTf] > [$C_n$mim][NT_2] result in higher ion-pairing or lower iconicity [6]. The anion size has 2 opposite effects in the σ: the anion size increases cause the decrease of the surface electrical charge density and mobility of ion in an area created of ions increase : Cl- < Br- < [BF_4] ; on the other hand the increased ion-size contributes to the difficult movement (hopping): [PF_6] < [ES] < [TY-]. The optimal anion size for electrical conductivity is [BF_4].

Electrical conducitivity in some cases follow the typical Arrhenius law. In fact, the temperature dependence of the electrical conductivity can be fitted with very high accuracy using a Vogel – Tamman –Fulcher (VTF) type equations. The value of ionic conductivity of investigated ILs was calculated using VFT equation from literature (Table 3.2).

Table 3.2. VFT equation for ionic conductivity of ILs. $\sigma = \sigma_o \times \exp [B/(T-To)]$

	σ_o (mS/cm)	B (K)	To (K)
[bmim][BF_4] [90]	1660	806.6	167
[bmim][OTf] [90]	951	767	166
[emim][NTf_2] [54]	657	571.6	164
[bmim][NTf_2] [53]	430	565	178
[hmim][NTf_2] [54]	610	731	168
[bmim][PF_6] [53]	1470	855	174

Table 3.3. Ionic conductivities of ionic liquids and solvents.

Solvent	σ (mS/cm)	Solvent	σ (mS/cm)	Solvent	σ (mS/cm)
[emim][BF_4] (25°C)	14[94]	[emim][NTf_2]	8.8[80]	ACN/0.1 M TBAP	7.6
[bmim][BF_4] (25°C)	1.73[95]	[hmim][NTf_2]	1.84[54]	DMF/0.1 M TBAP	4.07
[bmim][PF_6]	1.5[96]	[emim][CF_3COO]	9.6[80]	DMSO/0.1 M TBAP	2.7
[bmim][dca] (25°C)	11.4[97]	[bmim][CF_3COO]	**3.2**[80]	KOH (30% wt.). Lead-acid battery (25°C)	621[98]
[emim]dca]	28[89]	[emim][BF_4] 0.2 M in ACN (25°C)	19.0[97]	Li[NTf_2] 1M in EC + DME (1:1). Li-ion battery (25°C)	13.3[99]
[bmim][NTf_2]	3.9[80]	[bmim][BF_4] 0.27 M + PC (25°C)	5.37[97]	Li[PF_6]1M in EC + DME (1:1). Li-ion battery (25°C)	16.6[99]
[emim][OTf]		[bmim][PF_6] 0.14 M + ACN (25°C)	14.9[97]	Li[OTf] 1M in EC + DMC (1:1). Li-ion battery (25°C)	3.1[99]
[bmim][OTf]	3.7[80]	[bmim][dca] 0.49 M+H_2O (25°C)	20.2[97]	Li[NTf_2] 1M in EC + DEC (1:1). Li-ion battery (25°C)	6.5[99]

3.3.5. Thermal and chemical stability

Compared to organic solvents, vapor pressure of ILs are undetectable at room temperature. This is a big advantage of ILs which named ILs as green solvents.

ILs are nonflammable. The temperature of decomposition of ILs is high which allows to access chemical processes which are not able to do in traditional solvents. [bmim][OTf] still stable after heating 10h at 200^0C while [bmim][PF_6] degrade [100]. The stability of ILs is in the range Br < [dca] < [BF_4] < [PF_6] < [OTf] < [NTf_2] [82]. ILs with longer alkyl chains are more stable with temperature compared to smaller one.

3.3.6. Electrochemical window

Electrochemical window (EW) is the potential range between reduction and oxidation of supporting electrolyte in solvents or of ILs. In the other words, EW is the range in which the solvent is electrochemically stable. EW is one of the most important parameter when choosing a solvent in electrochemical application. EW depends on electrode materials and the composition of solution (Table 3.4). Aqueous solution has small EW. Organic solvents with electrolyte give higher value of EW. For ILs, the EW is often in the range of 3 -6 which is large in comparison to traditional organic solvents with supporting electrolyte.

EW of ILs based on tetraalkylammonium cation and pyrrolidium cation is wider than those of imidazoliun cation.

Anions composing ILs have a strong effect on EW. ILs based on [dca], [CF_3COO], X (halogen) have narrow EW while ILs based on [NTf_2], [BF_4],[PF_6] have wide EW.

Table 3.4. Electrochemical windows (EW) of ionic liquids and traditional solvents/supporting electrolytes

Ionic liquid	WE	RE	Cathodic limit	Anodic limit	EW
[emim][BF_4]	Pt	Ag/AgCl-wire	- 2.1	+ 2.2	4.3 [101]
	Pt	Ag/Ag^+ in DMSO	- 1,6	+ 1	2,6 [102]
	Pt	Al in $AlCl_3$ + EmimCl (1.5:1.0)	- 2.1	+ 2.2	4.3[94]
	GC	Li/Li^+	+ 1	+ 5	4[103]
[bmim][BF_4]	W(RDE)	Pt(QRE)	- 1.6	+ 4.5	6.1 [104]
	GC(RDE)	Pt(QRE)	- 1.8	+ 3.65	5.45[104]
	Au(RDE)	Pt(QRE)	- 1.85	+ 2.35	4.2[104]
	Pt(UME)	Pt(QRE)	- 1.5	+ 2.5	4.0[104]
	GC	Li/Li^+	+ 1.2	+ 5	4.2 [103]
[bmim][PF_6]	GC(RDE)	Pt(QRE)	- 2.5	+ 3.85	6.35[104]
	Au (RDE)	Pt(QRE)	-2.5	+ 3.45	5.95[104]
	Pt(UME)	Pt(QRE)	-2	+ 3	5[104]
	Pt	Ag wire	- 1.1	+ 2.1	3.2[105]
	Pt	Pt	- 2.3	+ 3.4	5.7[104]
	Pt	Ag/Ag^+ in DMSO	- 1.9	+ 2.5	4.4[102]
[emim][OTf]	Pt	I^-/I_3^-	- 1.8	+ 2.3	4.1[80]
[bmim][OTf]	Pt	Pt (QRE)	- 2.2	+ 2.0	4.2[106]
[emim][NTf_2]	Pt	I^-/I_3^-	- 1.8	+ 2.5	4.3[80]
	Pt	Ag wire	- 2	+ 2	4.0[105]
	Pt	Ag/Ag^+ in DMSO	- 2	+2.5	4.5[102]
[bmim][NTf_2]	Pt	Ag/Ag^+ in DMSO	- 2	+2.6	4.6[102]
[emim][dca]	Pt	Ag wire	- 1.6	+1.4	3.0[105]

[emim][CF_3COO]	Pt	I^-/I_3^-	- 1.8	+1.6	3.4[80]
[bmim]Br	Pt	Ag/Ag^+ in DMSO	- 2	0.2	2.2 [102]
Organic solvents [51] $TBABF_4$/ACN	Pt	SCE	- 2.5	+ 2.5	5
$TBAClO_4$/DMF	Pt	SCE	- 2.5	+ 1.7	4.2
$TBAClO_4$/THF	Pt	SCE	- 3.1	+ 1.4	4.5
$TBAClO_4$/PC	Pt	SCE	- 2.5	+ 2.2	4.7
$TBAClO_4/CH_2Cl_2$	Pt	SCE	- 1.7	+ 1.8	3.5
KCl/H_2O	C	SCE	- 1.3	+ 1.1	2.3
1M H_2SO_4/H_2O	Pt	SCE	- 0.3	+ 1.3	1.5
NH_3/H_2O	Hg	SCE	- 2.4	0	2.4

3.3.7. Surface tension

Surface tension is given by the change of force per length (N/m) or surface free energy per area (J/m^2). The molecule which is inside the solution has neighbours with lower energy than the one near the surface. The molecule in the bulk liquid is surrounded by other molecules at all direction cause a zero net force. In contrast, a surface molecule does not have all the surrounding molecules at all sides which give a net force pointing to the interior.

The value of surface tension of the used ILs is shown in Table 3.5. surface tension decrease significantly with the increase of alkyl chain length for the imidazolium-based ILs ($n \leq 8$) [107]. The alkyl group was aggregate to the surface of ionic liquids, [108] which is attributed to surface tension following the Langmuir's principle that surface tension is caused only by the structure of the molecul. The outer layer at the surface are normally the alkyl chains, ionic part face toward the bulk solution. Therefore when then alkyl chain increase, the van der Waals increase. However the contribution of Van der Waals interaction is smaller compared with the Coulombic interaction explaining the decrease of surface

tension when the alkyl chain increases. For ILs with symmetric anion such as [BF_4] and [PF_6], the ST increase from [BF_4] to [PF_6] due to bigger size of anion [PF_6] [107]. The Coulombic interaction in the solution is similar[109]. The surface tension is in the order: [[OTf] > [NTf_2] > [PF_6] > [FAP] with the increase of molecule volume in that order. This can be explained by the decrease of Coulombic interaction when the size of anion becomes bigger.

Table 3.5. Values of surface tension of ILs

ILs	[emim][dca]	[emim][NTf_2]	[emim][OTf]	[bmim][NTf_2]
ST (mN/m)	60.5[110]	41.8[111]	44.6[111]	33.6[112]
ILs	[bmim][OTf]	[hmim][NTf_2]	[bmim][BF_4]	[bmim][PF_6]
ST (mN/m)	35.5[112]	36.1[111]	44.4[113]	48.2[111]

3.4. Impurities in ILs

3.4.1. Effect of water

There is always such a certain amount of water in ILs, even for immiscible ILs, this causes the dramatic changes in the properties of the ILs. Water contamination have low effect on hydrophobic ILs but higher in the case of hydrophilic ILs [112]. Hydrogen bond between H of cation and O of water determine solubility of ILs. A replacement H of C_2 in [bmim][PF_6] by methyl group decrease the polarity of Ils equal to [omim][PF_6] [114]. Interaction strength of hydrogen bonding in case of [BF_4] and [PF_6] –ILs is in the order: [C_4C_1mim] < [omim]< [hmim]< [bmim] [112] while for same cation [bmim] and different anion in the range of [NTf_2] < [PF_6] < [OTf] < [BF_4]. Therefore, the hydrophobicity of the anions is in the order: [BF_4] < [PF_6] < [NTf_2]. ILs which contain anion [PF_6], [NTf_2] is immiscible in water while ILs which contain [BF_4], [OTf], X^- are miscible in water. However, for long chain ILs result in higher hydrophobicity and decrease in the solubility in water [114]. For example, [omim][BF_4] is immiscible in water.

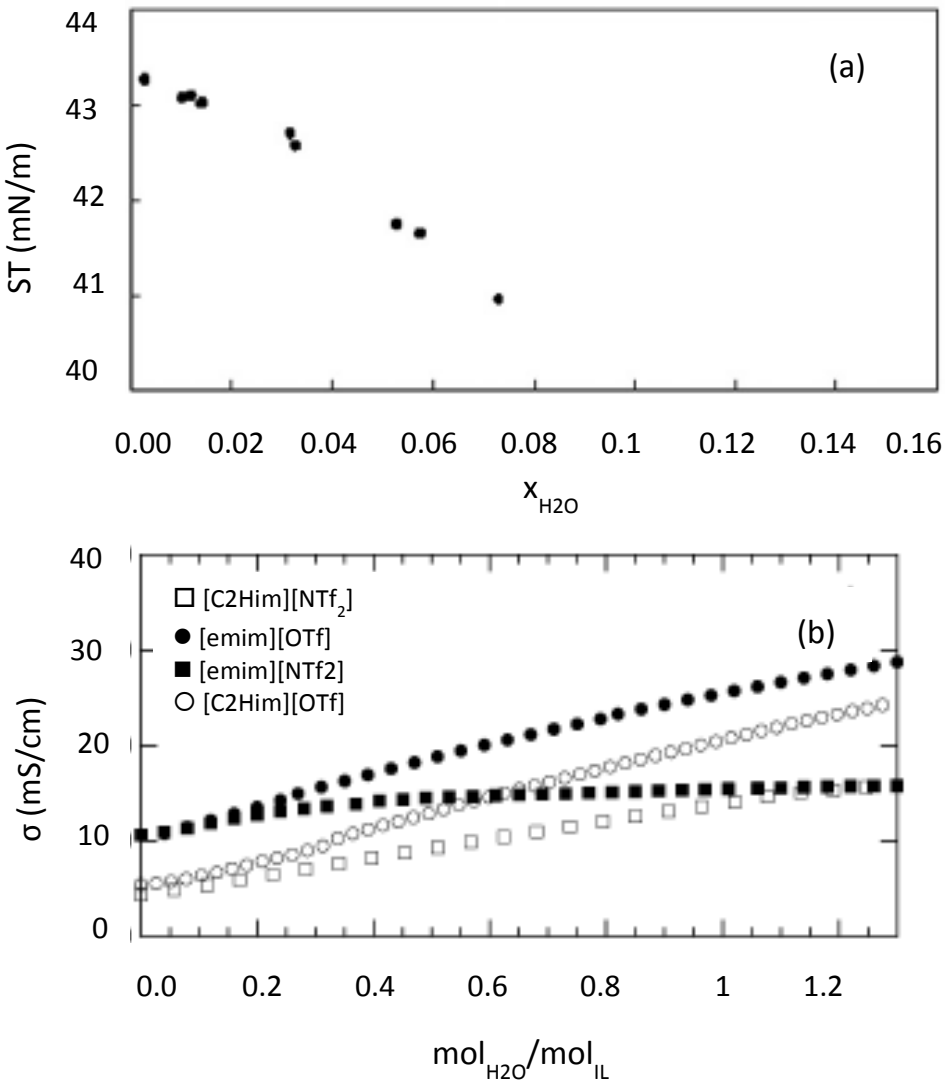

Figure 3.4. (a) Dependence of surface tension on water content in [bmim][PF_6] at 30^0C. Adapted from Ref. [112]. (b) Ionic conductivity of ILs in the presence of added water at 30^0C. Adapted from Ref. [115].

Surface tension of ILs is smaller (Fig. 3.4a) in the presence of water which can be explain by a reduce in the interactions between cation and anion formed ILs. When water introduce to ILs, ILs will form H bond with both cation and anion. The cation and anion have to arrange water can get in. cause the lower surface energy [112]. It is known that the interactions cation anion in ILs and water-water is stronger than the one form the mixture.

Water can be removed under high vacuum at 60°C. For $[PF_6]$–Ils, the temperature must not higher than 60°C because $[PF_6]$ can react with water to form HF and complex oxo- and hydrophosphate [116]. Water can be detected by IR spectroscopy or more precise Karl Fischer titration, NIR spectroscopy or cathodic stripping voltammetry.

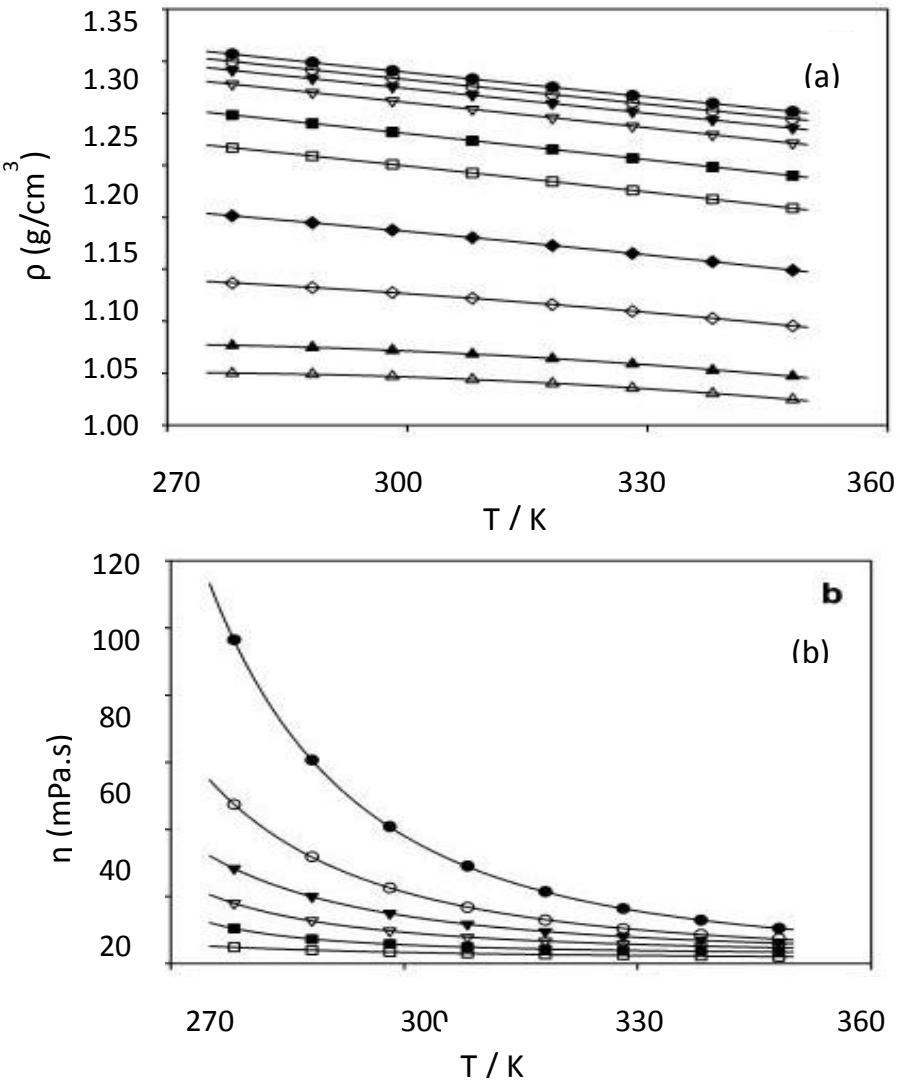

Figure 3.5. (a) Density of $[emim][NTf_2]$ + water: ● 0%; ○ 2%; ▼ 5 %; ▽ 10%; ■ 20%; □ 30%; ◆ 50 %; ◇ 70%; ▲ 90 %; △ 100%. (b) Dynamic viscosity of [emim][OTf] +water: ● 0%; ○ 2%; ▼ 5 %; ▽ 10%; ■ 20%; □ 30%; ◆ 50 %. Adapted from Ref. [117].

Water also has a strong effect on other properties: increases conductivity (Fig. 3.4b) [115], decreases density and viscosity (Fig. 3.5). Moreover, water can contract largely the electrochemical window of ILs (Fig. 3.6).

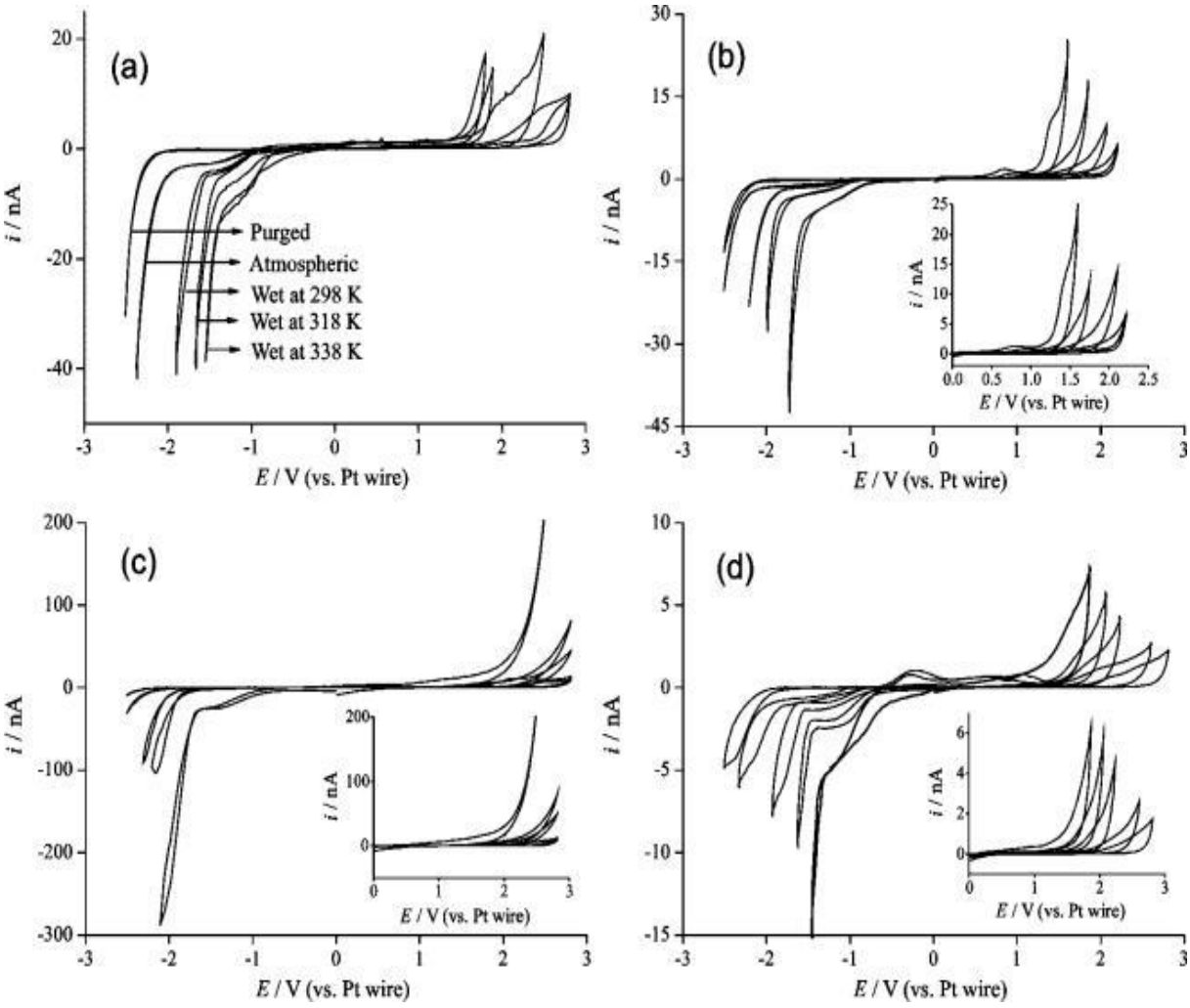

Figure 3.6. Effect of water on electrochemical window of (a) [emim][NTf_2], (b) [bmim][OTf], (c) [bmim][BF_4], (d) [bmim][PF_6]. WE: Pt 10 µm, v: 100 mV/s. Adapted from [106].

3.4.2. Other impurities

Impurities can be from starting materials such as imidazole, alkyl halide, and chloride. The presence of chloride in ILs reduces densities and increases viscosities of ILs (Fig. 3.7). To detect chloride titration using $AgNO_3$ which is can be modified by Volhard method. The limit detection is 1.8 ppm. Cl^- can be detected more appropriate by inductively coupled plasma mass spectrometry (ICP-MS). Electrochemical methods such as linear sweep and square sweep voltammetry and cathodic stripping voltammetry with the LOD about 0.16 ppm also are used in determination of chloride in ILs [118]. Halide can be removed by washing with water in the case of immiscible ILs. Chloride can be removed using

other methods such as electrochemistry followed by vacuum to evaporate chlorine gas or using ion exchange chromatography [119]. The starting materials which still remain under vacuum can be extracted using volatile organic solvent. For ILs using for spectroscopy, the colourless ILs is required. Decolourization of ILs can be achieved using active charcoal and silicagel [116].

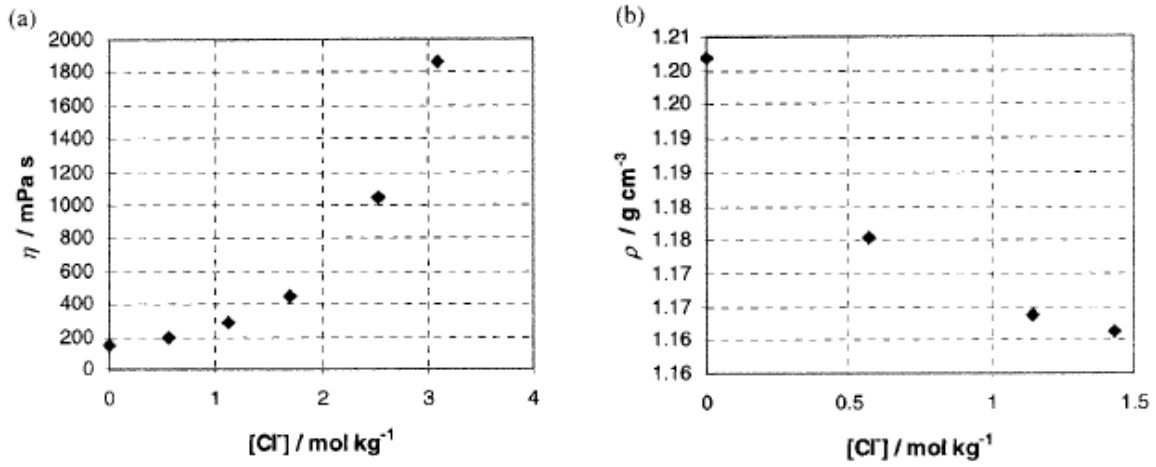

Figure 3.7. (a) Viscosity at 20°C, (b) Density at 30°C of [bmim][BF_4] with added chloride from [bmim]Cl. Adapted from [76].

4. Experimental work

"If your result needs a statistician then
you should design a better experiment."

Ernest Rutherford

This chapter brings a detail of experimentation section. The first part relates to characteristic and problems of ILs such as: removing chloride and water from ILs, measuring their physical properties. The second part focuses on synthesis/ purification of compounds used and their behavior in ILs. The final part is the presentation of two special electrochemical cells for millimeter and micro-electrodes used for ILs. Sample preparation; conducting the cyclic voltammetry experiments, steady-state measurements and impedance measurements of determining resistance of ILs are described in detail.

4.1. Instrumentation

4.1.1. High vacuum pump system

Ionic liquids, especially water-miscible ionic liquids, contain a large amount of water at ambient conditions. It is necessary to use high vacuum to remove water from ionic liquids before preparing solution of substances in ILs. The high vacuum works based on using an oil vapour diffusion pump. The diagram of the system is illustrated in Fig. 4.1. The pressure can reach $2 – 6 \times 10^{-5}$ Torr.

4.1.2. Solvent Characterization

Densities of the ILs were measured by a home-made densimeter. The dynamic viscosity of [emim][NTf_2], [bmim][NTf_2], [hmim][NTf_2], [bmim][BF_4], [bmim][PF_6] were measured by a Micro-Ubbelohde capillary viscometer type IIc from SI Analytics GmbH, Germany. The measurement ranges for IIc capillary is in 30-300 mm^2/s with K = 0.3144 mm^2/s^2.

The kinematic viscosity θ and dynamic viscosity η can be calculated by the following equations:

$$\theta = K \times t \qquad (4.1)$$

$$\eta = \theta \times \rho \qquad (4.2)$$

Where ρ is density of IL and t is flow time which is the average value of three measurements.

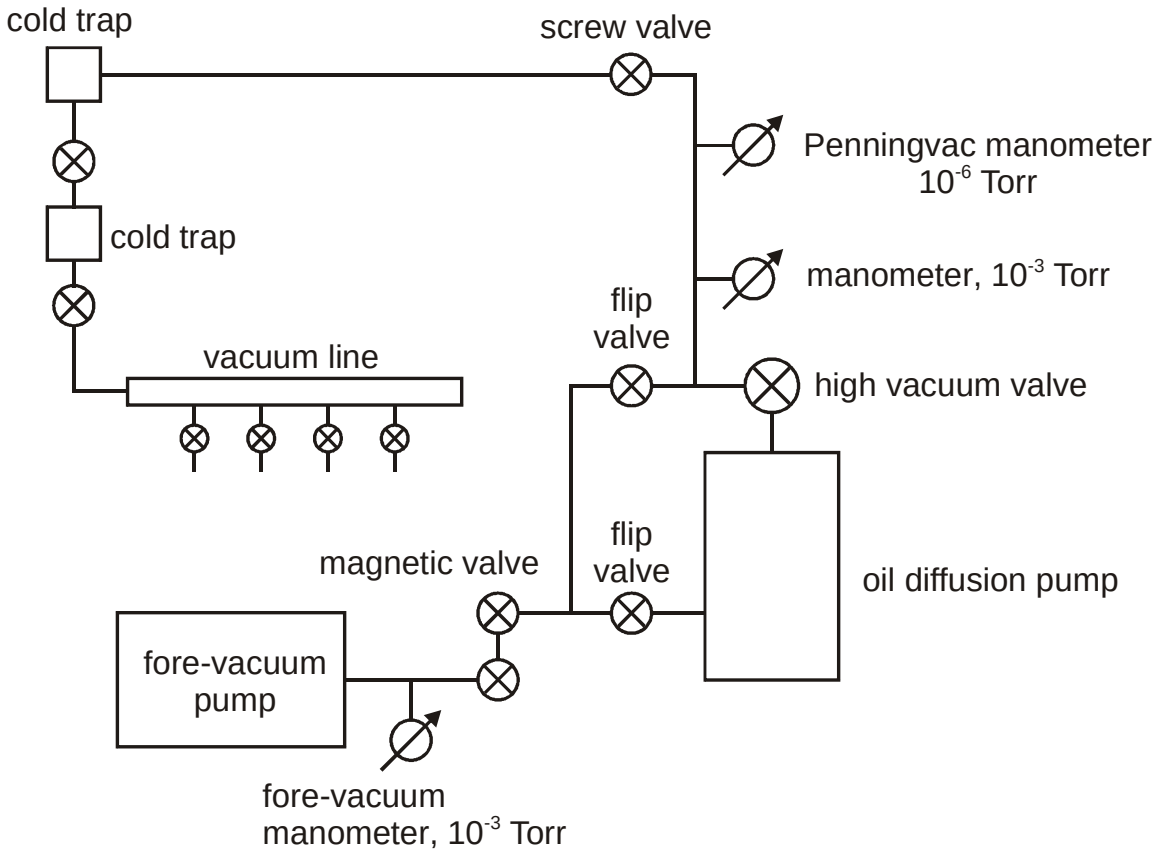

Figure 4.1. Scheme of high vacuum diffusion pump.

4.1. 3. UV –Vis and NIR spectroscopy

To understand the behaviour of substances in ILs in comparison to organic solvents, UV-Vis spectroscopy is a useful tool. UV-Vis spectra were recorded using a Shimadzu UV-3101 PC spectrometer. UV-Vis spectra of $TCNE^{\cdot-}Na^{\cdot+}$ in ACN was measured in a 5mm cuvette.

UV-Vis spectra of TTF and $TTF^{\cdot+}ClO_4^-$ in ILs and organic solvents were recorded in 2 mm and 1 mm - quartz cuvettes, respectively.

The water content in ionic liquids was determined by using NIR absorption spectroscopy. NIR spectra was done using a Shimadzu UV-3101 PC spectrometer with a usable wavelength range of 190 – 3200 nm. NIR spectra of ionic liquids were measured in a 5 mm cuvette filled with 1.2 ml of ionic liquids under nitrogen atmosphere. Prior to use the cuvette was first evacuated and then purge with argon for three times. Wet ionic liquids were made by adding exact amounts of water into high vacuum-dried ionic liquids using Hamilton syringe. NIR spectra were obtained in the wavelength range of 800- 3000 nm and at slow scan in the wavelength range of 1790- 2065 nm. Water adsorbs at 1920 cm^{-1}.

4.1.4. Electrochemical measurement

All electrochemical measurements were performed using an Autolab PGSTAT302N potentiostat (Eco Chemie B.V., Utrecht, The Netherlands) with the software version 4.9.

4.1.4.1. Temperature controlled electrochemical cell for millimeter-working electrode

In order to measure small volumes of samples at different temperatures and to use the commercial millimeter working electrodes, a three-electrode cell was constructed (Figs 4.2a, 4.3). The cell contained two lines of thermostated water inlet and outlet. These lines were connected with a thermostat. The temperature in the cell was controlled by a digital thermometer. The cell body was made from Teflon and thermal paste was used for better thermal transport between the cell and surrounding temperature unit.

Ag/AgCl with 0.1 M [bmim]Cl in the relevant IL was chosen as reference electrode, a Pt wire as counter electrode, and (1 ± 0.04) mm diameter glassy carbon-disk electrode (GC) as a working electrode. The reference electrode is located 1mm away from working electrode. The working electrode could be dismantled from the cell.

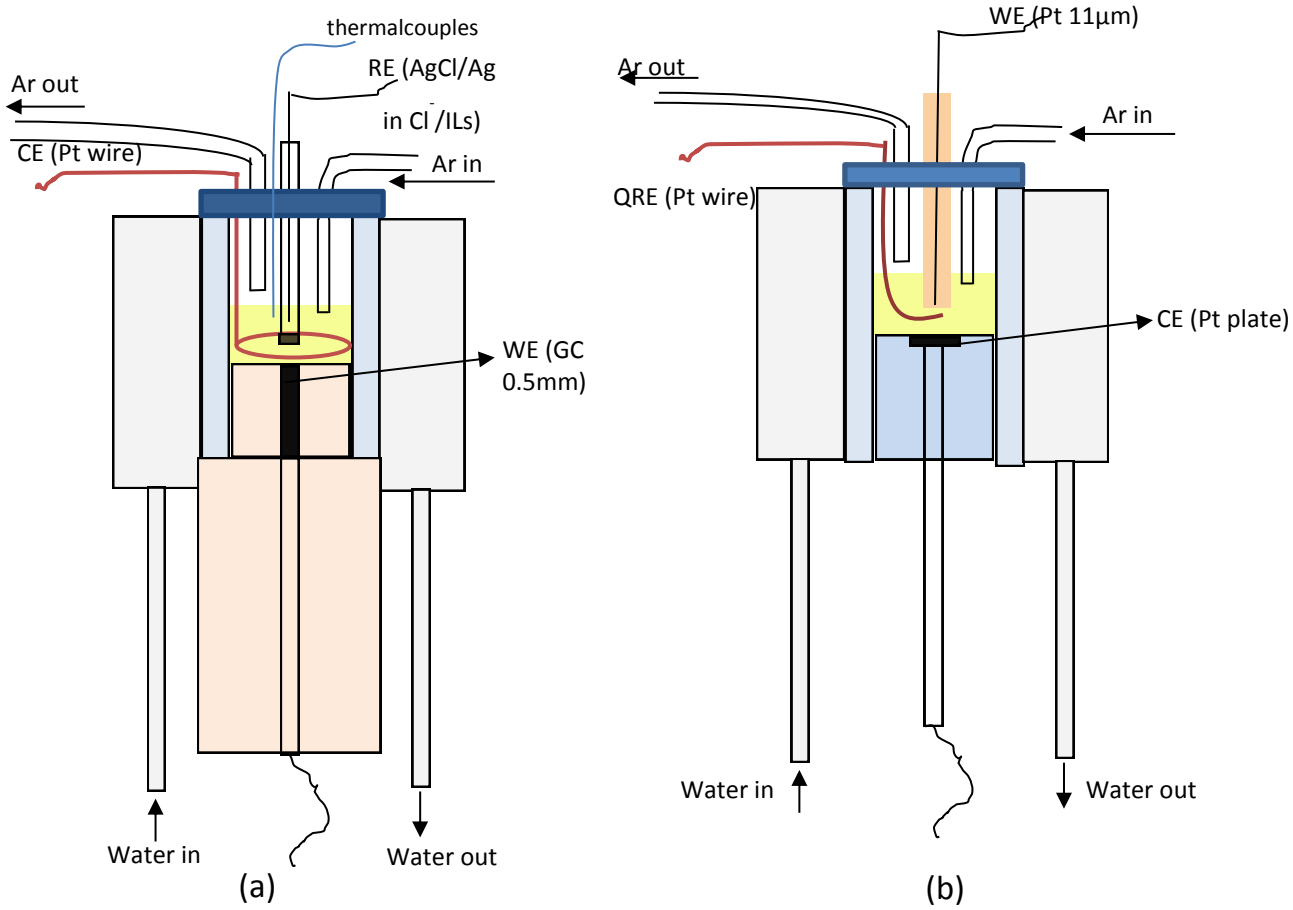

Figure 4.2. Scheme of the temperature-controlled electrochemical cells for (a) millimeter-, and (b) micrometer-working electrodes.

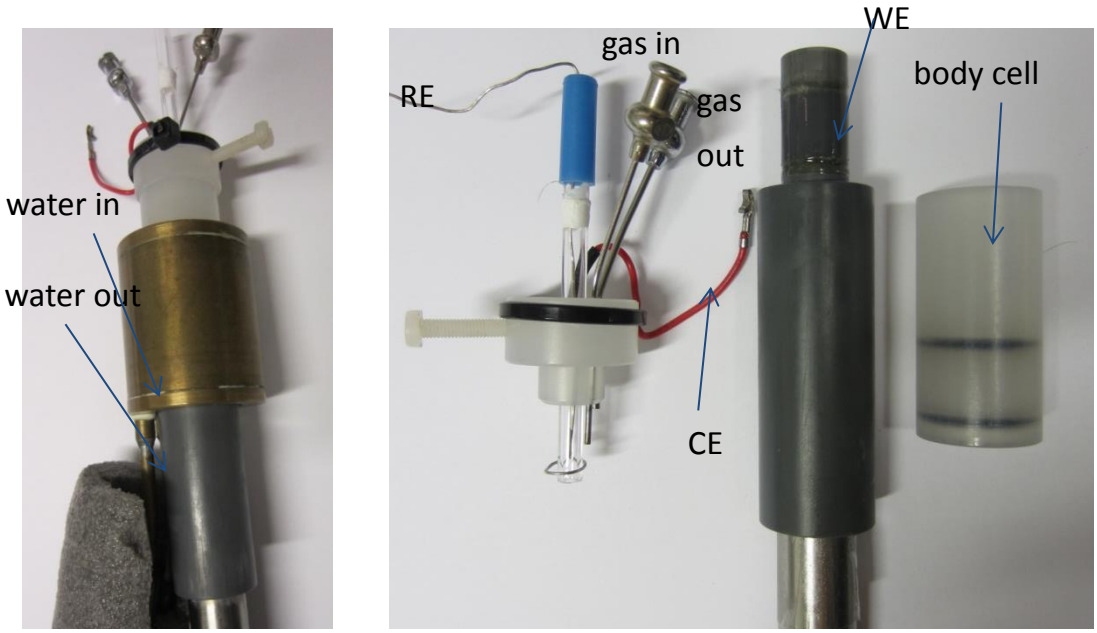

Figure 4.3. Temperature-controlled millimeter-working electrode electrochemical cell

4.1.4. 2. Temperature controlled electrochemical cell for micrometer working electrode

Ultramicroelectrodes were made following procedure from literature with modifications. A 10 µm, 15 µm or 20 µm diameter Pt wire was soldered with a 0.5 mm Ag wire. The Pt wire was then inserted into a 6mm diameter glass capillary. The end of the capillary was sealed under vacuum condition using burner and finally was polished to expose Pt disk-shaped surface. At first, the surface was polished by sand paper (K800 and later K1200). The WE was then polished by alumina with the decreasing diameter from 5, 1, to 0.25 µm until a mirror surface is formed.

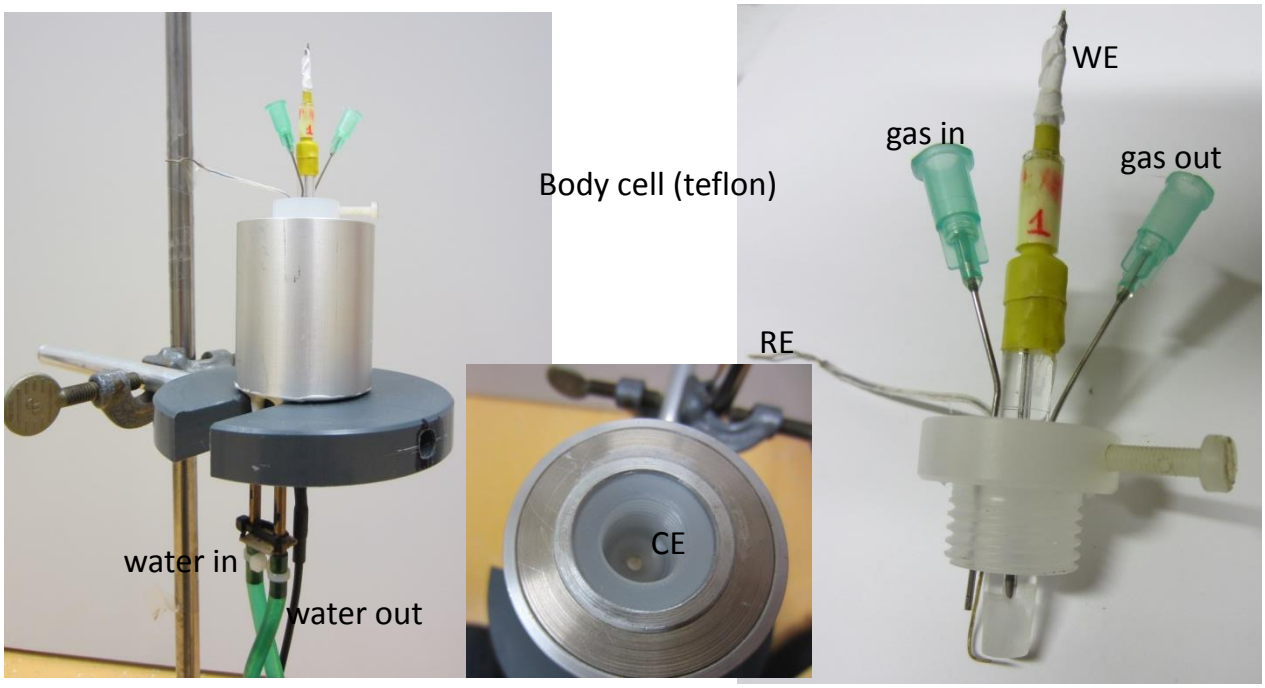

Figure 4.4. Temperature-controlled electrochemical cell for micro-working electrode.

The electrode diameter was calibrated using steady-state voltammetry, using a solution of Fc 2 mM in acetonitrile (ACN) / tetra n-butylammonium hexaflourophosphate ($TBAPF_6$) 0.1 M with a value of D of 2.13×10^{-5} cm^2 s^{-1} [9]. A silver wire served as a quasi-reference electrode (Ag QRE).

The cell using micro-working electrode was modified to allow temperature dependence measurements. The design was similar to the cell above (Figs. 4.2b,

4.4). Temperature calibration was done, comparing the temperature inside the cell, measured by a thin thermocouple compared with the temperature adjusted in the thermostat.

4.1.5. Impedance measurements

ILs have high resitance causing potential drops. The Ohmic drop was measured by impedance measurements using a wave generator SS0603. Voltage and current were measured usng a Voltcraft VC 920 and a Volcraft plus VC 920 multimeters, respectively.

4.2. Chemical reagents

4.2.1. Solvents

[emim][NTf_2], [emim][OTf], [bmim][NTf_2], [hmim][NTf_2], [bmim][BF_4], [bmim][PF_6], [emim][dca], and [bmim]Cl were purchased from Iolitec, Germany except [bmim][OTf] which was from Solvent Innovation, Germany. ACN, acetone, n-hexane, and methanol (MeOH) (Aldrich) were dried over molecular sieves, followed by distillation. Sulfolane was purified by bi-distillation [120].

All ILs received from the company contain 1-methyimimadole (< 2 %) which can react with TCNE (except for [bmim][BF_4]). The solution of TCNE in ILs shows a light yellow colour. Therefore, the ILs used for preparing TCNE solution were purified carefully to remove this impurity. The density and viscosity of purified IL and initial IL are similar.

Purification procedure: Method A: Using solution of HCl (for [bmim][NTf_2], [hmim][NTf_2], [bmim][PF_6]. In a separatory funnel, a slight excess of 1M HCl was added to ionic liquids. The volume of HCl was calculated based on the nominal purity of higher than 98% from Iolitec with assuming that all the impurities are 1-methylimidazole. 1-methylimidazolium chloride and any residual HCl were removed from ILs by washing with bi-distilled water. The washing procedure was repeated at least 5 times and the aqueous layer was tested using a pH indicator

and $AgNO_3$ for residual acid and $AgNO_3$, respectively. In addition to, chloride content also was tested by stripping method [118]. Method B: Using Alumina (for [emim][NTf_2]). Alumina Chromatography purchased from Fluka was packed in a column chromatogram. Then, ionic liquids were poured in and flushed through the column.

Water content in ILs were checked by NIR spectroscopy. Fig. 4.5a shows the NIR spectra of [bmim][OTf] in the presence of water. There is a dramatic increase in intensity of an adsorption at 1920 cm-1 which is assigned to overtone and combination transitions of O-H groups o water[121]. The other absorptions at around 1450 and 1800 cm^{-1} are also related to those transitions. A plot of absorbance at 1922 cm^{-1} vs. concentration of water is shown in Fig. 4.5b. Using this standard curve, it is easy determine the concentration of water in IL.

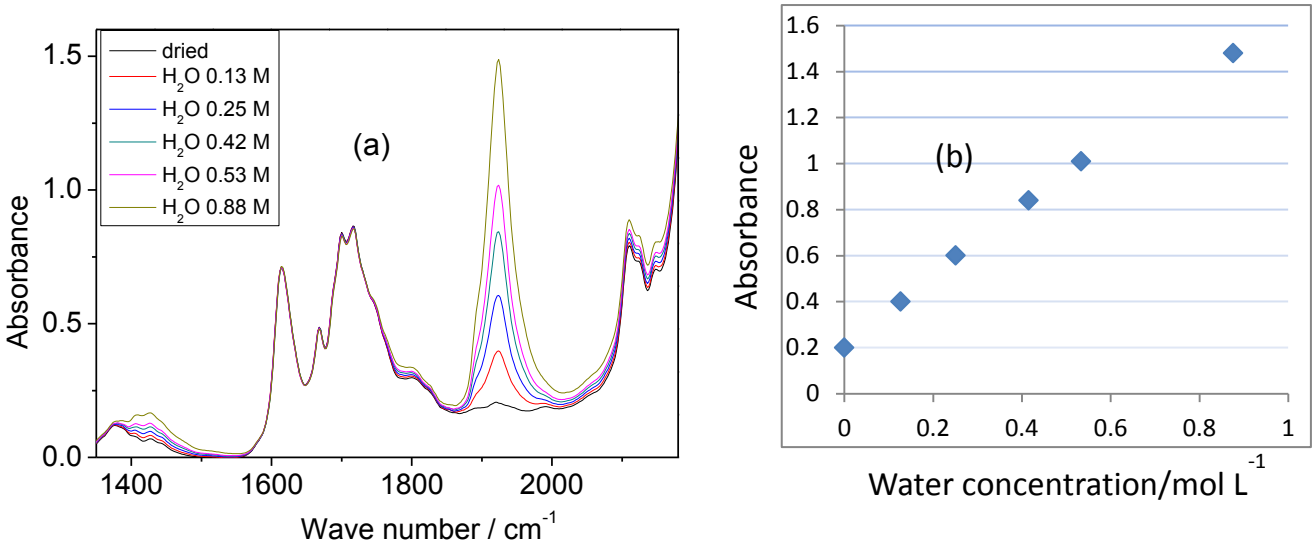

Figure 4.5. (a) NIR sepectra of dired and undried [bmim][OTf] and (b) plot of the absorption peaks at 1920 cm^{-1} vs. concentration of water in [bmim][OTf].

The values of density and viscosity of some ILs from our measurement are presented in Table 4.1 and 4.2. Those values are compared well with the ones from literature.

Table 4.1. Densities of some ionic liquids (g/cm^3)

T / K	[emim][NTf_2]	[bmim][NTf_2]	[hmim][NTf_2]	[bmim][BF_4]	[bmim][PF_6]
293	1.52	1.44	1.37	1.21	1.37
303	1.51	1.43	1.366	1.21	1.36
313	1.5	1.42	1.358	1.2	1.355
323	1.49	1.41	1.35	1.19	1.35
333	1.48	1.41	1.34	1.18	1.34
343	1.47	1.4	1.33	1.17	1.33

Table 4.2. Dynamic viscosities (cP) of some ionic liquids

T/K	[emim][NTf_2]	[bmim][NTf_2]	[hmim][NTf_2]	[bmim][BF_4]	[bmim][PF_6]
293	40	63	90	144	366
303	29	40	55	86	212
313	22	27	39	54	127
323	16	20	29	34	79
333	12	15	21	23	50
343	10	12	16	15	33

4.2.2. Electrochemical probes

The redox substances used in this work include: TCNE and its radical anion; TTF and its radical cation; TEMPO and TEMPOL.

- TCNE and $TCNE^{\cdot+}$ salt: TCNE was sublimated. $TCNE^{\cdot-}Na^+$, $TCNE^{\cdot-}K^+$, $TCNE^{\cdot-}TBA^+$ was prepared according to ref. [122]. The purity of $TCNE^{\cdot-}$ radical was checked using UV-Vis spectra. Fig. 4.6 shows the typical absorption peak of $TCNE^{\cdot-}$ at 428 nm with 17 vibrational overtones. The slight decrease of absorption peak from 296 K to 343 K indicates that the radical is stable over the range of measuring temperatures. Solution of TCNE in ILs is very stable while TCNE radical form dimer or ion-pairing in ILs at the concentration higher than 10 mM. Indeed, the colour of solution of $TCNE^{\cdot-}$ radical in ILs is

pinkish caused by dimerization. Therefore, it is impossible to perform measurements of $TCNE^{\cdot-}$ in ILs.

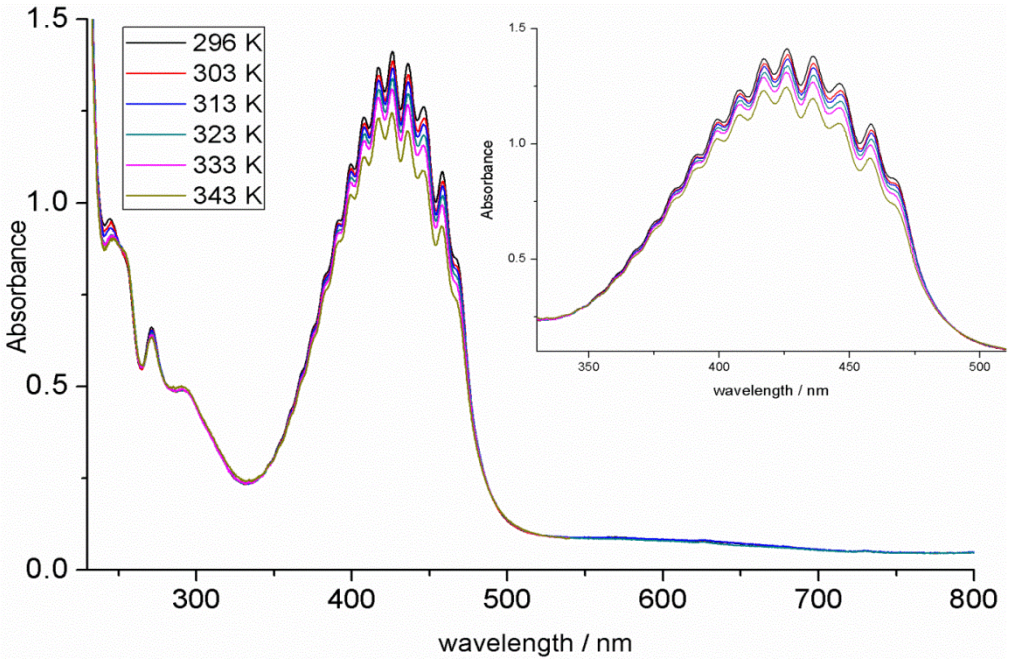

Figure 4.6. UV-Vis spectra of 0.1 mM $TCNE^{\cdot-}Na^{+}$ in ACN at different temperatures.

- TTF and $TTF^{\cdot+}ClO_4$: TTF was sublimated and $TTF^{\cdot+}ClO_4^{-}$ synthesized according to ref. [123]. To get insight into identities of TTF and $TTF^{\cdot+}$ in ILs, absorption spectra were recorded. Fig.4.7. shows UV-Vis spectra of TTF and $TTF^{\cdot+}$ in selected ionic liquids and traditional solvents at room temperature (296 K). Fig. 4.7a displays typical absorption peaks of 2.7 – 3.9 mM TTF in all solvents at ca. 356 nm and ca. 447 nm in agreement with the published data [123]. A red shift was observed due to the decrease in polarity of media, notably in n-hexane. Dividing those spectra by the maxima absorptions at ca. 447 nm, normalized spectra were formed (Fig. 4.7b). The shapes of the spectra in ILs are virtually the same as the spectra in organic solvents which indicates the identical species of TTF in all solvents. The same behavior was observed for $TTF^{\cdot+}$ in all solvents. Fig. 4.7c, d show the UV-Vis and normalized spectra of 1.4 – 1.9 mM $TTF^{\cdot+}$ which are analogous in all solvents. Four absorption peaks are readily seen, which are attributed to $TTF^{\cdot+}$ including a very intense band at 433 nm, two peaks at 339 nm and 578 nm, and a shoulder at 402 nm

in conformity with the results in ref. [123,124]. No absorption peak of $(TTF^{\cdot+})_2$ dimer is observed.

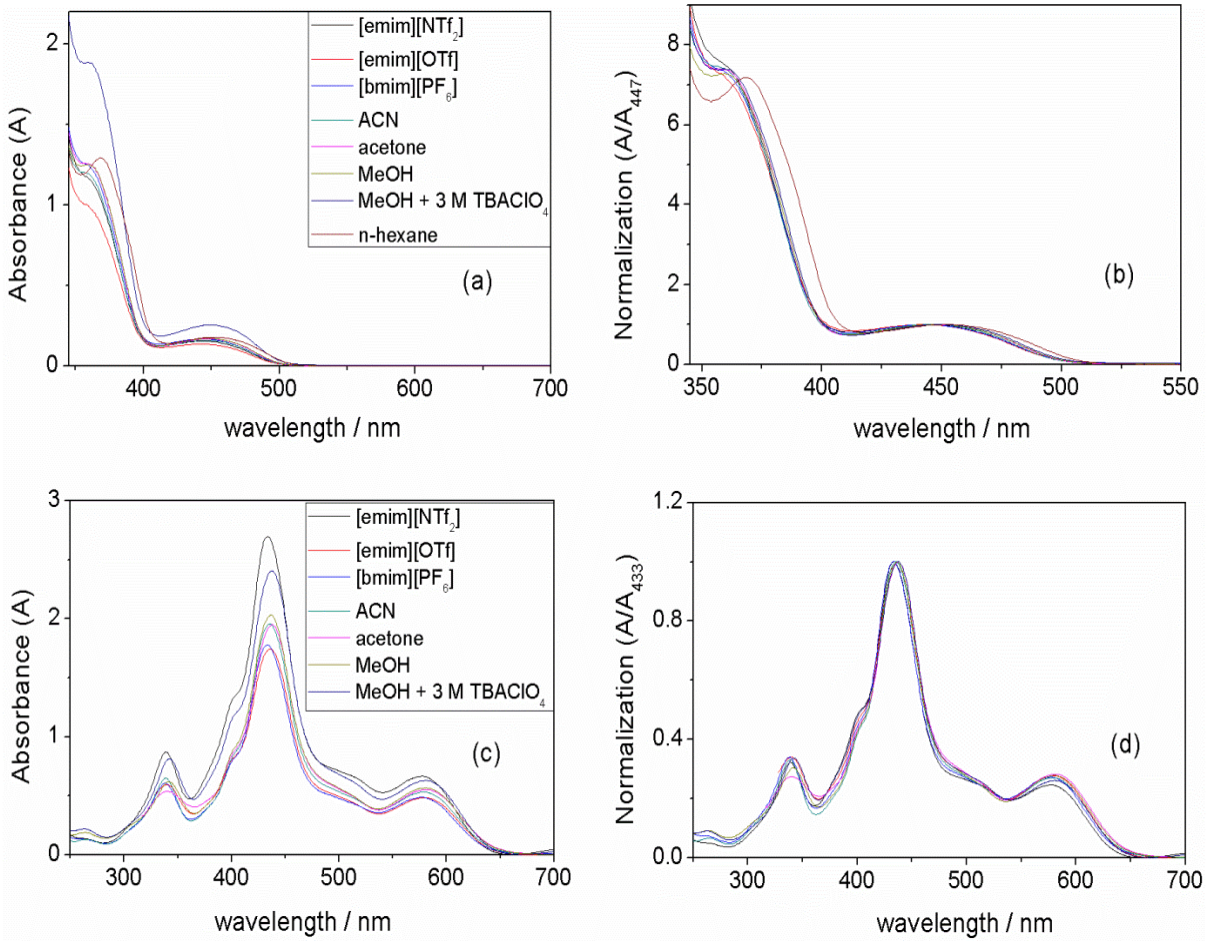

Figure 4.7. UV-Vis spectra of (a) TTF 2.7-3.9 mM and (b) $TTF^{\cdot+}$ 1.4 - 1.9 mM in various solvents; plots of normalized absorption curves (c), (d) respectively at room temperature (296 K).

- TEMPO was sublimated.
- TEMPOL was used as received.
- Tetrabutylammonium perchlorate ($TBAClO_4$) and $TBAPF_6$ was purchased from Sigma Aldrich. TTF was sublimated and $TTF^{\cdot+}ClO_4^-$ was synthesized according to Ref. [123]. $TBAPF_6$ was used as supporting electrolyte for measurements in ACN and sulfolane at a concentration of 0.1 M.

4.3. Sample preparation and measurements

Prior to use, the ILs were dried under high vacuum (2 - 6 × 10^{-5} Torr) for 24 hours at 323 K. The ILs were kept in round bottom flasks under argon in a desiccator. For TCNE, purified ILs were used while for other compounds, ILs were used from company without any further purification.

To prepare solutions in ionic liquids is more difficult than in organic solvents. Solutions were made in Schlenk tubes by dissolving appropriate amounts of the substances in ILs using magnetic stirring for 1-2 h under vacuum (exception for TEMPO and TEMPOL under argon due to high volatile pressure of the substances). It should be noted that only the values of weight instead of volumes of ILs is reliable due to their high viscosity. The volumes of ILs were calculated using their weights and the densities.

TCNE, TTF, $TTFClO_4$, TEMPO and TEMPOL are stable under the investigated conditions. The CVs of the substances in ILs were checked again after 3 hour increasing the temperature from 293 K to 343 K (interval 10 K). There was is no evaporation during electrochemical measurement recorded. For one concentration, three solutions was prepared and measured to get precise value of diffusion coefficient.

4.3.1. iR drop measurement

The theoretical resistances were calculated at different temperatures using the following equation [125]:

$$R = \frac{arctan\,(z/r)}{2\pi\kappa r} \tag{4.3}$$

With z is the distance between working electrode and reference electrode (z = 1 mm); r is the radius of working electrode (0,5 mm); κ is specific conductivity of ILs at the corresponding temperature taking from literature: [emim][NTf_2], [bmim][NTf_2], [bmim][OTf], [hmim][NTf_2], [bmim][BF_4], [bmim][PF_6]. The values of the theoretical resistances are shown in Table 4.3.

Table 4.3. Theoretical resistances of ILs calculated by using equation 4.3.

R_u / Ω						
T/ K	[emim][NTf_2]	[bmim][NTf_2]	[bmim][OTf]	[hmim][NTf_2]	[bmim][BF_4]	[bmim][PF_6]
293	455	1115	1528	2002	1293	3163
303	330	753	986	1298	798	1812
313	250	539	675	894	528	1125
323	196	403	485	646	369	744
333	159	314	362	485	270	519
343	131	252	280	377	205	377

At first the impedance measurement was carried out using a dummy cell (Fig. 4.8). R_u symbols for resistance of the solution between WE and RE. Z_f is polarization impedance and C_d is capacitance of double layer between WE and solution. Z_f and C_d were set to be 500 Ω and 1μF, respectively, in this test.

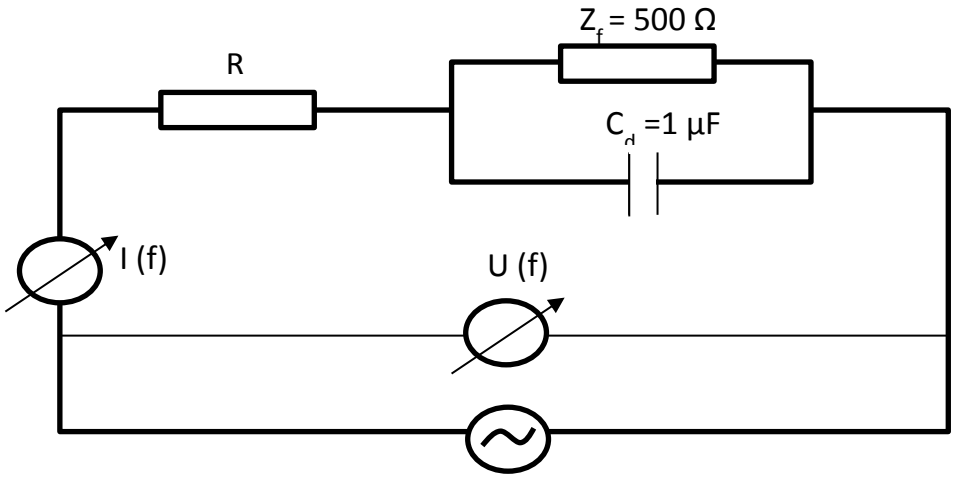

Figure 4.8. Schematic circuit of impedance measurement using dummy cell.

The impedance of capcitor is proportinal to the inverse frequency. At low frequency, the impedance is high and capacitor become open AC circuit. Therefore, the total impedance measued in this case is R_u + 500 Ω. In contrast, at high frequency, capacitor if short AC circuit which means that the resistance us very low and the current now flows through the capacitor, not through the resistance 500 Ω. In the other words, the impedance measured is equal to the value of R_u.

After testing on the dummy cell, the impedance measurement was done on the temperature-controlled milimeter working electrode cell (Fig. 4.9). The impedance (Z = U/I) was then ploted vs. frequency in a logarithm scale (Bode plot). Bode plots of selected ILs at 293 K and 343 K were shown in Figs. 4.10-4.12. From those plots, the resistances of ILs are readily determined (Table 4.4.).

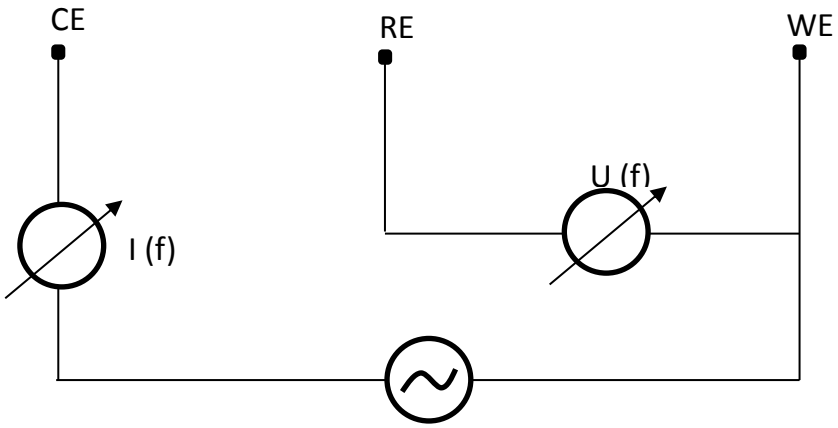

Figure 4.9. Schematic circuit of impedance measurement for ionic liquids using the milimeter-working electrode temperature controlled electrochemical cell.

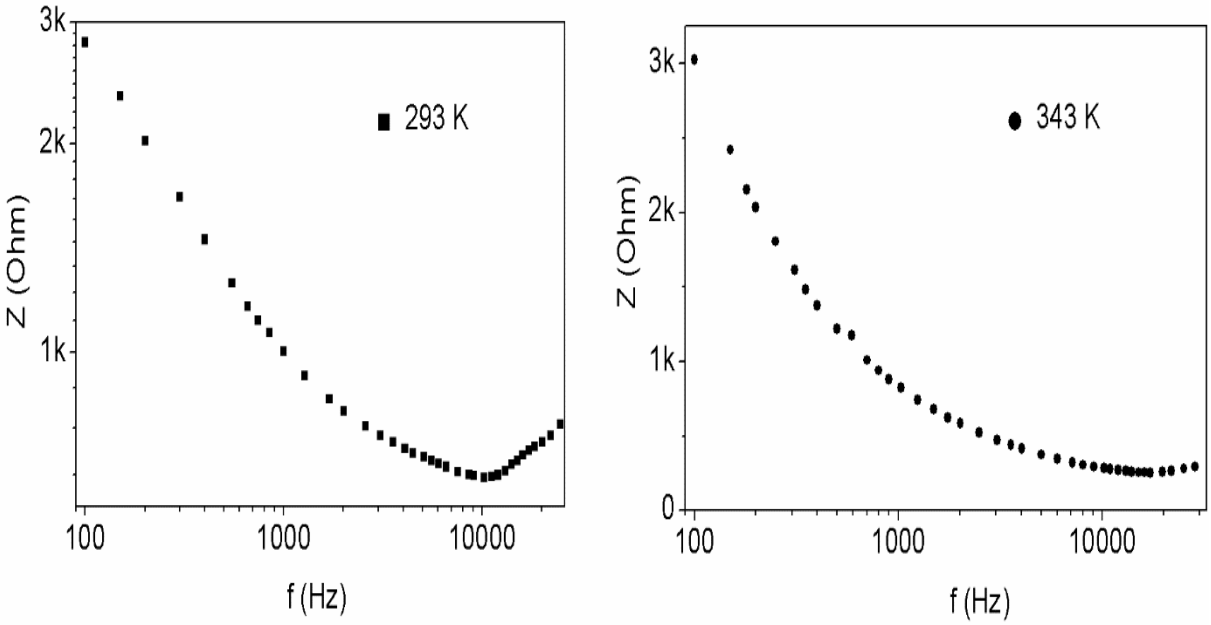

Figure 4.10. Bode plots of [emim][NTF_2] at 293 K and 343 K.

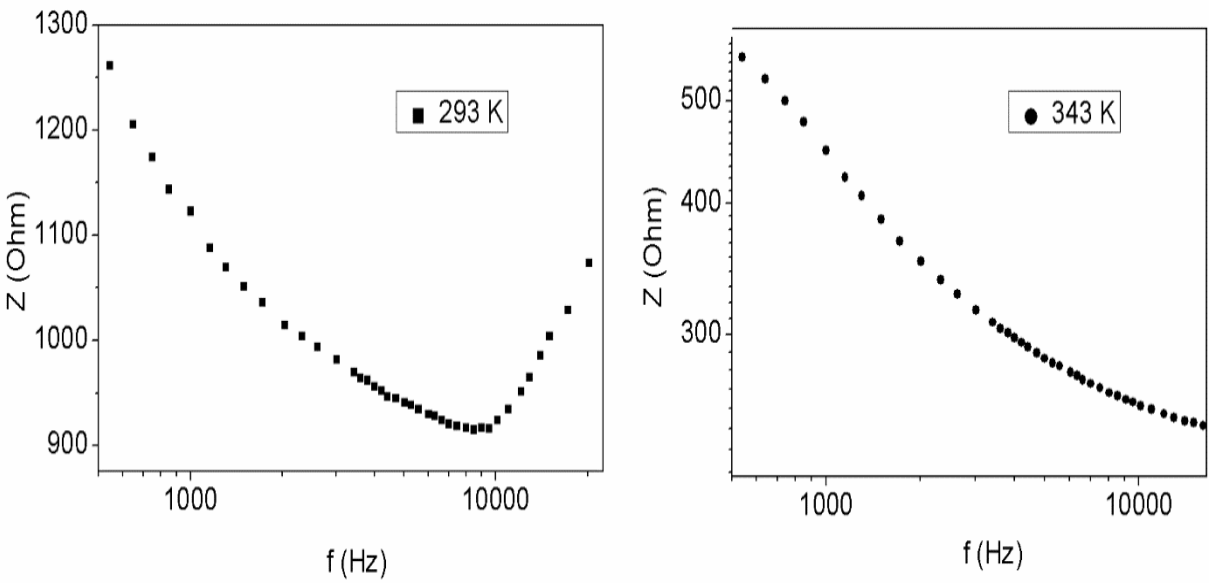

Figure 4.11. Bode plots of [bmim][OTf] at 293 K and 343 K.

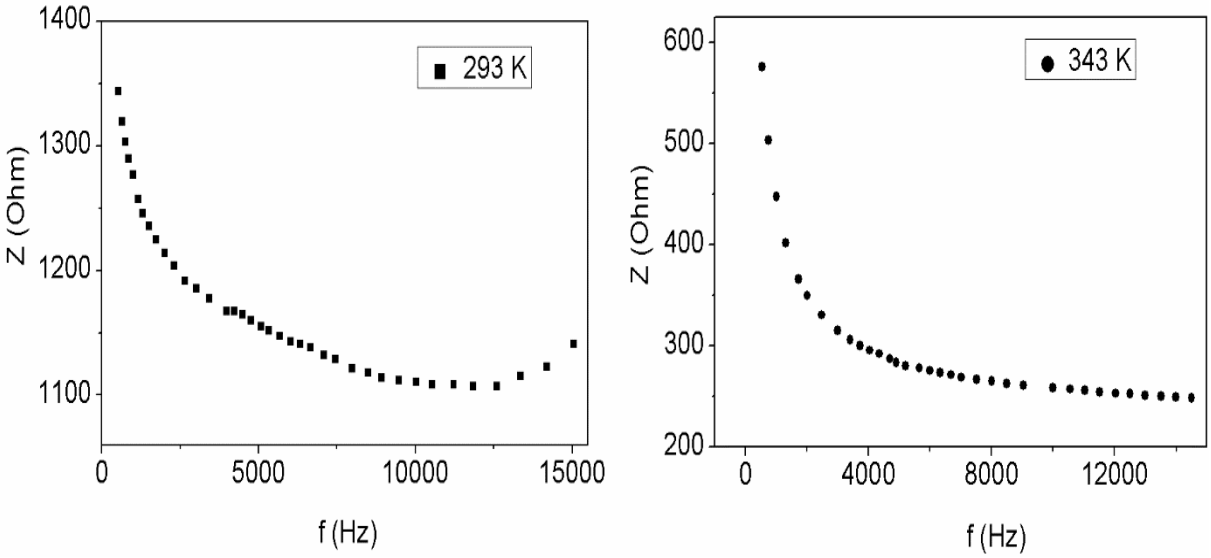

Figure 4.12. Bode plots of [bmim][BF_4] at 293 K and 343 K.

Table 4.4. Resistances of ILs measured by impedance methods.

R_u / Ω							
T/K	[emim][NTf_2]	[bmim][NTf_2]	[bmim][OTf]	[hmim][NTf_2]	[bmim][BF_4]	[bmim][PF_6]	[emim][OTf]
293	660	1220	940	2200	1300	2850	596
303	520	797	708	1680	770	1900	490
313	416	650	510	1280	540	1158	437
323	349	570	390	990	400	900	384
333	293	550	306	770	310	715	352
343	258	500	246	623	250	579	285

4.3.2. Electrochemical measurement

Electrochemical experiments in ILs were carried out over a temperature range from 293 to 343 K by 10 K intervals with an accuracy of 1 K. Measurements of TTF and $TTF^{\cdot+}ClO_4^-$ in sulfolane were performed at temperature higher than 303 K due to the high melting point of sulfolane. A slight stream of argon was purged through the electrochemical cell during experiments. No volatilization of all the compounds was observed.

Working electrode plays an important role especially for diffusion measurements. Defects in the working electrode can cause the deviation in diffusion mechanism leading to an error in diffusion coefficient (Fig. 4.13). Therefore, treating the surface of working electrode in a proper way becomes more important in measuring precise value of diffusion coefficients and then electron transfer rate constants.

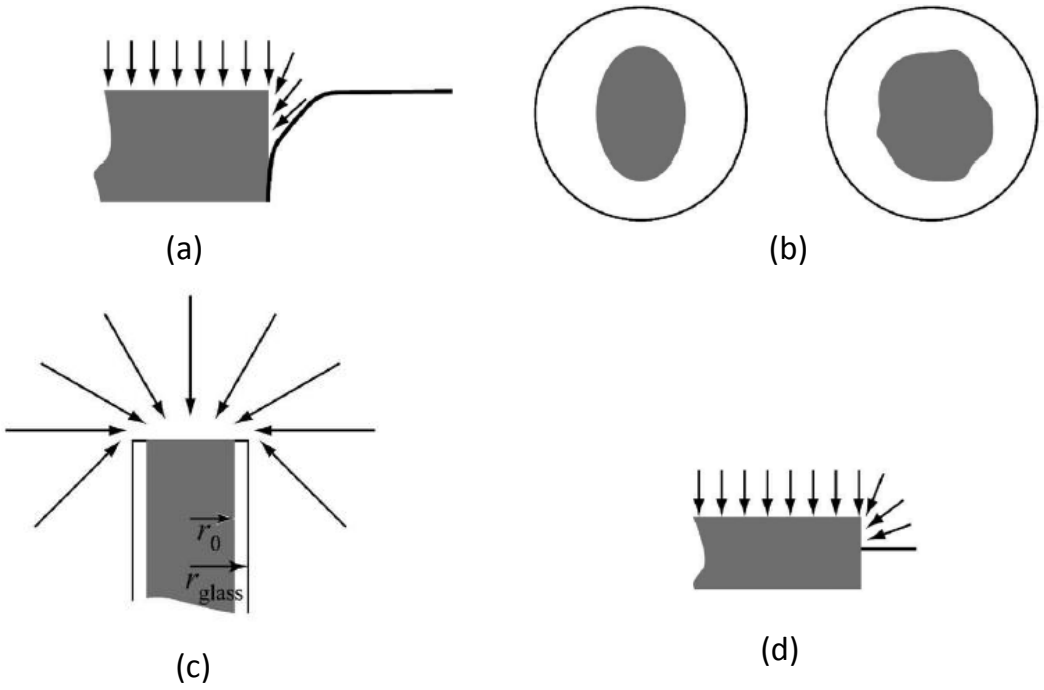

Figure 4.13. Defects of working electrode: (a) poor –sealed electrode (b) asymmetric electrode (c) thin insulator microelectrode (d) electrode jutting out from insulator. Adapted from Ref.[48].

Before measurement, working electrodes were checked and polished carefully (Fig 4.14). For microelectrode, the ratio r_{glass}/a (r_{glass} is the radius of the insulator) was chosen to be higher than 100 (Fig.4.14b) [48].

4.3.2.1. Cyclic voltammetry at macro-electrodes

Before each measurement the working electrode was polished using diamond paste (IDA Industrie-Diamant-Aachen, Germany) in steps of decreasing particle size 15, 6, 3, 1 and 0.25 (in µm units) on polishing ads, and then the polished working electrode was rinsed with distilled water (Fig. 4.15a,b).

A 0.3 mL of solution was transferred into the cell under argon. The thermometer probe was inserted into the cell. Cyclic voltammograms were recorded at scan rates (100, 200, 300, 400, 500, 700, 900, 1100 mV s^{-1}) in order to avoid any aggregation of products on surface of the electrode due to the slow movement in highly viscous ionic liquids. Due to the high viscosity of ionic liquids, leading to

the slower movement of the species, larger amount of products are built up on the surface of electrode at lower scan rates.

More reasons for choosing scan rates (100, 200, 300, 400, 500, 700, 900, 1100 mV s^{-1}) for CV in ILs are listed below.

- Non-Faradaic current is proportional to double layer capacitance and scan rate. Faradaic current is proportional to the square root of scan rate. Obviously, higher scan rates cause higher increase in non-Faradaic currents in comparison to Faradaic current. Moreover, ILs have high resistance leading to the assumption that using slow scan rate is more reliable than higher scan rates. However, from the baseline of the forward scan [51] it is readily seen that CV of TTF and $TTF^{\cdot+}$ in the investigated ILs did not present high double-layer charging currents in the range of scan rates 100-1100 mV/s
- The concentration of TTF and $TTF^{\cdot+}$ were higher than 10mM. Thus, the charging current is negligible compared with the Faradaic current. However, for TTF in highly viscous ILs and for $TTF^{\cdot+}$, the CV at low scan rates gave higher charging current in comparison to the Faradaic current. This is explained by the small scale of observed Faradaic current. This is readily seen in the two examples of scan rate 20 mV/s and 500 mV/s.
- The picture of double layer is different in the case of ionic liquids. Multiple layer structure has been proposed. It means that the charging current increase with measuring time.
- CVs of TTF and $TTF^{\cdot+}$ in ILs was also scanned at scan rates less than 100 mV/s (10, 20, 30, 40, 50, 70, 90, 100) giving the same value of diffusion coefficient (within the experimental error) as determined from higher scan rates (100-1100). For instance, D of TTF in [bmim][NTf_2] at same temperature is (2.9 ± 0.3) $\times 10^{-7}$ (10 – 100 mV/s) while (3.0 ± 0.3) $\times 10^{-7}$ (100-1100 mV/s). For $TTF^{\cdot+}$ in [emim][NTf_2] the value is (2.4 ± 0.3) $\times$ 10^{-7} (10 – 100 mV/s) and (2.7 ± 0.3) $\times 10^{-7}$ (100-1100 mV/s).

The CV only registered for the first circle and the solution was shaken to renew the working electrode surface. The temperature was increased from 293 to 343 K

at 10K intervals with the accuracy is 1K. A slight stream of argon was purged through the cell during experiment.

Because ILs are very viscous, the concentration of substances is in the range of 10-20 mM to get the good signal/noise ratio.

(a) (b)

Figure 4.14. (a) Millimeter working electrode with PVC (blue) and Teflon (white) insulator; (b) micrometer working electrode.

(a) (b) (c)

Figure 4.15. Polishing machine (a), diamond pastes and polishing pads for millimeter working electrode (b) and alumina and special holder for micrometer working electrode (c).

4.3.2.2. Steady - state voltammetry at microdisc electrodes

Prior to each measurement, the working electrode was polished with cloth pads using alumina suspensions, with decreasing size 5 µm (Buehler), 1 µm (Alfa Aesar) and 0.25 µm (Schmitz metallographie GmbH) and then sonicated in deionised water (Fig. 4.15a, c).

Scan rates were chosen to reach steady- state according to Eq. 2.27 and were different depending on viscosity of solvents, for example 0.5 - 2 mV s^{-1} for ILs, while for organic solvents 10 mV s^{-1} at room temperature was used. The measurements at several scan rates were done to confirm a true steady state, for instance the SSV measurement of TTF in [emim][NTf_2] were carried out at 1 mV/s, 0.8 mV/s and 0. 6 mV/s at 293 K and the same plateau was obtained regardless scan rate.

5. Results and discussion

All my life through, the new sights of
nature made me rejoice like a child.
Marie Curie

Diffusion coefficients of the compounds in ILs were measured by using cyclic voltammetry. In addition, steady state voltammetry was used for comparison in the cases of TTF and TEMPO. The values of D were then analysed under the effects of measuring method, concentration, temperature, viscosity and nature of the substances. The mechanism of diffusion was taken into account using the classical and hole theory. The second part of this chapter is results of heterogeneous electron transfer rate constant k_{het}. From experimental values of k_{het}, activation energies were determined and analysed using Marcus theory.

5.1.Diffusion coefficients in ILs

5.1.1. Dependence on concentration

A non-linear relationship between the concentration and diffusion coefficient is reported in literature for Fc in ILs [44,63], which has been attributed to the inaccurate values of concentration [8]. To the best of our knowledge, there are two methods to check the reliability of the concentration of solute in ionic liquids. The first is using chronoamperometry which gives concentrations and diffusion coefficients by fitting the chronoamperomogram using the Shoup-Szabo equation. Recently Compton et al. reported on large deviations of concentration as well as diffusion coefficients on the measuring time [49]. Therefore, choosing the optimal transient time to get reliable diffusion coefficients and concentrations is still a question when using this method. The second method was suggested by Vorotyntsev et al. [8] UV-Vis spectroscopy and CV were used at the same time to get precise values of diffusion coefficients.

The normalized UV-Vis spectra (Fig. 4.7) of TTF and $TTF^{\cdot+}$ in ionic liquids are very similar to those in organic solvents. Thus, the nature of the absorbing

species is unchanged in all solvents lead us to the conclusion that UV–Vis can be used to check the reliable concentration of TTF and $TTF^{\cdot+}$ in ionic liquids. CV was carried out in parallel for the corresponding concentrations. Indeed a good linear relationship between maxima absorptions at 447 nm (A_{447}, for TTF), 578 nm (A_{578}, for $TTF^{\cdot+}$) and the corresponding concentrations in Figs. 5.1a and 5.2b showed that concentrations determined by weight are reliable. In addition, the plot of oxidation peak current I_{pa} for TTF and anodic peak current I_{pc} for $TTF^{\cdot+}$ against concentration in Figs. 5.1b and 5.2b also give good straight lines and illustrate the independence of diffusion coefficient on concentration. Thus, it is possible to determine the diffusion coefficient using a single concentration.

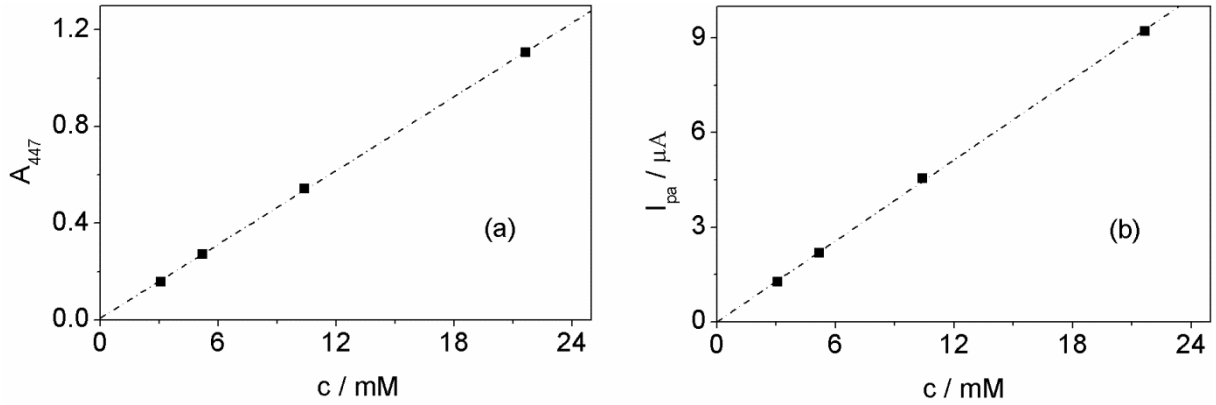

Figure 5.1. Plots of (a) maxima absorption at 447 nm (A_{447})and (b) oxidation peak current (I_{pa}) vs. concentration of TTF in [emim][NTf_2] at 100 mV s^{-1} at 296 K.

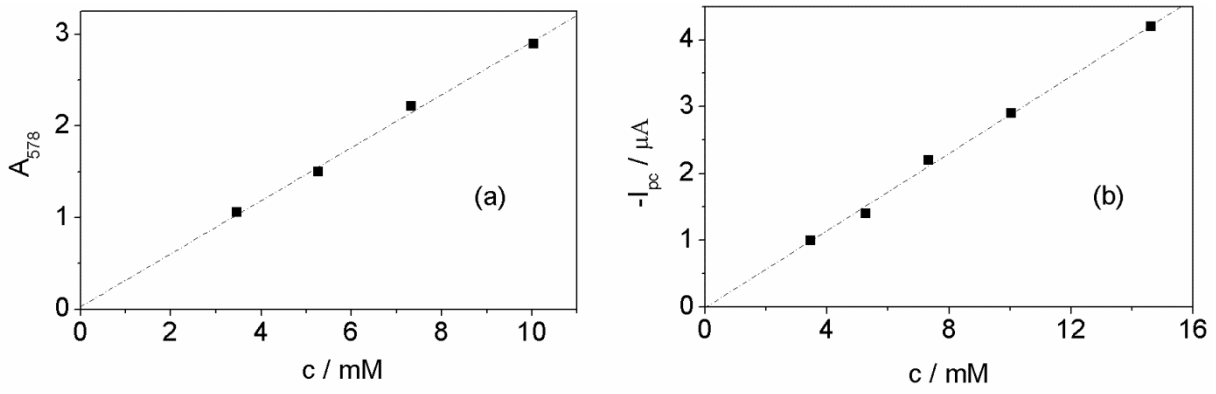

Figure 5.2. Plots of (a) maxima absorption at 578 nm (A_{578})and (b) reduction peak current (I_{pc}) vs. concentration of $TTF^{\cdot+}$ in [emim][NTf_2] at 100 mV s^{-1} at 296 K.

5.1.2. Diffusion coefficients determined from cyclic voltammetry and steady-state voltammetry

5.1.2.3. Cyclic voltammetry

The values of diffusion coefficients of all investigated substances in ILs were first determined using cyclic voltammetry. Figs. 5.3a – 5.10a show cyclic voltammograms of TCNE, TTF, TEMPO, TEMPOL in selected ILs at 293 K at different scan rates over the range of 100-1100 mV s^{-1}. For TCNE, the scanning potential, starting at 0.7 V, was swept towards a negative potential. In contrast, for TTF, TEMPO and TEMPOL, the potential was scanned toward positive direction starting from 0 to 0.7 for TTF, from 0.3 to 1.0 for TEMPO and TEMPOL. There was no absorption peak observed for all compounds in ILs.

Before doing any further calculations, it is necessary to correct all the cyclic voltammograms in each ionic liquid using the uncompensated resistances, obtained by separate impedance measurements. The highest resistance (2850 Ω) was recorded for [bmim][PF_6] and the lowest (500 Ω) for [emim][NTf_2] at 293 K (Table 4.4). The values are comparable to those from theoretical calculations using the distance between working and reference electrode and the conductivity of the solvents (Table 4.3).

Cyclic voltammograms of TCNE in selected ILs at 293 K

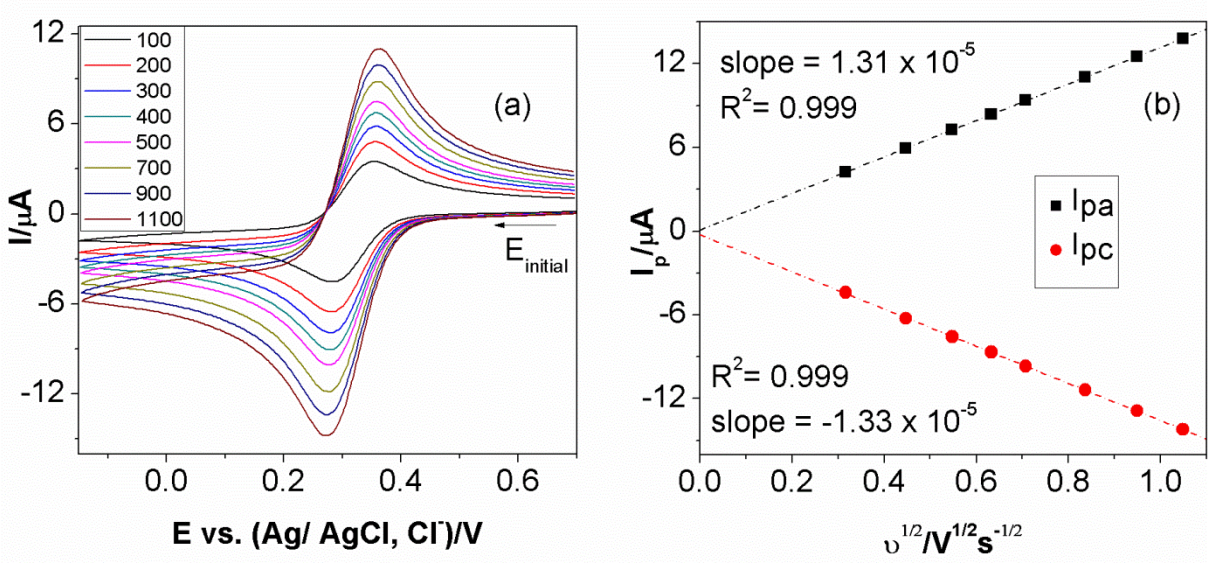

Figure 5.3. (a) CVs of TCNE 26.4 mM at 0.5 mm radius GC in [bmim][BF_4] at 293 K at different scan rates (100 - 1100 mV/s); (b) plots of corresponding I_{pa} and I_{pc} vs. $v^{1/2}$.

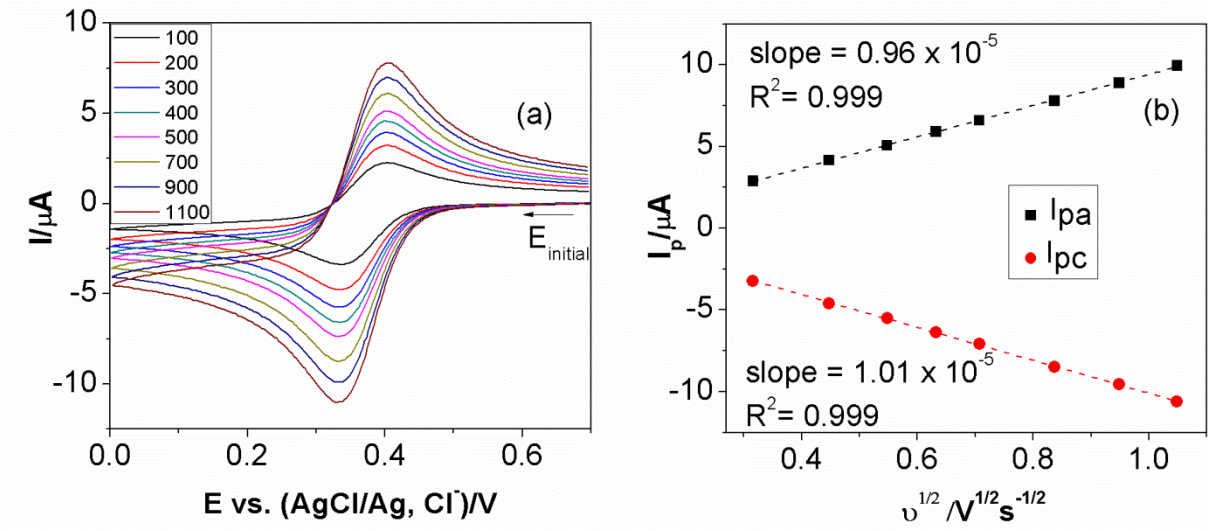

Figure 5.4. (a) CVs of TCNE 14.9 mM at 0.5 mm radius GC in [bmim][NTf_2] at 293 K at different scan rates (100 - 1100 mV/s); (b) plots of corresponding I_{pa} and I_{pc} vs. $v^{1/2}$.

Cyclic voltammograms of TTF in selected ILs at 293 K

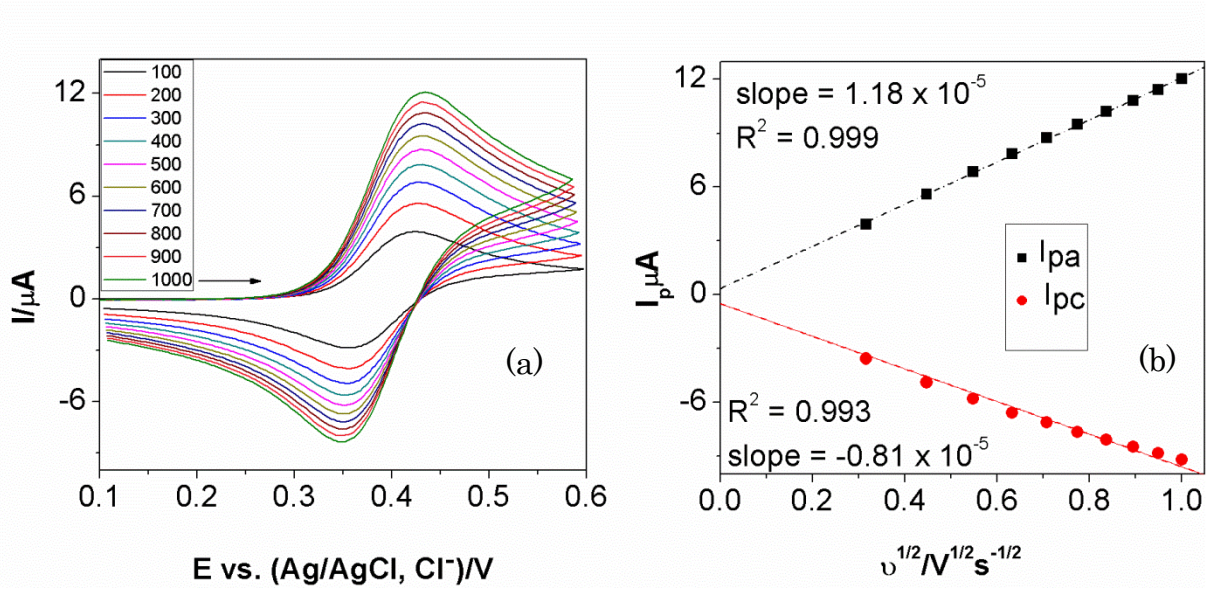

Figure 5.5. (a) CVs of TTF 13.3 mM at 0.5 mm radius GC in [hmim][NTf_2] at 293 K at different scan rates (100 - 1100 mV/s); (b) plots of corresponding I_{pa} and I_{pc} vs. $v^{1/2}$.

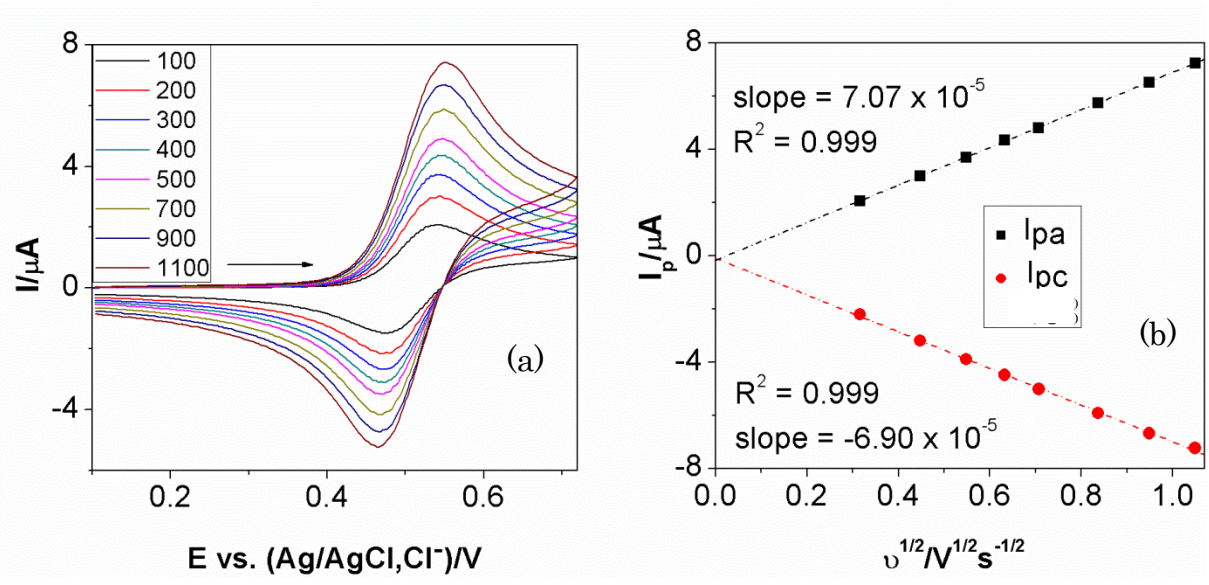

Figure 5.6. (a) CVs of TTF 9.94 mM at 0.5 mm radius GC in [bmim][OTf] at 293 K at different scan rates (100 - 1100 mV/s); (b) plots of corresponding I_{pa} and I_{pc} vs. $v^{1/2}$.

Cyclic voltammograms of TEMPO in selected ILs at 293 K

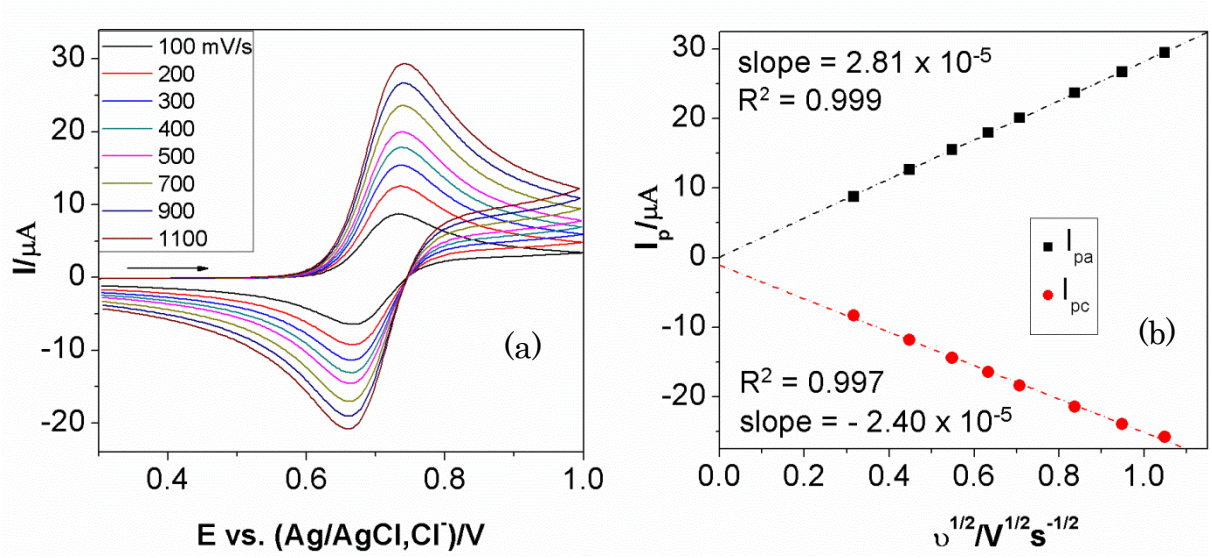

Figure 5.7. (a) CVs of TEMPO 21.7 mM at 0.5 mm radius GC in [emim][NTf_2] at 293 K at different scan rates (100 - 1100 mV/s); (b) plots of corresponding I_{pa} and I_{pc} vs. $v^{1/2}$.

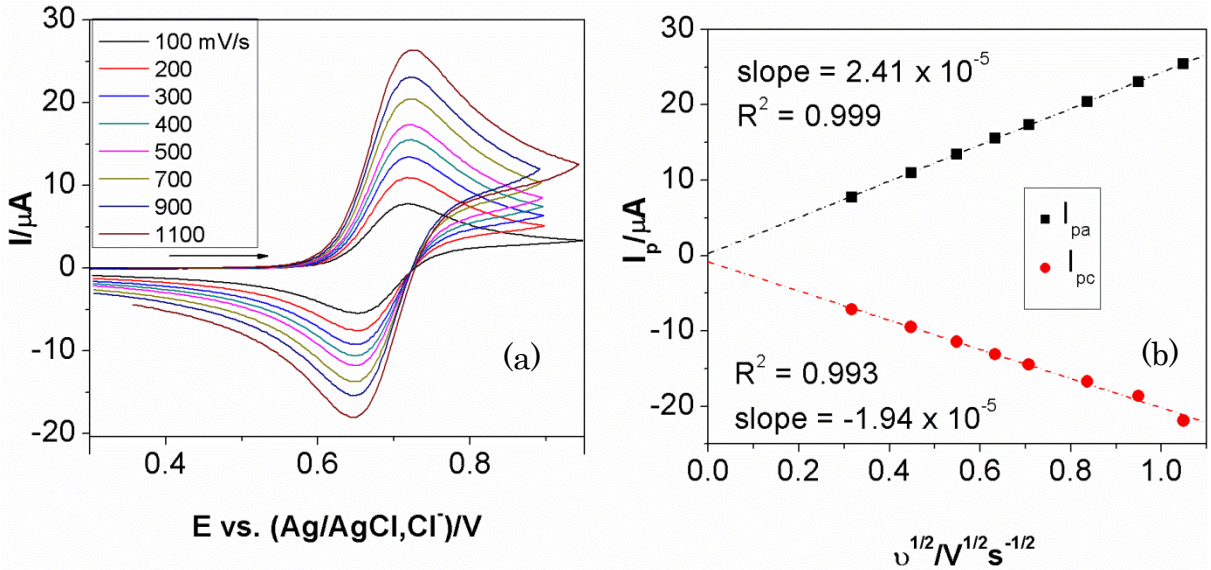

Figure 5.8. (a) CVs of TEMPO 25.4 mM at 0.5 mm radius GC in [emim][OTf] at 293 K at different scan rates (100 - 1100 mV/s); (b) plots of corresponding I_{pa} and I_{pc} vs. $v^{1/2}$.

Cyclic voltammograms of TEMPOL in selected ILs at 293 K

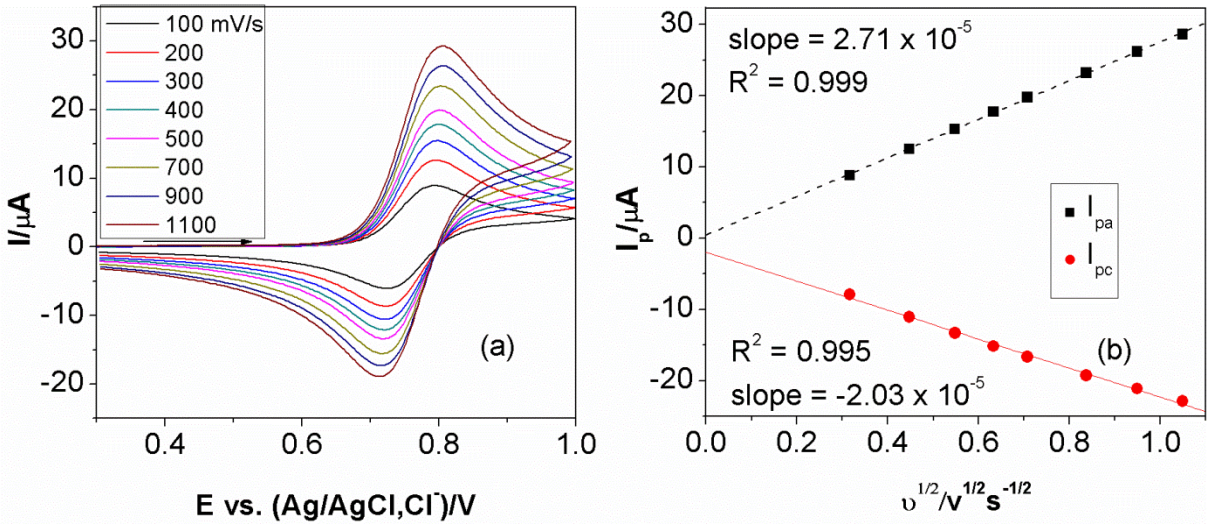

Figure 5.9. (a) CVs of TEMPOL 27.7 mM at 0.5 mm radius GC in [emim][NTf_2] at 293 K at different scan rates (100 - 1100 mV/s); (b) plots of corresponding I_{pa} and I_{pc} vs. $v^{1/2}$.

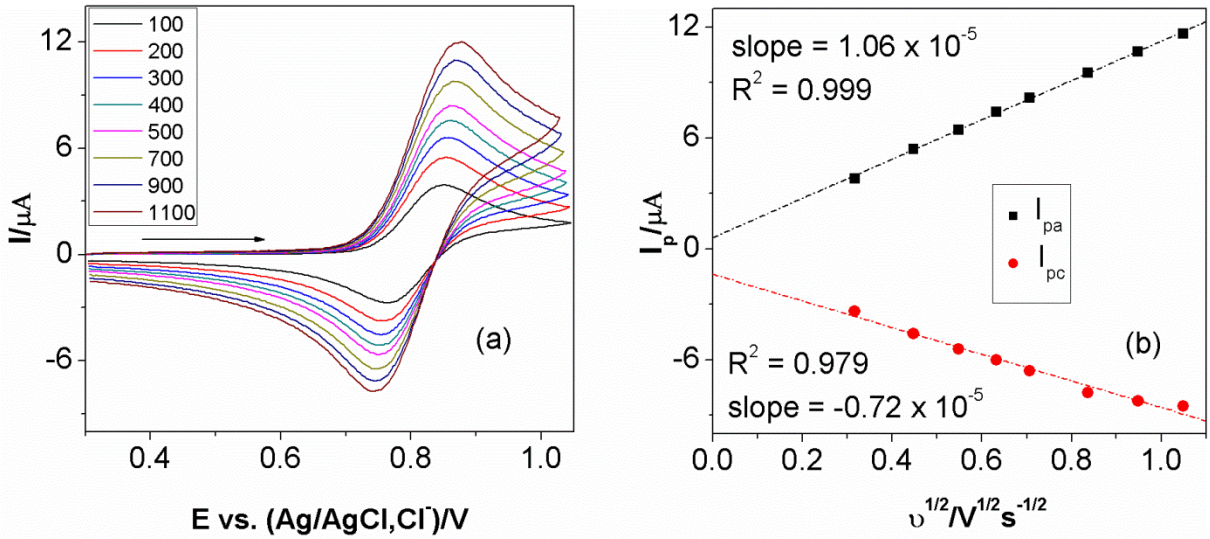

Figure 5.10. (a) CVs of TEMPOL 23.6 mM at 0.5 mm radius GC in [bmim][PF_6] at 293 K at different scan rates (100 - 1100 mV/s); (b) plots of corresponding I_{pa} and I_{pc} vs. $v^{1/2}$.

The reversibility of redox process of each substance in ionic liquids was then analysed in terms of the peak potential separation $\Delta E_p = E_{p_a} - E_{p_c}$, the half-peak potential difference $\Delta E_{p_a/2} = E_{p_a} - E_{p_a/2}$, and the ratio of anodic to cathodic peak currents I_{p_a} / I_{p_c} where E_{p_a}, E_{p_c} and I_{p_a}, I_{p_c} are potential and current peaks for the oxidation and the reduction, respectively; $E_{p/2}$ the potential equivalent to the half-peak current. ΔE_p (293 K), calculated using the Ohmic drop correction, was found to be 60-70 mV for low-viscous ILs, such as [emim][NTf_2], [emim][OTf], and [bmim][OTf], and 70-90 mV for high-viscous ILs, e.g., [hmim][NTf_2], and [bmim][PF_6]. The above results were similar for TTF and TCNE in ILs. In the case of TEMPO and TEMPOL, the potential differences were higher, especially in high-viscous ILs. For example, ΔE_p was in the range of 80-130 mV. In addition, the $\Delta E_{p_a/2}$ for all compounds in ILs were about 56-75 mV at 293 K. Such large values of ΔE_p and $\Delta E_{p_a/2}$ may originate from a slower increase in rate constant of a sluggish electron-transfer compared with the increase in D [47]. Figs. 5.3b - 5.10b present good linear relations between I_{pa} and $\nu^{1/2}$ (for TTF, TEMPO and TEMPOL, between I_{pc} and $\nu^{1/2}$ (for TCNE), intersecting the origin. This indicates that the processes are planar diffusion-controlled. The same behaviour was found for the other ILs. From the slopes of lines such as those in Figs. 5.3b -5.10b, the diffusion coefficients in the given ILs [50,51] were determined by the Randles–Sevčik equation (Eq. 2.25) for a reversible redox process.

5.1.2.4. Steady-state voltammetry

In order to check the reliability of the diffusion coefficients obtained from CV, steady-state voltammetry (SSV) was applied for TTF and TEMPO in ILs. To achieve true steady-state currents, optimal scan rates were determined following the inequality in Eq. 2.27, corresponding to each IL and each temperature. Indeed, steady-state could be observed at scan rate of 0.8 mV s^{-1} for TTF in [emim][NTf_2], and 0.3 mV s^{-1} in [hmim][NTf_2] at 293 K. Figs. 5.11 - 5.14 illustrate steady-state voltammograms of TTF and TEMPO in selected ILs. The small panel in each figure indicates that steady-state condition is achieved. From the limiting current, diffusion coefficients were calculated using Eq. 2.28.

Steady-state voltammograms of TTF in selected ILs

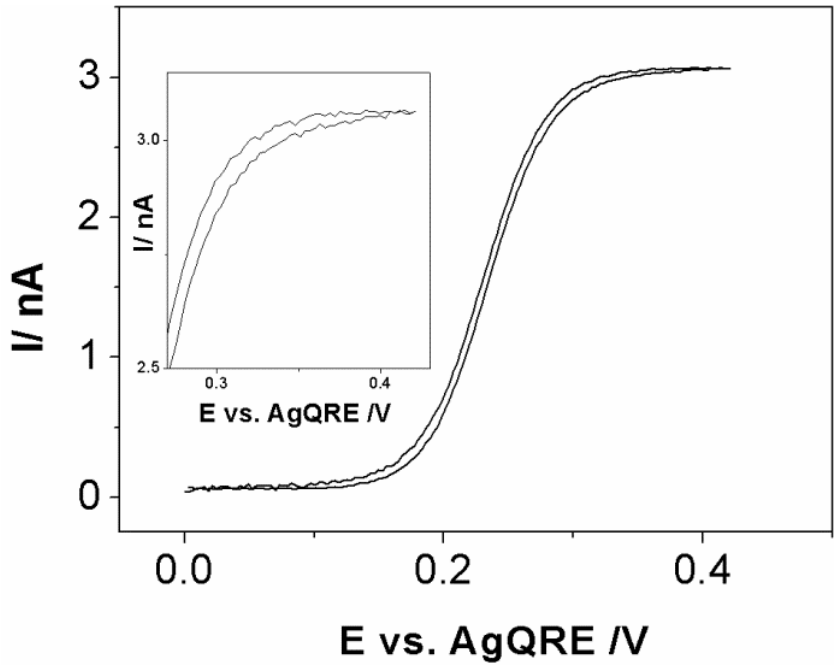

Figure 5.11. Steady-state voltammograms of 8.0 mM TTF in [bmim][OTf] at a 5.5 μm radius Pt electrode at 293 K at scan rate of 0.25 mV s^{-1}.

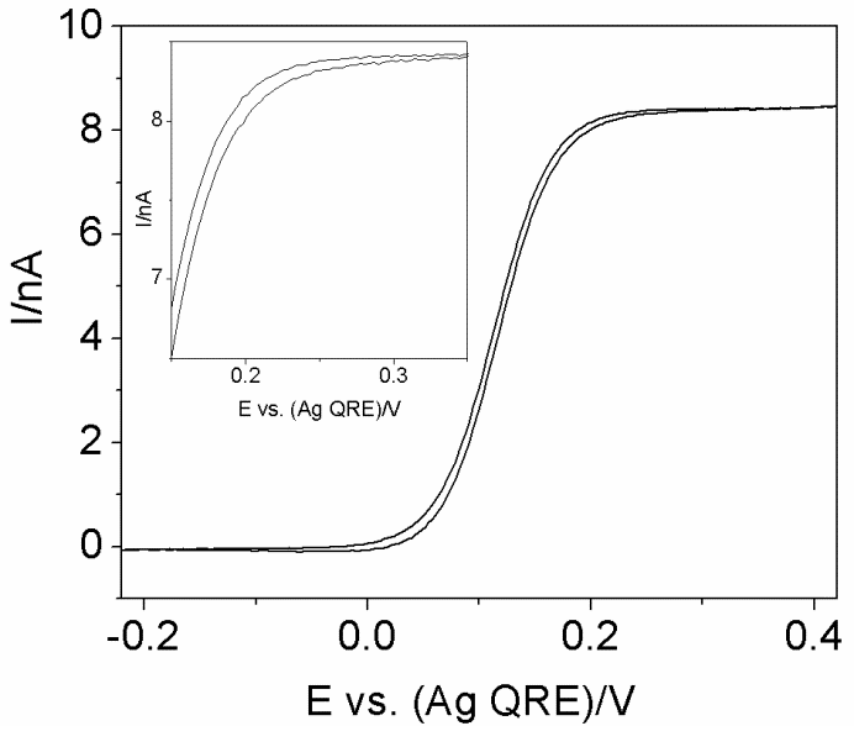

Figure 5.12. Steady-state voltammograms of 8.2 mM TTF in [emim][NTf_2] at a 5.5 μm radius Pt electrode at 303 K at scan rate of 1.5 mV s^{-1};

Steady-state voltammograms of TEMPO in selected ILs

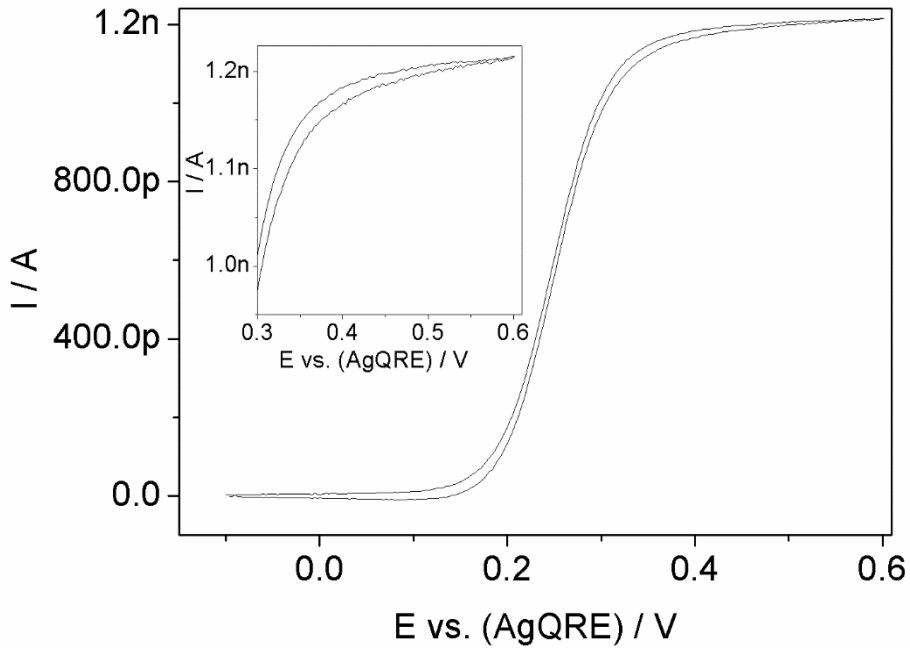

Figure 5.13. Steady-state voltammograms of 20.6 mM TEMPO in [hmim][NTf_2] at a 5.5 μm radius Pt electrode at 303 K at scan rate of 1 mV s^{-1};

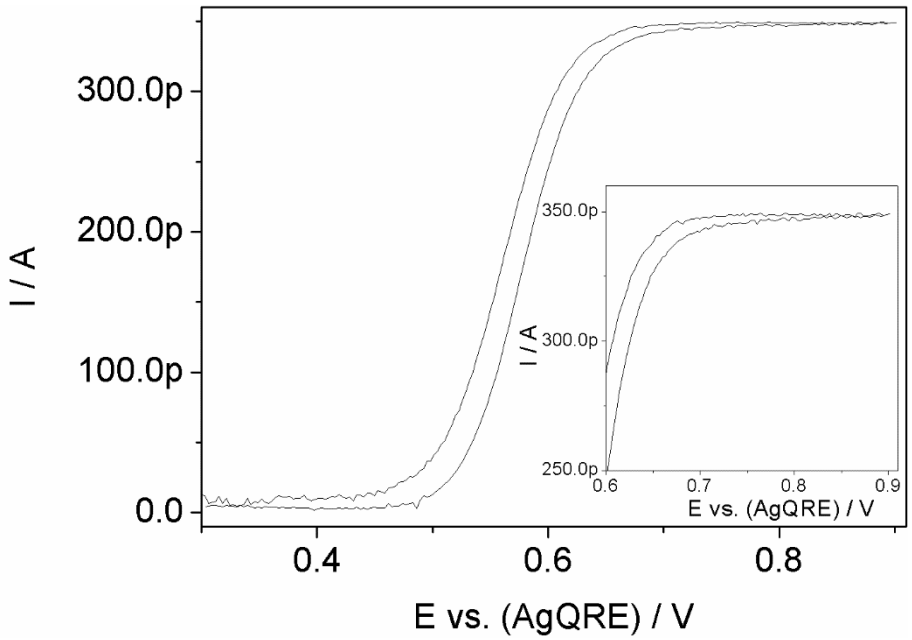

Figure 5.14. Steady-state voltammograms of 21.5 mM TEMPO in [bmim][PF_6] at a 5.5 μm radius Pt electrode at 293 K at scan rate of 0.2 mV s^{-1}.

The values of diffusion coefficients of TTF and TEMPO measured from CV and SSV are listed in Table 5.1.

For TTF in ILs, it is obvious that diffusion coefficients determined from SSV are systematically larger than those measured by CV by about a factor of 1.1 - 1.3, which can be attributed to convection. For the same reason, values of diffusion coefficients of $TTF^{\cdot+}$ (discussed later in section 5.1.4) measured by SSV in the ionic liquids are larger than those are from CV. Larger values of diffusion coefficients using steady-state methods in comparison to those for CV have also been reported in literature [15].

In contrast, convection seems not to be the case for the uncharged TEMPO molecules. The value of D from SSV is comparable to those from CV (Table 5.1), and it becomes smaller at higher temperature (Table. 5.3). One explanation for the lower D of TEMPO using SSV is the slight volatilization of TEMPO at high temperature with long measuring time.

Table 5. 1. Diffusion coefficients of TTF and TEMPO in ILs obtained using cyclic voltammetry (CV) as well as steady-state voltammetry (SSV) at 293 K.

ILs	η / cP	TTF		TEMPO	
		CV	SSV	CV	SSV
[emim][NTf_2]	38[a]	3.1±0.4	3.6±0.2	3.7±0.4	3.5±0.2
[emim][OTf]	48[b]	2.3±0.2	2.5±0.1		
[bmim][NTf_2]	62 [a]	1.8±0.2	2.3±0.1	2.5±0.3	2.4±0.1
[bmim][OTf]	89[c]	1.3±0.2	1.69±0.09	-	-
[hmim][NTf_2]	87 [a]	1.6±0.2	1.9±0.1	1.3±0.2	1.86±0.09
[bmim][PF_6]	374 [a]	-	-	0.47±0.06	0.56±0.03

[a]: from our measurements

[b, c]: from ref. [126] and [84] respectively

5.1.3. Dependence of D on Temperature

Figs. 5.15 -5.22 show cyclic voltammograms of TCNE, TTF, TEMPO, TEMPOL in selected ILs recorded over a temperature range of 293 – 343 K at 500 mV s^{-1} scan

rate. The ratios of I_{p_a}/I_{p_c} are close to 1 in all cases. Plots of I_p vs. $v^{1/2}$ show the transients rising with increasing temperature. Diffusion coefficients calculated from Eq. 2.25 present a trend of increasing D corresponding to an increase in temperatures due to the decrease in viscosity.

Cyclic voltammograms of TCNE at different temperatures in selected ILs

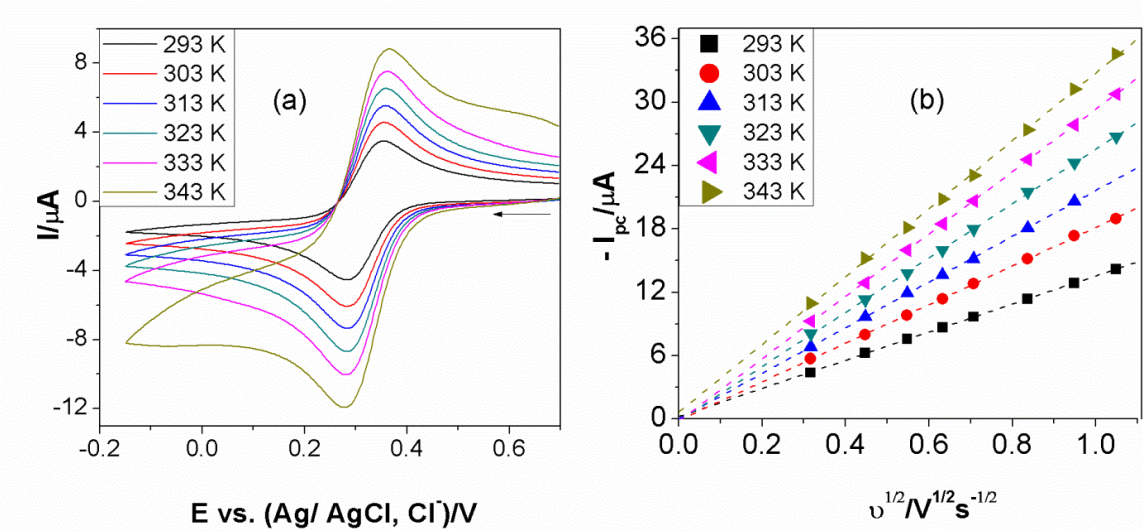

Figure 5.15. (a) CVs of TTF 26.4 mM in [bmim][BF4] obtained at 0.5 mm radius GC over the range 293-343 K at 100 mV s-1; (b) plots of corresponding Ipc vs. $v^{1/2}$.

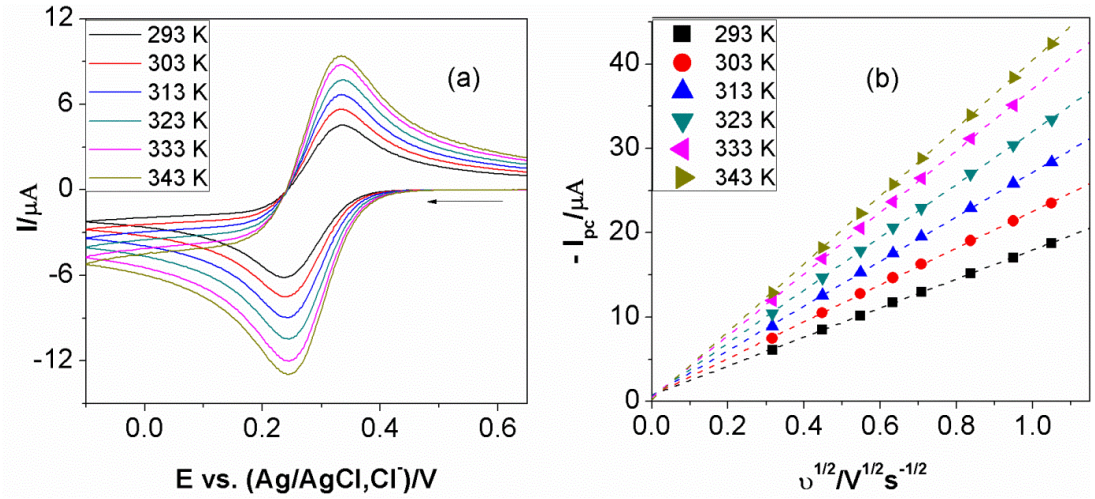

Figure 5.16. (a) CVs of TTF 20.1 mM in [hmim][NTf_2] obtained at 0.5 mm radius GC over the range 293-343 K at 100 mV s^{-1}; (b) plots of corresponding I_{pc} vs. $v^{1/2}$.

Cyclic voltammograms of TTF at different temperatures in selected ILs

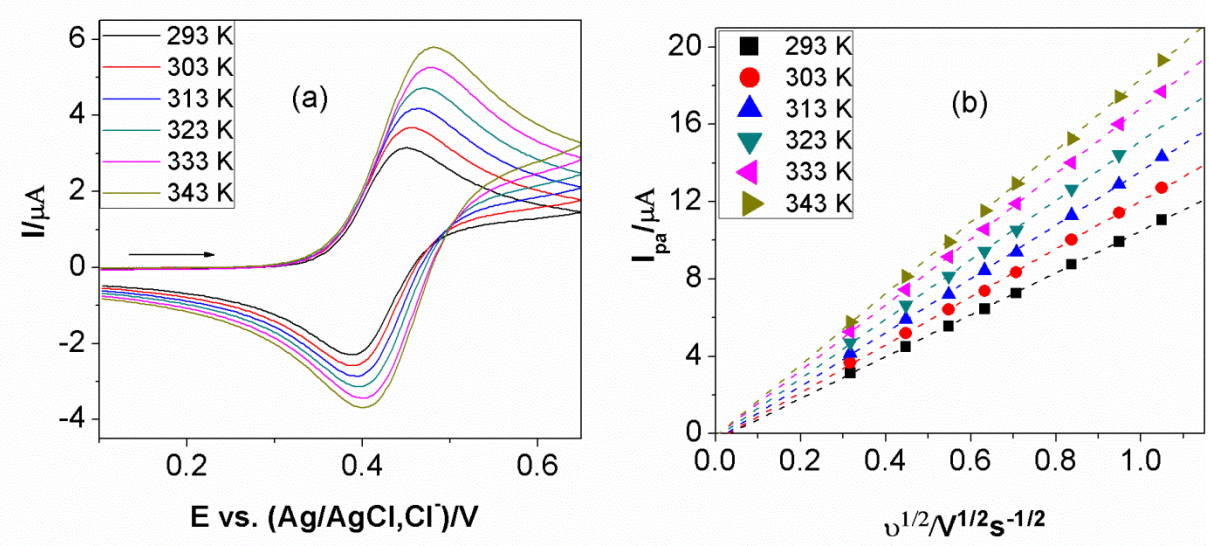

Figure 5.17. (a) CVs of TTF 9.04 mM in [emim][NTf_2] obtained at 0.5 mm radius GC over the range 293-343 K at 100 mV s^{-1}; (b) plots of corresponding I_{pc} vs. $v^{1/2}$.

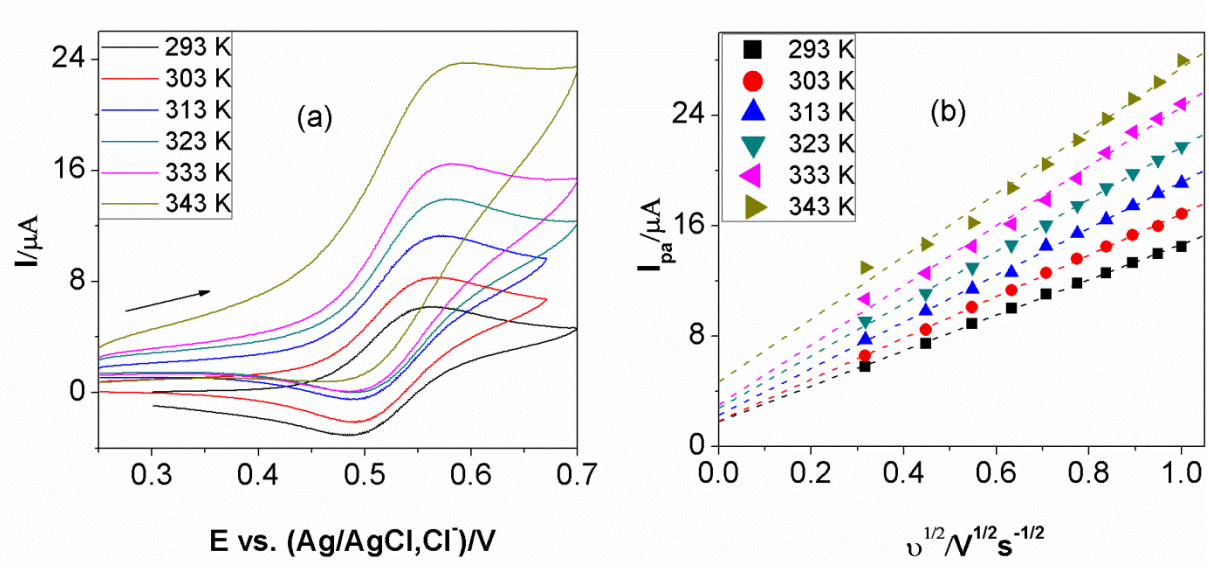

Figure 5.18. (a) CVs of TTF 9.4 mM in [emim][dca] obtained at 0.5 mm radius GC over the range 293-343 K at 100 mV s^{-1}; (b) plots of corresponding I_{pc} vs. $v^{1/2}$.

Cyclic voltammograms of TEMPO at different temperatures in selected ILs

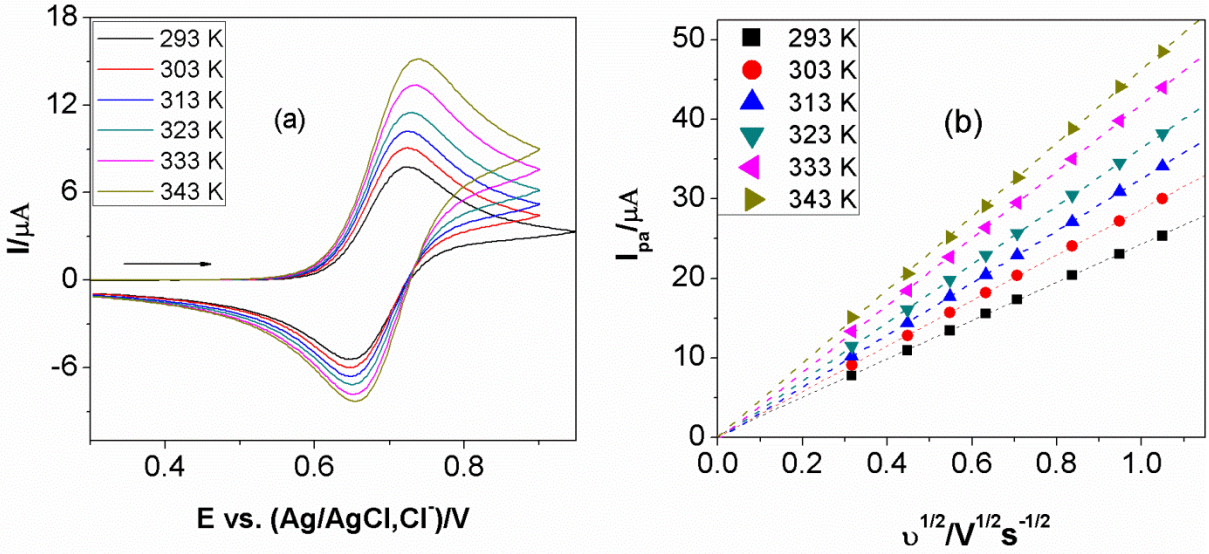

Figure 5.19. (a) CVs of TEMPO 23.3 mM in [emim][OTf] obtained at 0.5 mm radius GC over the range 293-343 K at 100 mV s^{-1}; (b) plots of corresponding I_{pc} vs. $v^{1/2}$.

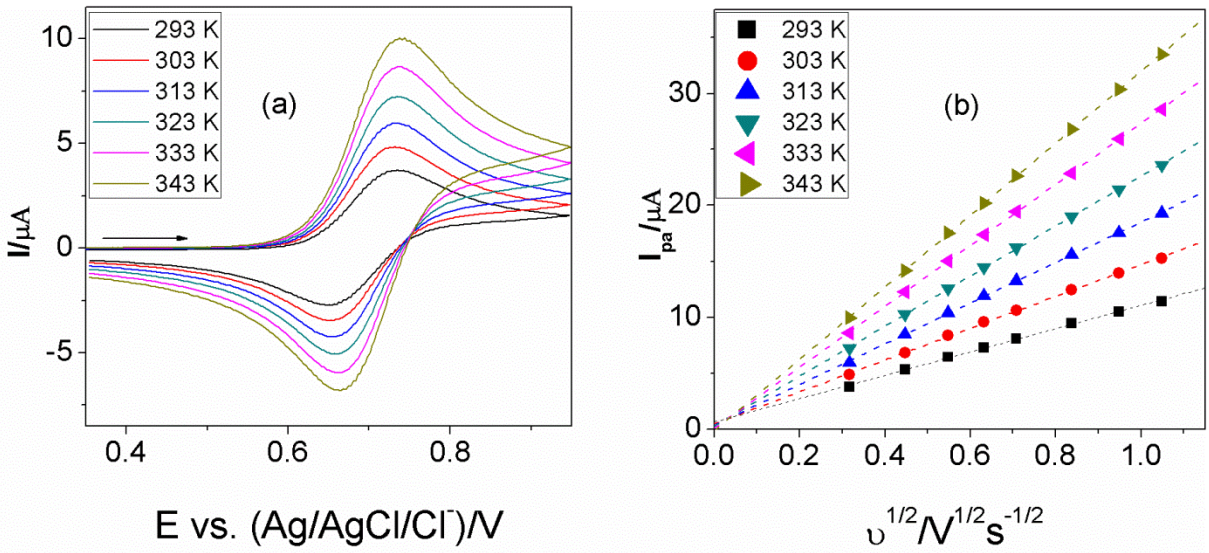

Figure 5.20. (a) CVs of TEMPO 17.6 mM in [bmim][PF_6] obtained at 0.5 mm radius GC over the range 293-343 K at 100 mV s^{-1}; (b) plots of corresponding I_{pc} vs. $v^{1/2}$.

Cyclic voltammograms of TEMPOL at different temperatures in selected ILs

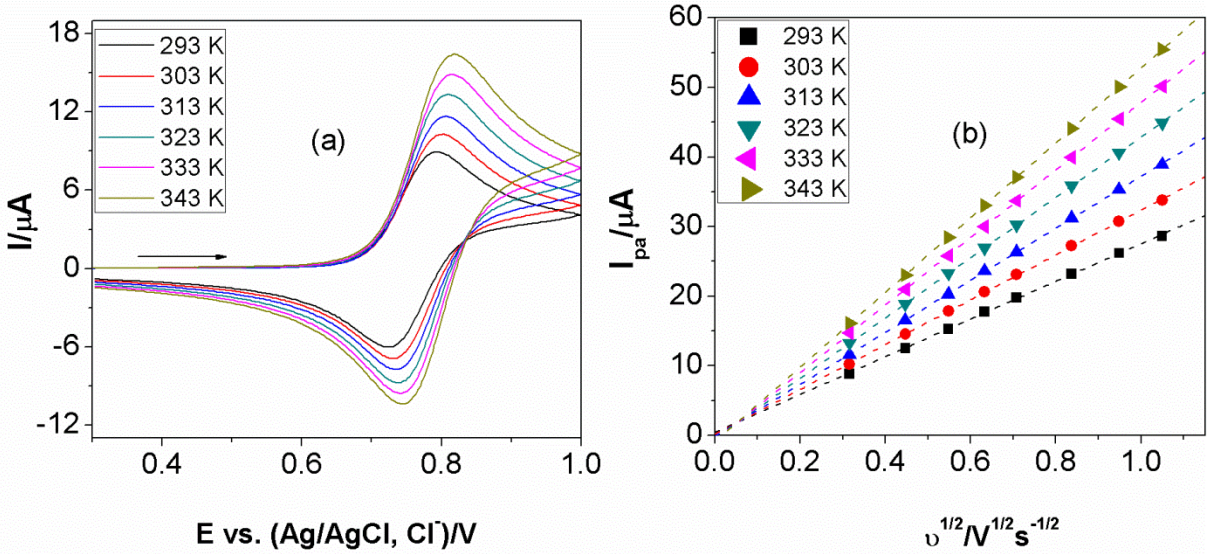

Figure 5.21. (a) CVs of TEMPOL 27.7 mM in [emim][NTf_2] obtained at 0.5 mm radius GC over the range 293-343 K at 100 mV s^{-1}; (b) plots of corresponding I_{pc} vs. $v^{1/2}$.

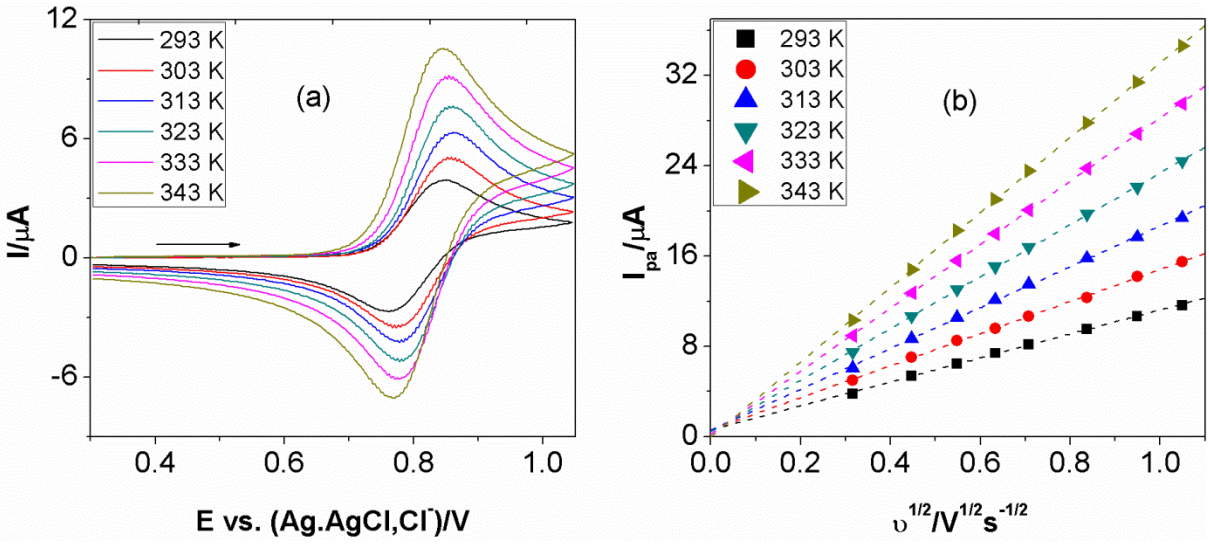

Figure 5.22. (a) CVs of TEMPOL 23.6 mM in [bmim][PF_6] obtained at 0.5 mm radius GC over the range 293-343 K at 100 mV s^{-1}; (b) plots of corresponding I_{pc} vs. $v^{1/2}$.

Diffusion coefficients of TTF and TEMPO at different temperatures were also measured by steady-state voltammetry and showed the same trend that the limiting current increases together with temperature (Figs. 5.23 - 5.26). The shape of steady-state voltammogram is shifted in some case due to the instability of the A-quasi-reference electrode (Ag-QRE).

Steady-state voltammograms of TTF at different temperatures

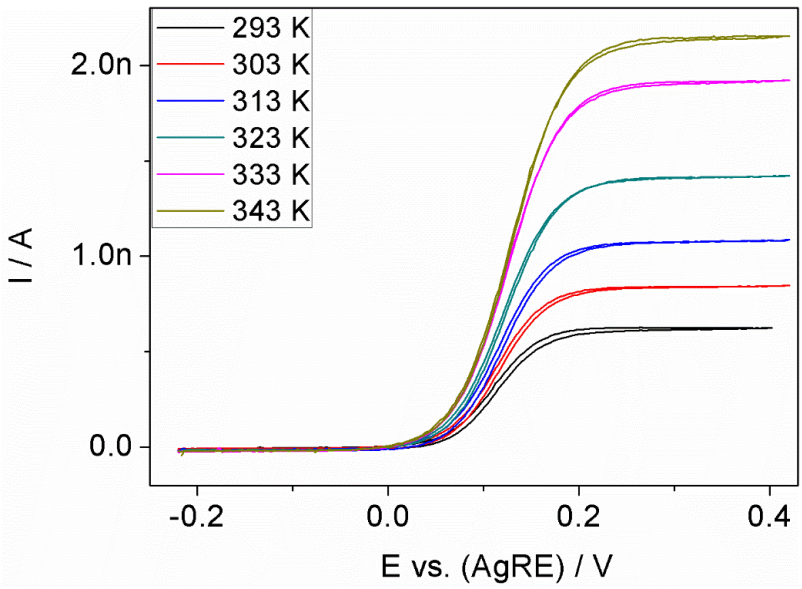

Figure 5.23. Steady-state voltammograms of 8.2 mM TTF in [emim][NTf_2] at a 5.5 µm radius Pt electrode at different temperatures.

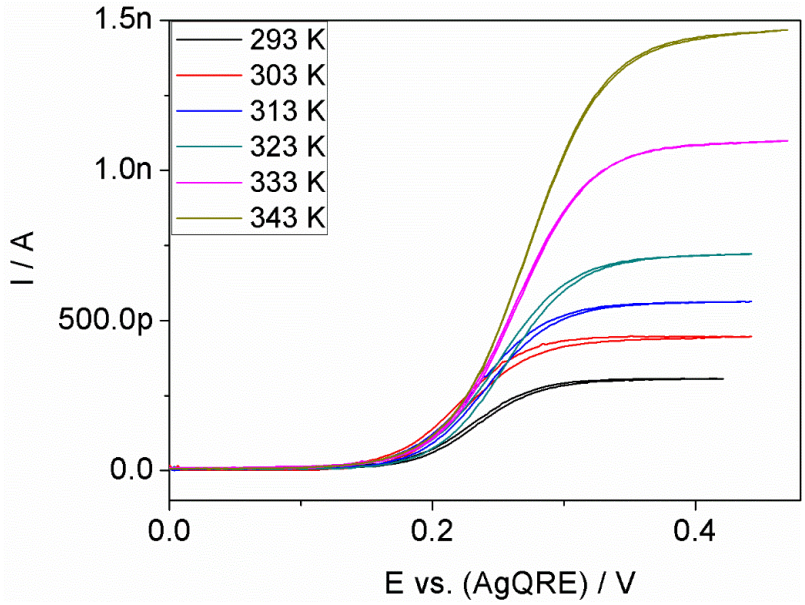

Figure 5.24. Steady-state voltammograms of 8.0 mM TTF in [bmim][OTf] at a 5.5 µm radius Pt electrode at different temperatures.

Steady-state voltammograms of TEMPO at different temperatures

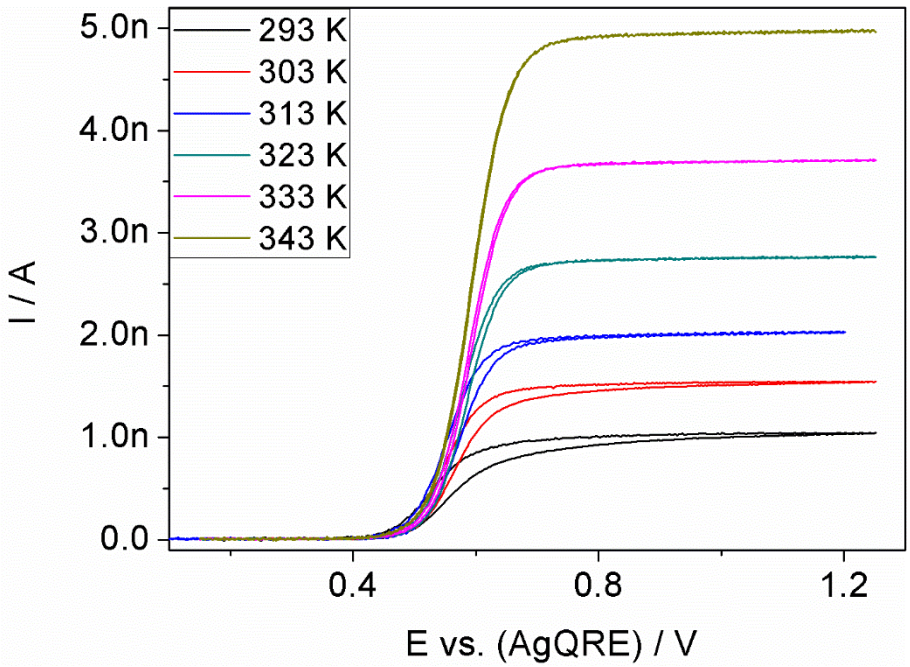

Figure 5.25. Steady-state voltammograms of 18.1 mM TEMPO in [bmim][NTf_2] at a 5.5 µm radius Pt electrode at different temperatures.

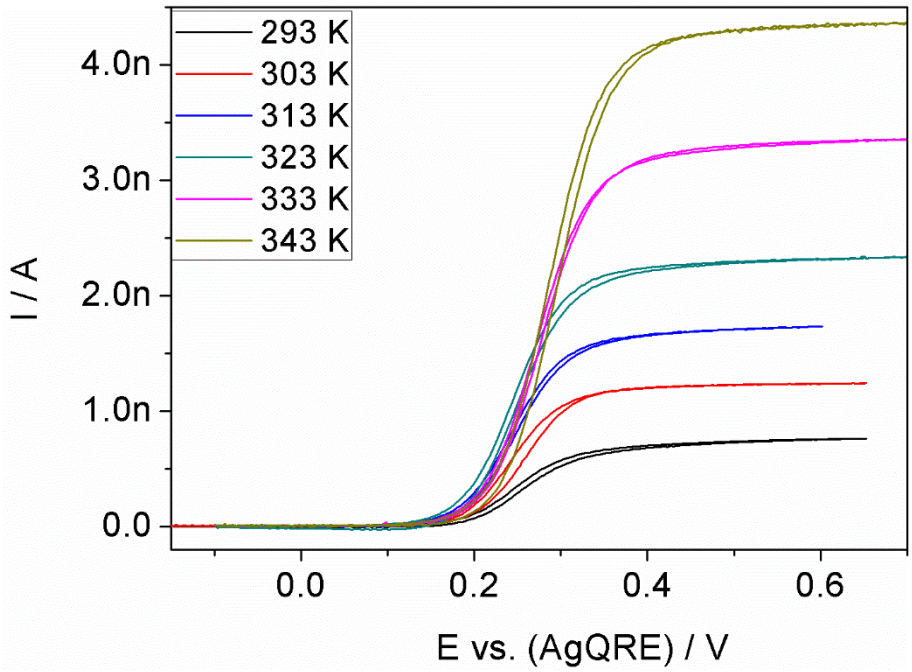

Figure 5.26. Steady-state voltammograms of 22.0 mM TEMPO in hmim][NTf_2] at a 5.5 µm radius Pt electrode at different temperatures.

Table 5.2. Diffusion coefficients of TTF in ILs and organic solvents at different temperatures.

	$D \times 10^7$ ($cm^2\ s^{-1}$)									
ILs	[emim][NTf_2]		[bmim][NTf_2]		[hmim][NTf_2]		[emim][OTf]		[bmim][OTf]	
T/K	CV	SSV	CV	SSV	CV	SSV	CV	SSV	CV	SSV
293	3.1±0.4	3.6±0.2	1.8±0.2	2.3±0.1	1.6±0.2	1.9±0.1	2.3±0.2	2.5±0.1	1.3±0.2	1.69±0.09
303	4.2±0.5	4.9±0.2	2.8±0.3	3.6±0.2	3.0±0.4	2.9±0.1	3.4±0.4	3.5±0.2	1.9±0.2	2.6±0.1
313	5.5±0.7	6.4±0.3	3.9±0.4	5.0±0.3	4.5±0.6	4.1±0.2	4.7±0.5	4.6±0.3	3.0±0.3	3.4±0.2
323	6.9±0.8	8.4±0.4	5.3±0.6	7.0±0.3	5.7±0.7	5.4±0.3	6.0±0.7	5.9±0.3	3.8±0.4	4.4±0.2
333	9±1	11.4±0.6	7.2±0.8	9.3±0.5	7.9±0.9	7.9±0.4	7.6±0.9	7.8±0.4	5.2±0.6	6.4±0.3
343	11±1	12.8±0.6	9.2±0.9	11.6±0.6	10±1	10.1±0.5	9±1	9.7±0.5	6.3±0.7	13.4±0.7

Table 5.2 (continued). Diffusion coefficients of TTF in ILs and organic solvents at different temperatures.

	$D \times 10^7$ ($cm^2\ s^{-1}$)				
T/K	[bmim][BF_4]	[bmim][PF_6]	[emim][dca]	ACN	sulfolane
	CV	CV	CV	CA	CV
293	0.88±0.09	0.50±0.08	4.2±0.6	200 ± 10	-
303	1.1±0.1	0.8±0.1	5.9±0.8	-	8 ± 1
313	2.2±0.2	1.4±0.2	8±1	-	
323	3.1±0.3	2.5±0.4	10±1	-	
333	4.2±0.4	3.5±0.5	13±2	-	-
343	5.5±0.6	4.7±0.7	16±3	-	-

Table 5.3. Diffusion coefficients of TEMPO in Ils at different temperatures.

	[emim][NTf_2]		[bmim][NTf_2]		[hmim][NTf_2]		[bmim][PF_6]		[bmim][OTf]	[emim][OTf]
T / K	CV	SSV	CV	SSV	CV	SSV	CV	SSV	CV	CV
293	3.7 ± 0.4	3.5±0.2	2.5 ± 0.3	2.4±0.1	1.3 ± 0.2	1.86±0.09	0.47 ± 0.06	0.56±0.03	1.3±0.2	2.4±0.3
303	5.4 ± 0.6	4.8 ± 0.2	4.0 ± 0.5	3.5±0.2	2.2 ± 0.3	2.7±0.1	0.9 ± 0.1	0.95±0.05	2.2±0.3	3.5±0.4
313	7.1 ± 0.7	6.3±0.3	5.8 ± 0.6	4.8±0.2	3.3 ± 0.4	4.0±0.2	1.6 ± 0.2	1.43±0.07	3.0±0.3	4.8±0.5
323	10 ± 1	8.1±0.4	8.3 ± 0.9	6.5±0.3	5.0 ± 0.6	5.5±0.3	2.5 ± 0.3	2.2±0.1	-	6.3±0.6
333	13 ± 1	11.0±0.6	11 ± 1	8.9±0.4	7.1 ± 0.8	7.8±0.4	3.9 ± 0.4	3.3±0.2	-	8.6±0.9
343	15 ± 2	13.8±0.7	14 ± 2	11.5±0.6	10.0 ± 1.0	10.3±0.5	5.7 ± 0.6	4.6±0.2	-	10.7±1.2

Table 5.4. Diffusion coefficients of TEMPOL in ILs at different temperatures.

	[emim][NTf_2]	[bmim][NTf_2]	[hmim][NTf_2]	[bmim][PF_6]	[bmim][OTf]	[emim][OTf]
T / K	CV	CV	CV	CV	CV	CV
293	2.1 ± 0.2	1.9 ± 0.2	1.0 ± 0.1	0.45 ± 0.05	1.4±0.2	2.3±0.3
303	3.1 ± 0.3	3.2 ± 0.4	1.7 ± 0.2	0.8 ± 0.1	2.3±0.3	3.5±0.4
313	4.4 ± 0.4	4.5 ± 0.5	2.5 ± 0.3	1.4 ± 0.2	3.5±0.4	4.3±0.6
323	6.2 ± 0.6	6.4 ± 0.7	3.7 ± 0.4	2.4 ± 0.3	5.0±0.6	-
333	8.1 ± 0.8	8.7 ± 0.9	5.3 ± 0.5	3.8 ± 0.4	6.6±0.7	-
343	10 ± 1	11 ± 1	7.2 ± 0.7	5.5 ± 0.6	10±1	-

Table 5.5. Diffusion coefficients of TCNE in Ils at different temperatures.

	[emim][NTf_2]	[bmim][NTf_2]	[hmim][NTf_2]	[bmim][BF_4]	[bmim][PF_6]
T / K	CV	CV	CV	CV	CV
293	2.7 ± 0.3	1.0±0.1	1.6 ± 0.2	0.55 ± 0.06	0.17 ± 0.02
303	4.1 ± 0.4	1.6±0.2	2.7 ± 0.3	1.1 ± 0.1	0.26 ± 0.03
313	5.7 ± 0.6	2.2±0.3	4.2 ± 0.4	1.6 ± 0.2	0.53 ± 0.07
323	7.6 ± 0.9	3.1±0.4	6.2 ± 0.6	2.2±0.2	0.9 ± 0.1
333	10 ± 1	4.2±0.5	8.8 ± 0.9	2.9±0.3	1.4 ± 0.2
343	12 ± 1	5.1±0.6	11 ± 1	3.4 ± 0.4	1.8 ± 0.2

Diffusion coefficients of TCNE, TEMPO, TTF, TEMPOL in ILs are presented in Tables 5.2 – 5.5. To test the temperature dependence of D, Arrhenius-type equations are used. Plots of ln D vs. 1/T for TTF, TCNE, TEMPO, TEMPOL in ILs are shown in Figs. 5.27 -5.34.

Arrhenius plots of lnD vs. T^{-1} for TCNE in ionic liquids

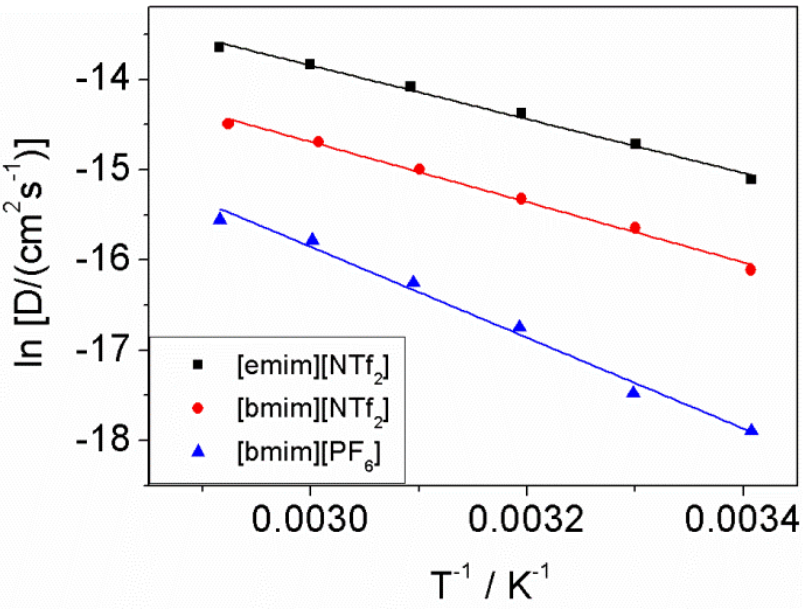

Figure 5.27. Arrhenius plots of lnD vs. T^{-1} for TCNE in [emim][NTf_2], [bmim][NTf_2], and [bmim][PF_6].

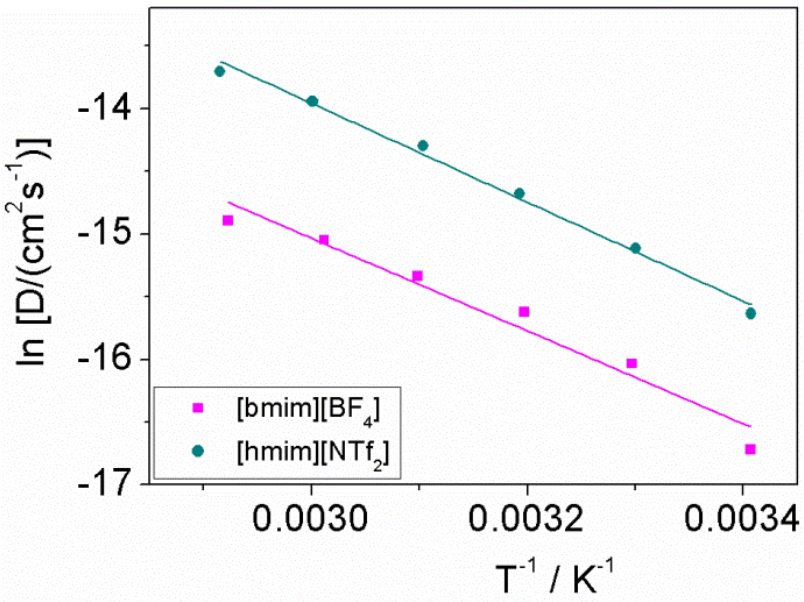

Figure 5.28. Arrhenius plots of lnD vs. T^{-1} for TCNE in [bmim][BF_4] and [hmim][NTf_2].

Arrhenius plots of lnD vs. T^{-1} for TTF in ionic liquids

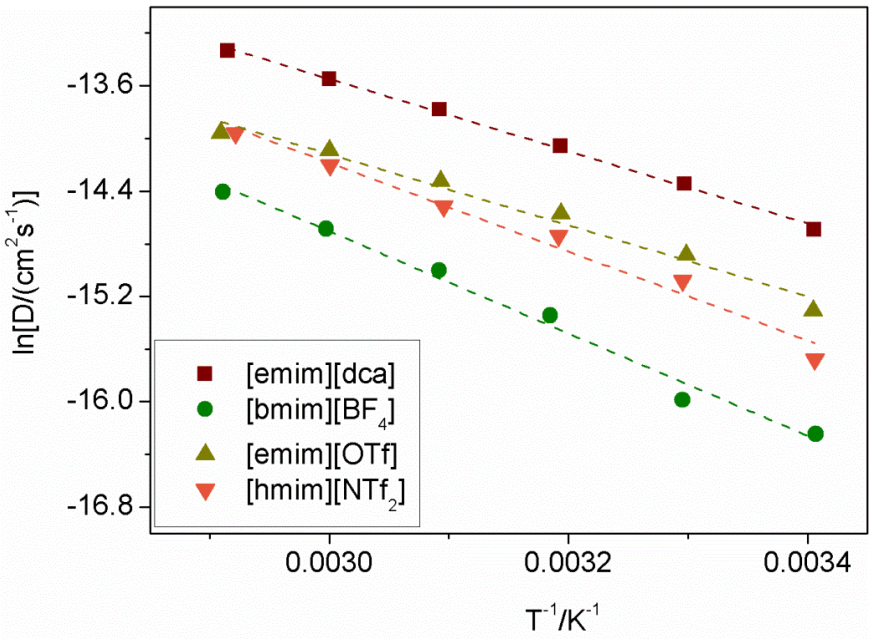

Figure 5.29. Arrhenius plots of lnD vs. T^{-1} for TTF in [emim]dca], [bmim][BF_4], [emim][OTf], and [hmim][NTf_2].

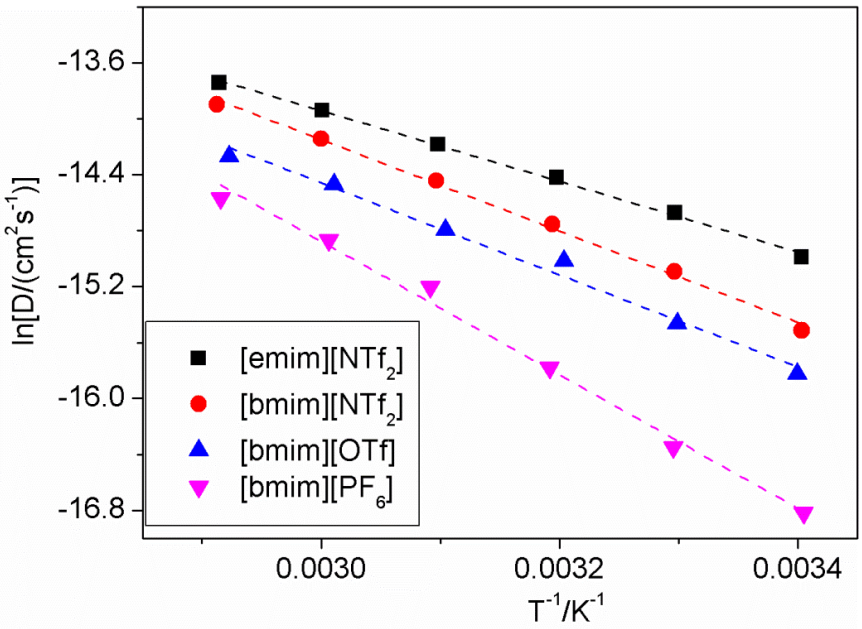

Figure 5.30. Arrhenius plots of lnD vs. T^{-1} for TTF in [emim][NTf_2], [bmim][NTf_2], [bmim][OTf] and [bmim][PF_6].

Arrhenius plots of lnD vs. T^{-1} for TEMPO in ionic liquids

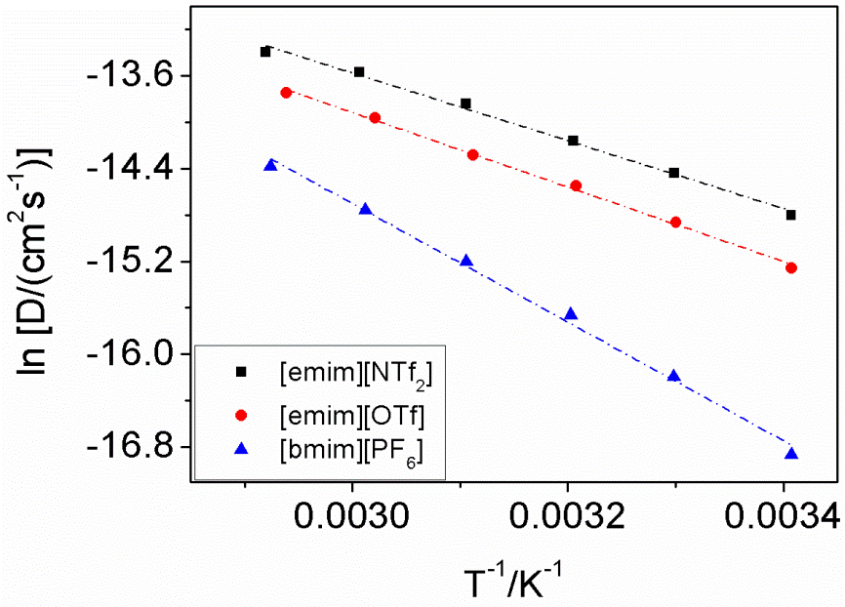

Figure 5.31. Arrhenius plots of lnD vs. T^{-1} for TEMPO in [emim][NTf_2], [emim][OTf] and [bmim][PF_6].

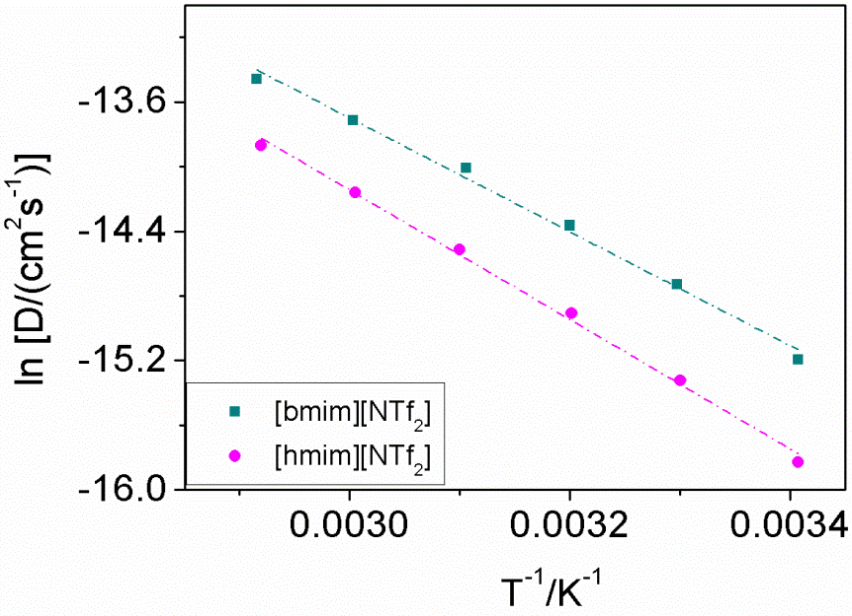

Figure 5.32. Arrhenius plots of lnD vs. T^{-1} for TEMPO in [bmim][NTf_2], [hmim][NTf_2].

Arrhenius plots of lnD vs. T^{-1} for TEMPOL in ionic liquids

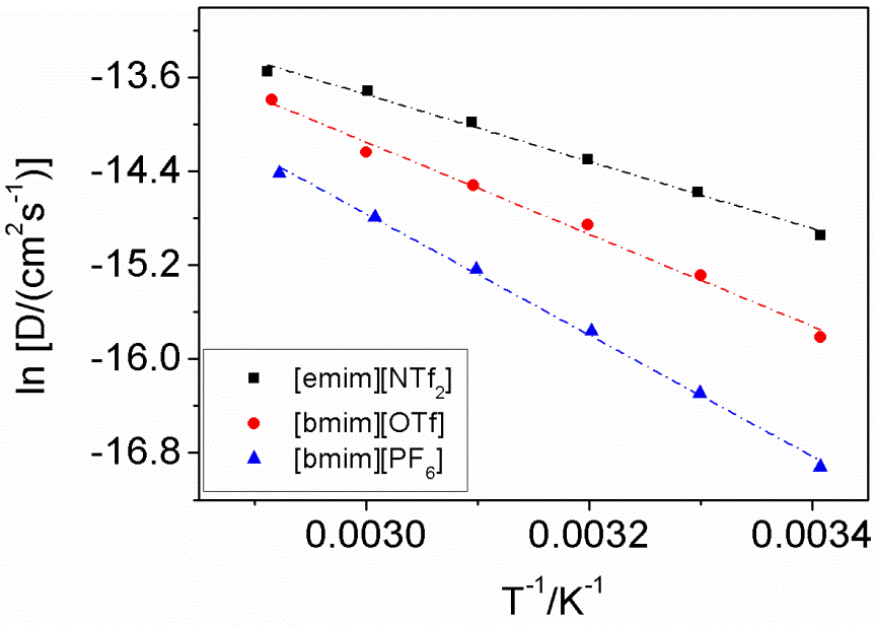

Figure 5.33. Arrhenius plots of lnD vs. T^{-1} for TEMPOL in [emim][NTf_2], [bmim][OTf] and [bmim][PF_6].

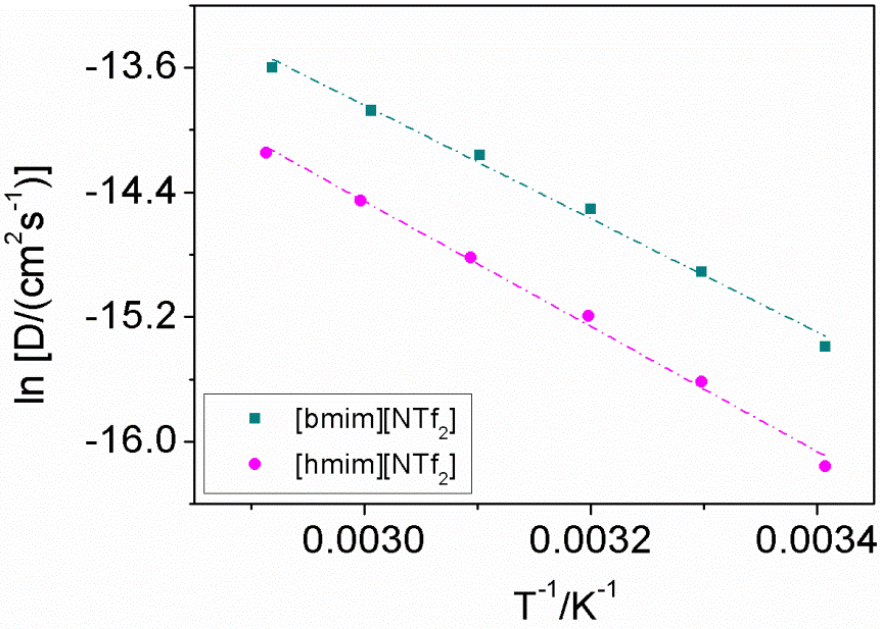

Figure 5.34. Arrhenius plots of lnD vs. T^{-1} for TEMPOL in [bmim][NTf_2], [hmim][NTf_2].

All the plots of lnD vs. T^{-1} present a good linearity leading to the conformity of the Arrhenius-type relationship of the system in the temperature range measured. The diffusional activation energies ($E_{a,D}$) have been calculated using Eq. 2.29. The activation energies of viscosity of IL are determined using the analogous equation.

$$\eta = \eta_o \, e^{E_{a,\eta}/RT} \tag{5.1}$$

Where $E_{a,\eta}$ is the activation energies of viscous flow of solvents, η_o is hypothetical values of η at infinite T.

$E_{a,D}$ and $E_{a,\eta,}$ are given in Table 5.6. The values of $E_{a,D}$ for the diffusion of TTF, TCNE, TEMPO, TEMPOL in each IL are similar. They compare well with the activation energy of viscous flow of the corresponding IL, suggesting the same mechanism of diffusion in each IL by changing the temperature. This means that the way of transport is independent on the nature and size of substances in ILs. Furthermore, the value of E_a is higher in more viscous ILs.

A slightly higher activation energy $E_{a,D}$ was obtained for TEMPO and TEMPOL in [emim][OTf] or in [bmim][OTf] in comparison with $E_{a,\eta}$. This observation can be explained by an additional hydrogen bonding which occurs between TEMPO or TEMPOL and anion [OTf]. Especially this hydrogen bonding is even stronger for TEMPOL due to the presence of -OH group.

Table 5.6. Activation energy (kJ mol^{-1}) for diffusion ($E_{a,D}$) of all compounds in ILs and for viscous flow of ILs ($E_{\eta,D}$).

	η (cP)	Solvent	TTF		$TTF^{\cdot+}$	TEMPO		TCNE	TEMPOL
Ionic liquid		$E_{\eta,D}$	$E_{a,D}$ (CV)	$E_{a,D}$ (SSV)	$E_{a,D}$ (CV)	$E_{a,D}$ (CV)	$E_{a,D}$ (SSV)	$E_{a,D}$ (CV)	$E_{a,D}$ (CV)
[emim][dca]	17[c]	19.1±0.4	22.9±0.5	-	-[e]	-	-	-	-
[emim][NTf_2]	38[a]	24.7±0.4	21.0±0.5	22.2±0.8	25.1±0.4	24.3±0.9	23.3±0.9	25±1	25.6±0.5
[emim][OTf]	48[d]	24.1±0.9	23±2	23.2±0.5	-[f]	26.7±0.6	-	-	28.4±0.8
[bmim][NTf_2]	62[a]	27.9±0.7	27.2±0.7	27±1	29±1	29±1	26.6±0.4	28±1	30±1
[bmim][OTf]	89[b]	29.5±0.8	29±2	26±1	27±2	32±3	-	-	33±1
[hmim][NTf_2]	87[a]	32.2±0.6	28±2	27.8±0.7	28±1	33.3±0.9	28.9±0.4	33±1	33±1
[bmim][BF_4]	129[a]	38±2	32±2	-	35±3	-	-	31±3	-
[bmim][PF_6]	374[a]	40±1	40±2	-	-[g]	42±1	35.6±0.5	42±2	43±1

[a]: from our measurement

[b, c, d]: from ref. [84], [86] and [126], respectively

[e]: $TTF^{\cdot+}$ is not stable

[f]: absorption peaks occurred at temperatures higher than 303 K

[g]: $TTF^{\cdot+}$ is not soluble at sufficiently high concentration

5.1.4. Dependence of charge on species

As shown in Figs. 5.5b and 5.6b, the ratio of I_{p_a} and I_{p_c} is close to unity which may lead to the incorrect conclusion that the values of D of TTF and $TTF^{\cdot+}$ are equal if one assumes the similar concentration of TTF and $TTF^{\cdot+}$ (Eq. 2.25). However, in this case cyclic voltammograms were scanned from the starting material TTF. Therefore, $TTF^{\cdot+}$ was not available in the bulk solution, but it was electro-generated on the surface of electrode. As a result, the actual concentration of $TTF^{\cdot+}$ is not the same as the TTF bulk concentration. Therefore, care must be taken in the extraction of the value of D of $TTF^{\cdot+}$ based only on cyclic voltammogram of TTF, especially in solvents with high viscosities.

Being aware of the above problem and also of a significant change in diffusion coefficients of each species in the presence of multiple solutes in the same solution [5,6], D of the $TTF^{\cdot+}$ was measured separately by using $TTF^{\cdot+}ClO_4^-$ instead of taking the value of D for the electro-generated species $TTF^{\cdot+}$ from using only the cyclic voltammogram of TTF in the section above. In addition, the determination of D of TTF from stock solutions of TTF and D of $TTF^{\cdot+}$ from the bulk resource of $TTF^{\cdot+}$, were done in order to make sure that the diffusion was measured under the concentration gradient of bulk concentration to the surface of the working electrode. In other words, D of TTF and $TTF^{\cdot+}$ was determined using the forward scans of cyclic voltammograms of TTF and $TTF^{\cdot+}$ respectively.

Cyclic voltammograms of $TTF^{\cdot+}$ in [bmim][OTf] and [bmim][NTf_2] at different scan rates are given in Figs. 5.35a and 5.36a, respectively. The voltammetric curves are obtained by scanning towards a negative potential direction starting from 0.7 V. Ohmic drop compensation was taken into account and an investigation of the reversibility of the system was also done in the same way as described for TTF. It must be mentioned that the ratio of I_{p_a}/I_{p_c} (Figs 5.35b, 5.36b) is also close to 1, but that I_{p_c} for the oxidation of $TTF^{\cdot+}$ is slightly higher than I_{p_a} for the reduction of TTF. The same behaviour was also observed in other ILs when scanning cyclic voltammograms from $TTF^{\cdot+}$ as the starting substance.

Cyclic voltammograms of $TTFClO_4$ in selected ionic liquids

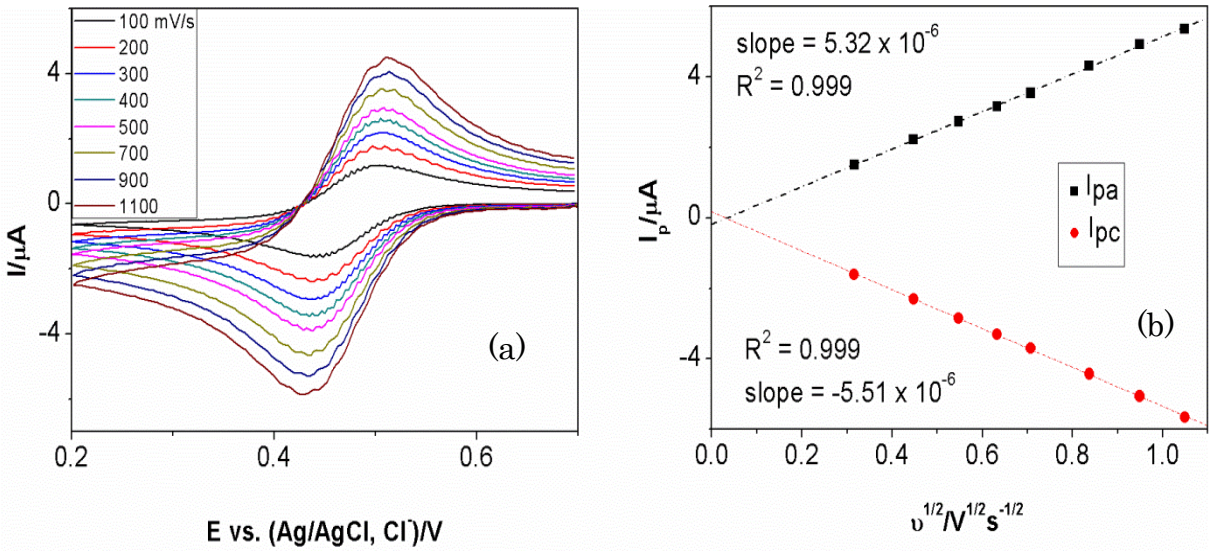

Figure 5.35. (a) Cyclic voltammograms of TTF^{+} 9.9 mM at 0.5mm radius GC in [bmim][OTf] at 303 K at different scan rates; (b) plots of corresponding I_{pa} and I_{pc} vs. $v^{1/2}$.

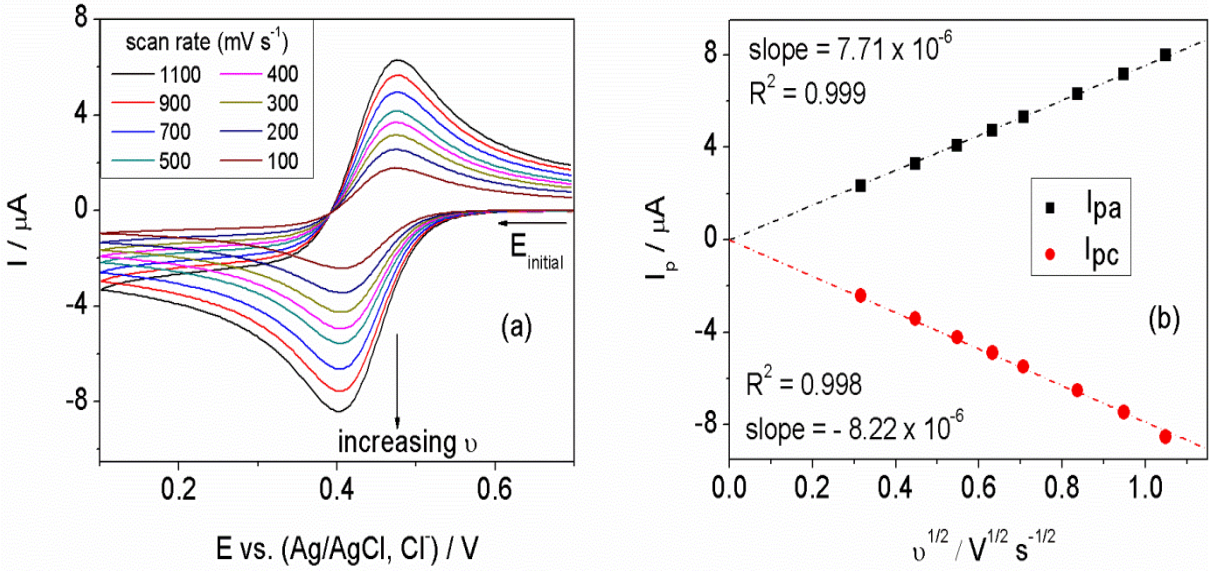

Figure 5.36. (a) Cyclic voltammograms of TTF^{+} 10 mM at 0.5mm radius GC in [bmim][NTf_2] at 303 K at different scan rates; (b) plots of corresponding I_{pa} and I_{pc} vs. $v^{1/2}$.

Cyclic voltammograms of $TTF^{\cdot+}$ in ILs were also recorded over a temperature range of 293 – 343 K (Figs. 5.37, 5.38). Diffusion coefficients of $TTF^{\cdot+}$ were then calculated following Eq.2.25 for five ILs and are summarized in Table 5.7. The values of the diffusion coefficients of TTF and $TTF^{\cdot+}$ are found to be $(2.0 \pm 0.1) \times 10^{-5}$ and $(1.8 \pm 0.1) \times 10^{-5}$ cm^2 s^{-1}, respectively in ACN (293 K, from SSV) and $(8 \pm 1) \times 10^{-7}$ and $(5.3 \pm 0.8) \times 10^{-7}$ cm^2 s^{-1}, respectively in sulfolane (at 303 K, from CV). The viscosities of ACN and sulfolane are 0.36 cP (293 K) and 10.29 cP (303 K) [120]. D of TTF in [bmim][NTf_2] is $(1.8 \pm 0.2) \times 10^{-7}$ cm^2 s^{-1}, which is two orders of magnitude lower than D of TTF in ACN. The data of D for TTF in ACN are comparable with values from literature [127]. More importantly, the results in Table 2 indicate the general trend that the diffusion of the cation $TTF^{\cdot+}$ is slower than that of the neutral form in each IL. The diffusion coefficient of $TTF^{\cdot+}$ is approximately half as large as that of the neutral TTF. Having a positive charge on TTF causes strong electrostatic interactions with ions of the IL-solvents, resulting in lower diffusion coefficients. The ratio $D_{TTF^{\cdot+}}/D_{TTF}$ at 293 K for ILs is in the range 0.43-0.62, while for ACN/$TBAPF_6$ and sulfolane/$TBAPF_6$ (303 K) it is 0.90 and 0.67, respectively. Implications of ion-paring have been reported for the smaller D of ferrocenium cation than that of Fc in organic solvents, when using $TBAClO_4$ or $TBAPF_6$ as supporting electrolytes, suggesting the formation of the ion-pair $FcClO_4$ or $FcPF_6$ [128,129]. However, in this case there are no big differences between the formal potentials of reduction of TTF in ILs, when scanning TTF or $TTF^{\cdot+}$ (from $TTF^{\cdot+}ClO_4^-$) as the starting species (Table 5.8). In addition, the concentration of ClO_4^- is much smaller than that of the anion in the ILs. As a consequence, the effect of ion-pairing of $TTF^{\cdot+}$ and ClO_4^- in ILs can be ruled out. The smaller ratio of $D_{TTF^{\cdot+}}/D_{TTF}$ in ILs can be attributed to electrostatic interactions between a positive charge on TTF and solvent which are stronger in ILs than in ACN/$TBAPF_6$ due to the three dimensional and highly charge-ordering structures of ILs. Moreover, for each ILs, the ratio $D_{TTF^{+}}/D_{TTF}$, showed a slightly smaller increase at higher temperature, as is already known at lower viscosity. This may be explained by considering two effects that hinder the diffusion of molecules: the friction force caused by viscosity and the interaction between species (TTF or $TTF^{\cdot+}$) and ILs. At higher viscosity it seems that the

effect of viscosity of the fluid is dominant compared to the total solute-ILs interactions (π-π interaction, coulombic interaction, etc.).

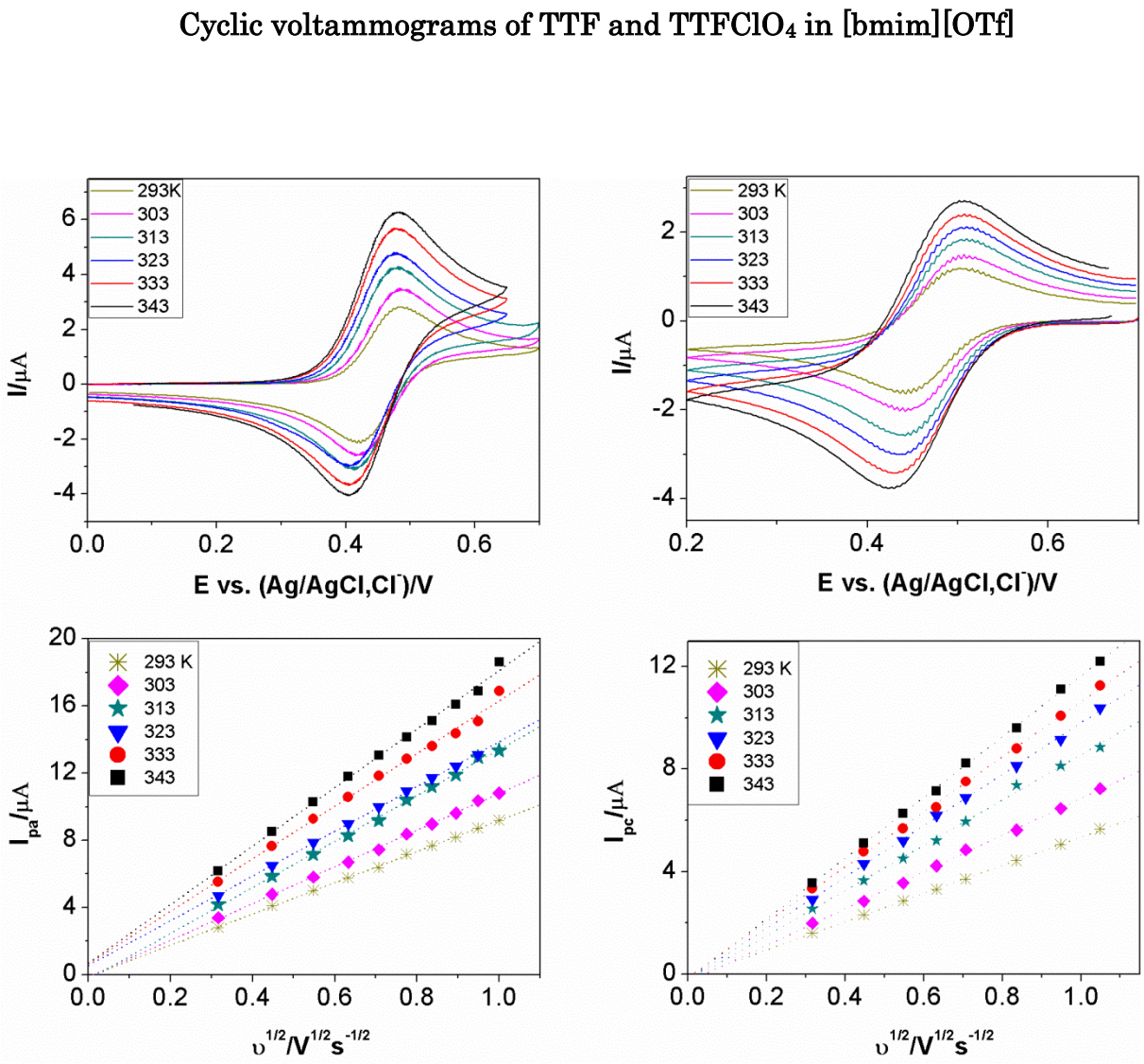

Figure 5.37. Cyclic voltammograms of (a) TTF 9.9 mM and (b) $TTF^{\cdot+}$ 9.9 mM in [bmim][OTf] obtained at 0.5 mm radius glassy carbon over the range 293-343 K at 100 mV s^{-1}; plots of corresponding I_{pa} and I_{pc} vs. $v^{1/2}$ (c), (d) respectively.

Cyclic voltammograms of TTF and $TTFClO_4$ in [bmim][NTf_2]

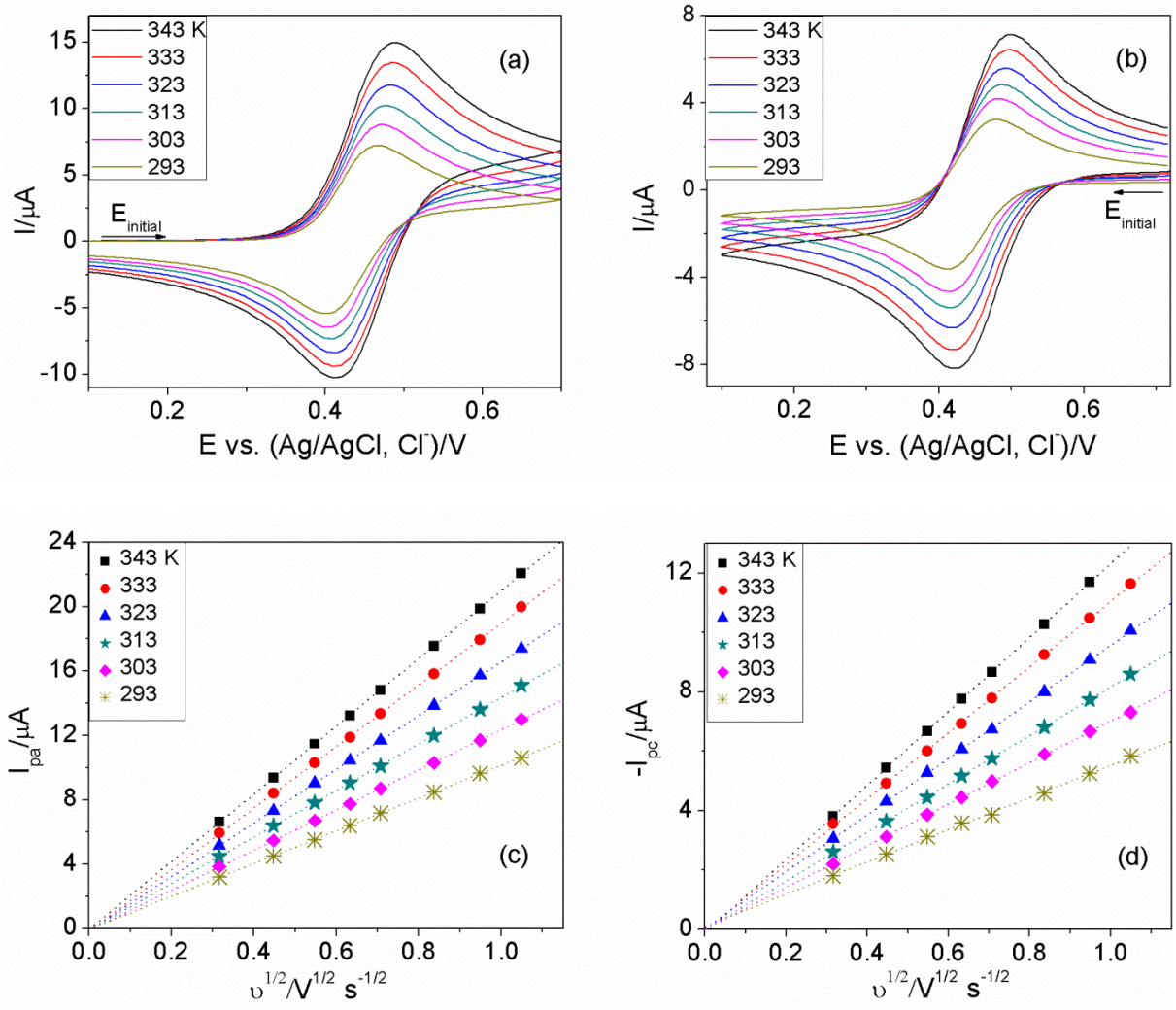

Figure 5.38. Cyclic voltammograms of (a) TTF 11.8 mM and (b) $TTF^{\cdot+}$ 10 mM in [bmim][NTf_2] obtained at 0.5 mm radius glassy carbon over the range 293-343 K at 500 mV s^{-1}; plots of corresponding I_{pa} and I_{pc} vs. $v^{1/2}$ (c), (d) respectively.

Table 5.7. Diffusion coefficients of TTF and $TTF^{\cdot+}$ in selected ILs at different temperatures measured by cyclic voltammetry.

	$D \times 10^7$ ($cm^2\ s^{-1}$)									
	[emim][NTf_2]		[bmim][NTf_2]		[bmim][BF_4]		[bmim][OTf]		[hmim][NTf_2]	
T/K	TTF	$TTF^{\cdot+}$	TTF	$TTF^{\cdot+}$	TTF	$TTF^{\cdot+}$	TTF	$TTF^{\cdot+}$	TTF	$TTF^{\cdot+}$
293	3.1±0.4	1.5±0.2	1.8±0.2	0.8±0.1	0.88±0.09	0.44±0.07	1.3±0.2	0.68±0.07	1.6±0.2	1.0±0.1
303	4.2±0.5	2.2±0.2	2.8±0.3	1.3±0.2	1.1±0.1	0.8±0.1	1.9±0.2	1.2±0.1	3.0±0.4	1.4±0.2
313	5.5±0.7	3.0±0.3	3.9±0.4	1.9±0.2	2.2±0.2	1.5±0.3	3.0±0.3	1.9±0.3	4.5±0.6	2.1±0.3
323	6.9±0.8	4.0±0.43.1	5.3±0.6	2.6±0.3	3.1±0.3	2.0±0.3	3.8±0.4	2.5±0.3	5.7±0.7	3.3±0.4
333	9±1	5.2±0.6	7.2±0.8	3.6±0.4	4.2±0.4	2.8±0.4	5.2±0.6	3.0±0.4	7.9±0.9	4.0±0.5
343	11±1	6.8±0.8	9.2±0.9	4.7±0.5	5.5±0.6	3.4±0.4	6.3±0.7	3.8±0.4	10±1	5.0±0.6

Table 5.8. Formal potential of oxidation of TCNE, reduction of TTF, TEMPO and TEMPOL from CV. In the case of $TTF^{\cdot+}/TTF$, $E^{o'} = (E_{p_a} + E_{p_c})/2 - (RT/F) \times \ln(D_{TTF^{\cdot+}}/D_{TTF})$. ($E^{o'}$ ±0.01) vs. (Ag/AgCl) / V in [bmim]Cl/ corresponding ILs.

	$E^{o'}$/ (V)				
ILs	TTF	$TTF^{\cdot+}$	TCNE	TEMPO	TEMPOL
[emim][NTf_2]	0.44	0.44	0.34	0.70	0.82
[bmim][NTf_2]	0.46	0.46	0.37	0.72	0.80
[bmim][OTf]	0.42	0.43	-	0.72	
[bmim][BF_4]	0.44	0.44	0.32	-	-
[hmim][NTf_2]	0.41	0.42	0.29	0.89	0.92
[emim][dca]	0.55	-	-	-	-
[emim][OTf]	0.43	0.42	-	0.69	0.81
[bmim][PF_6]	0.44	-	0.36	0.68	0.81

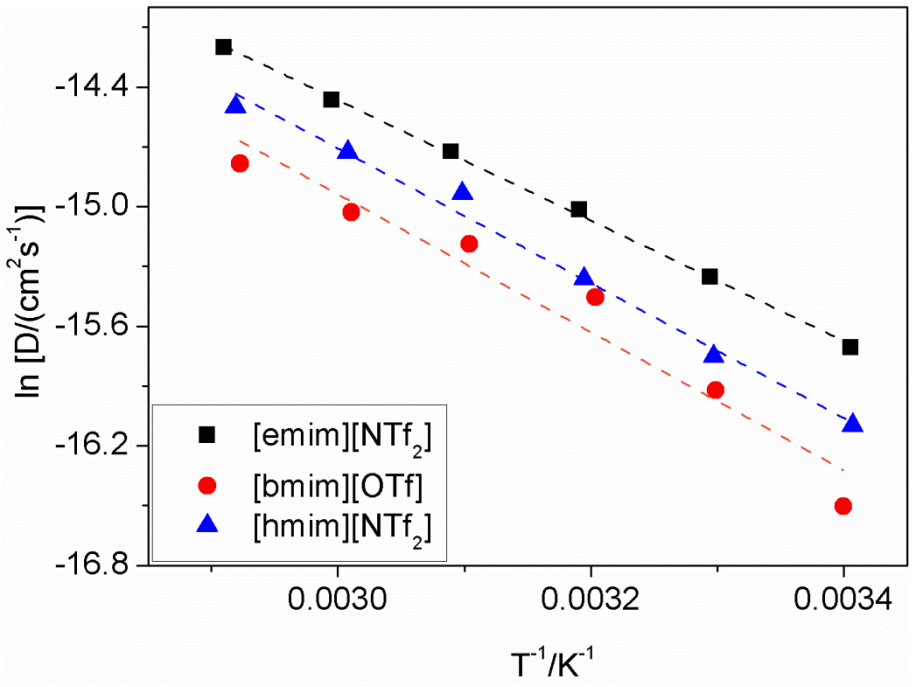

Figure 5.39. Arrhenius plots of lnD vs. T^{-1} for $TTF^{\cdot+}$ in [emim][NTf_2], [bmim][OTf], [hmim][NTf_2].

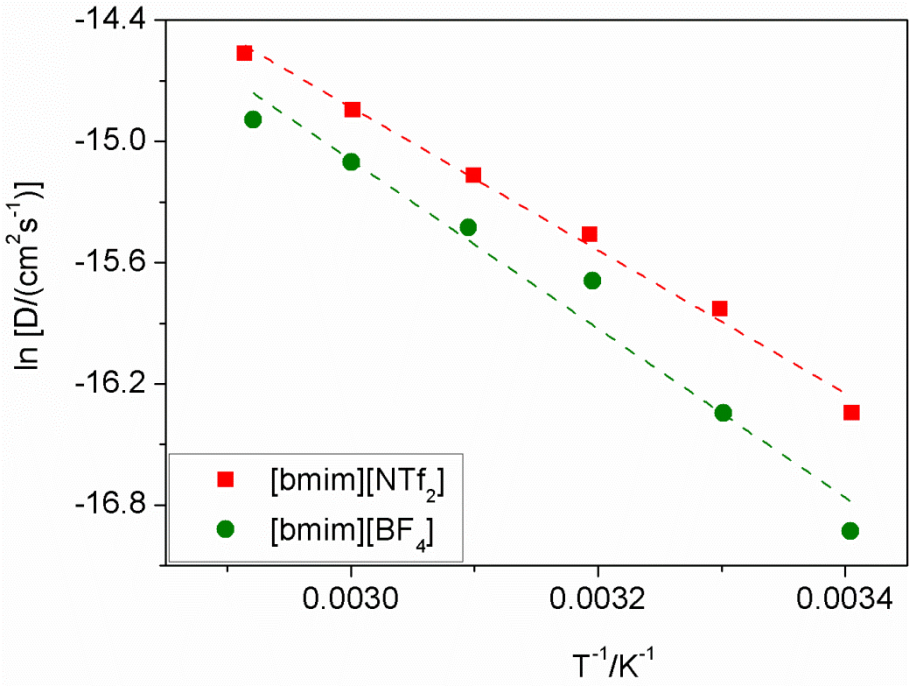

Figure 5.40. Arrhenius plots of lnD vs. T^{-1} for $TTF^{\cdot+}$ in [bmim][NTf_2], [bmim][BF_4].

The diffusion coefficients of $TTF^{\cdot+}$ in ILs are investigated by means of Arrhenius-type equation. Plots of ln D vs. 1/T for $TTF^{\cdot+}$ in ILs are shown in Figs. 5.39, 5.40 indicating a good linearity. Therefore, the Arrhenius-type relationship also holds well for $TTF^{\cdot+}$ in ILs. The same behaviour is observed for all other ILs. From Eq. 2.29, the diffusional activation energies, $E_{a,D}$, were computed and shown in Table 5.5. The values of E_a for the diffusion of TTF (from CV and SSV) and $TTF^{\cdot+}$ (from CV) in each IL were approximately the same. They are similar to the activation energy of viscosity of the equivalent IL, which may lead to the same mechanism of diffusion of TTF and $TTF^{\cdot+}$ in ILs. In addition, the above observation also predicted that $TTF^{\cdot+}$ is only in ion-paring with anions of IL or only in the free ion form.

5.1.5. Dependence on the substance

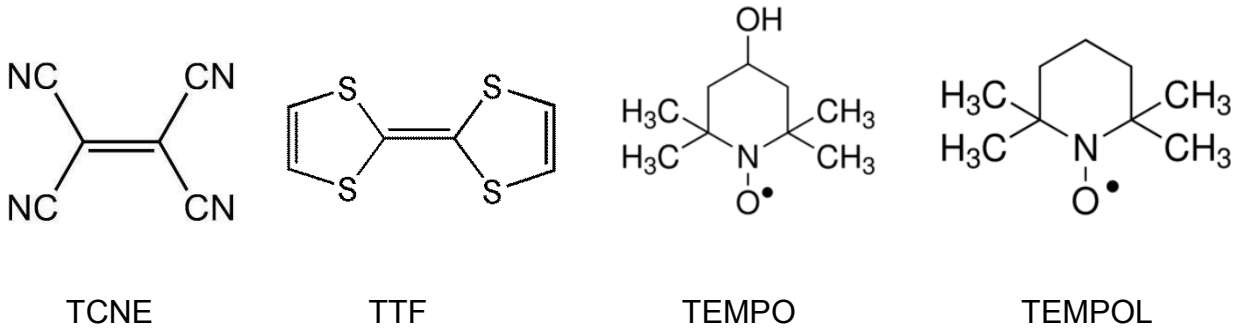

Figure 5.41. Structure of investigated diffusing molecules in ILs.

To investigate the role of molecular structure on diffusion in ILs, all D of the above substances are listed in Table 5.9. The general trend for D in the same ILs is: TCNE < TTF ≈ TEMPO < TEMPOL. Surprisingly, size and weight of diffusing molecule does not play an important role in diffusion. For example, TCNE molecule is smaller than TEMPO and TEMPOL but D of TEMPO and TEMPOL are higher than those of TCNE in ILs (except for in [hmim][NTf_2]). Another example is TTF. Having the same size as TCNE but the D of TTF is1.6-1.8 times lower than that of TCNE in (except for in [hmim][NTf_2]).

The question is what makes diffusion of molecules different in the same IL, if not size and weight of particle. Geometries of the investigated redox probes are

shown in Fig. 5.41. TCNE is planar with the angle of C-C-C is 116.5°[130]. TTF has a boat-like shape with C_{2v} symmetry which is in equilibrium with planar structure [131,132]. TEMPO and TEMPOL have more spherical structure [133]. Only TTF and TCNE are π-systems, therefore, interaction between TTF and TCNE is mainly based on π - π interaction with the immidazolium ring of IL. For TEMPO and TEMPOL the interaction is described in Fig. 5.42 a,b.

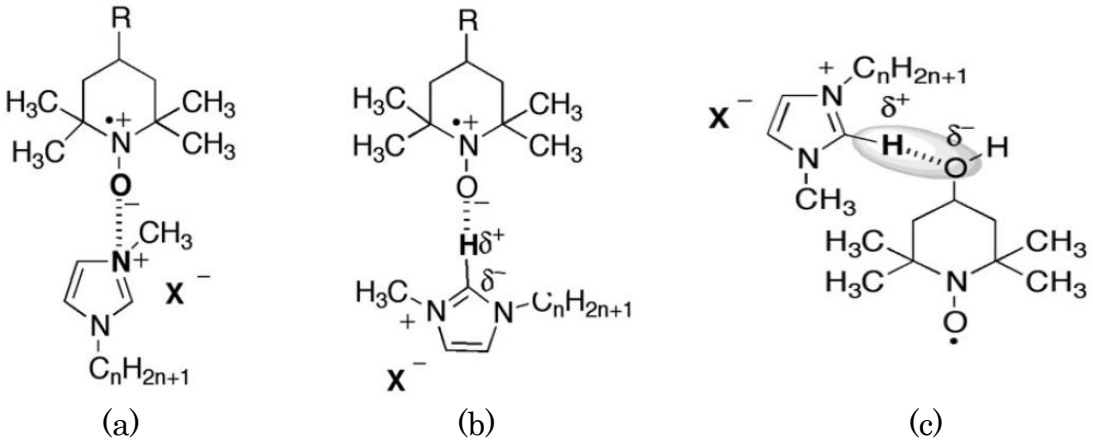

Figure 5.42. Interactions between TEMPO, TEMPOL and IL (a) ionic interaction, (b) hydrogen bonding; (c) additional hydrogen bonding between -OH of TEMPOL and IL. Adapted from [134].

The low value of D for TCNE in each IL may be attributed to a strong interaction with IL due to the fact that TCNE has planar structure and it is a strong π-acid [135]. The higher value of D for TEMPO and TEMPOL can be explained by a weaker interaction with ILs. Interactions in this case include ionic interactions and hydrogen bondings, however, the contact with ions of ILs is hindered (it is caused by the bulky structure of TEMPO and TEMPOL).

In a given IL, D of TEMPO is higher than that of TEMPOL which is assigned to a weaker interaction between TEMPO with IL. Indeed, TEMPOL has –OH group which cause an additional hydrogen bonding with IL (Fig. 5.42c). Grampp et al and Strehmel et al. obtained a smaller average rotational correlation time for TEMPO (0.1 ns) in [emim][BF_4] compared with that for TEMPOL (1.1 ns) which again confirms the additional interaction above [133,136].

Table 5.9. Diffusion coefficients of TCNE, TTF, TEMPO and TEMPOL and ILs measured by cyclic voltammetry.

solvents	η (cP) 293 K	TCNE	TTF	TEMPO	TEMPOL
		r = 3.1 Å [137] M=128.09	r = 3.04 Å [137] M=204.36	r=3.73 Å [133] M=156.25	r = 3.9 Å [133] M=172.24
[emim][NTf_2]	38[a]	2.7±0.3	3.1±0.4	3.7±0.4	3.0±0.3
[emim][OTf]	48[d]	-	2.3±0.2	2.4±0.3	2.3±0.3
[bmim][NTf_2]	62[a]	1.0±0.1	1.8±0.2	2.5±0.3	1.9±0.2
[bmim][OTf]	89[b]	-	1.3±0.2	1.3±0.02	1.4±0.2
[hmim][NTf_2]	87[a]	1.6±0.2	1.6±0.2	1.3±0.2	1.0±0.1
[bmim][BF_4]	129[a]	0.55±0.06	0.88±0.09	-	-
[bmim][PF_6]	374[a]	0.17±0.02	0.5±0.08	0.47±0.06	0.45±0.05

[a]: from measurements presented in this work
[b], [c], [d]: from Ref. [84], [86] and [126], respectively

5.1.6. Dependence of viscosity

5.1.6.1. Classical model

Before attempting to analyse the diffusion based on the classical model, plots of ln D vs. T/η were made to check the fractional Stokes-Einstein relation in Eq. 2.32. Good linearity was found with correlation coefficients > 98%. The slopes of these lines, i.e. the exponent m, were in the range of 0.8 - 1.0 (Table 5.10).

Table 5.10. Values of the exponents m in Eq. 2.32 from the slopes of plots of ln D vs. ln (T/η).

	Exponent m				
ILs	TTF	$TTF^{\cdot+}$	TCNE	TEMPO	TEMPOL
[emim][NTf_2]	0.80 ±0.01	0.96 ±0.01	0.95±0.02	0.92±0.04	0.92±0.06
[bmim][NTf_2]	0.89 ±0.01	0.96 ± 0.02	0.91±0.02	0.96±0.02	0.96±0.02
[bmim][OTf]	0.87 ±0.06	0.87 ± 0.09	-	0.99±0.09	1.01±0.04
[bmim][BF_4]	0.90 ±0.05	0.97 ± 0.07	0.93±0.04	-	-
[hmim][NTf_2]	0.89 ±0.04	0.85 ± 0.03	1.00±0.02	1.008±0.006	1.01±0.01
[emim][dca]	1.05 ±0.01	-	-	-	-
[emim][OTf]	0.84 ±0.04	-	-	0.99±0.01	0.98±0.01
[bmim][PF_6]	0.92 ±0.03	-	0.98±0.09	0.99±0.01	0.998±0.002

Because of a inconformity with of the fractional Stokes-Einstein relation, the classical relationship between D and η (Eq. 2.33) was then considered. The diffusion coefficients of TCNE, TTF, $TTF^{\cdot+}$, TEMPO and TEMPOL have been plotted as a function of the inverse of viscosity of the ILs (Figs. 5.43 - 5.47), at 293 K showing a good linearity.

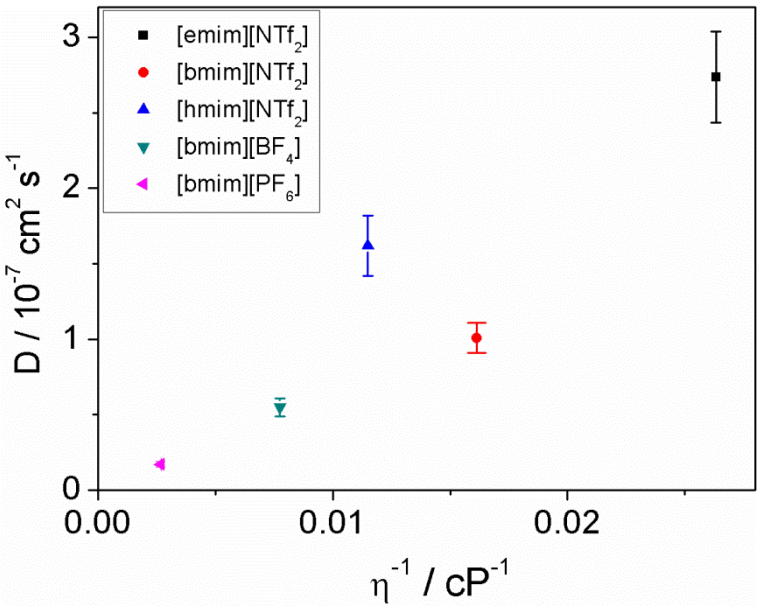

Figure 5.43. Plots of D vs. η^{-1} for TCNE in five ILs. Values of diffusion coefficients were obtained from CV.

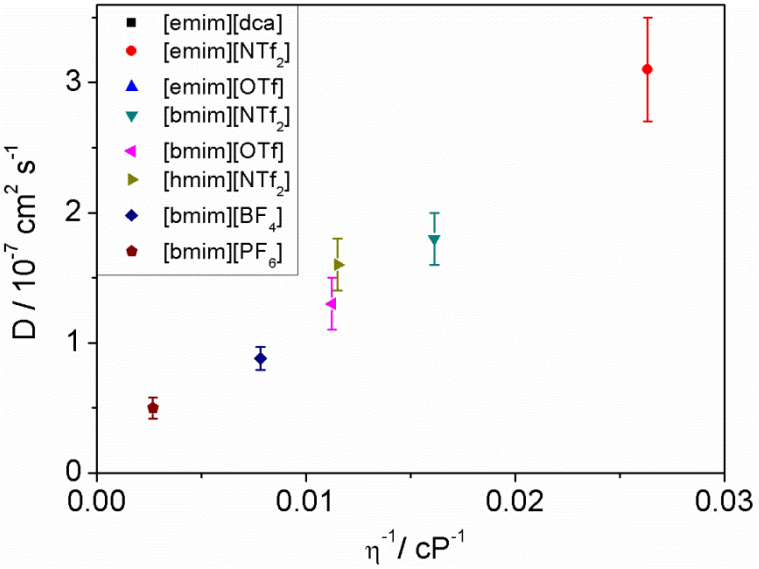

Figure 5.44. Plots of D vs. η^{-1} for TTF in eight ILs. Values of diffusion coefficients were obtained from CV.

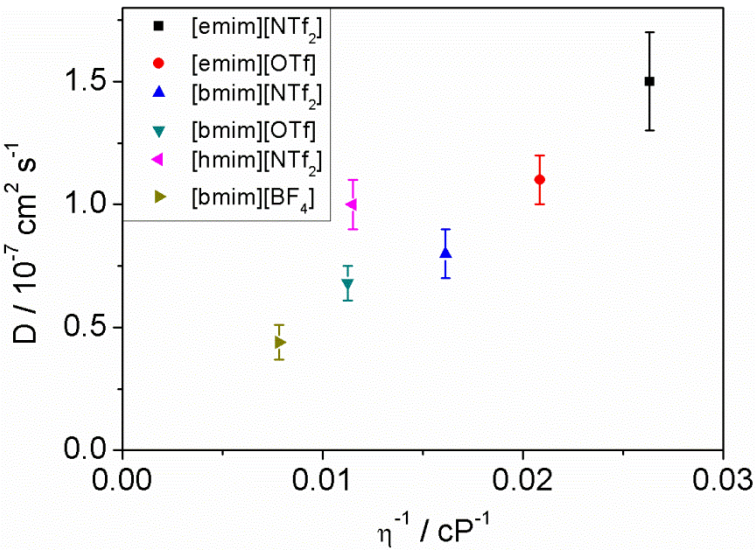

Figure 5.45. Plots of D vs. η^{-1} for $TTFClO_4$ in six ILs. Values of diffusion coefficients were obtained from CV.

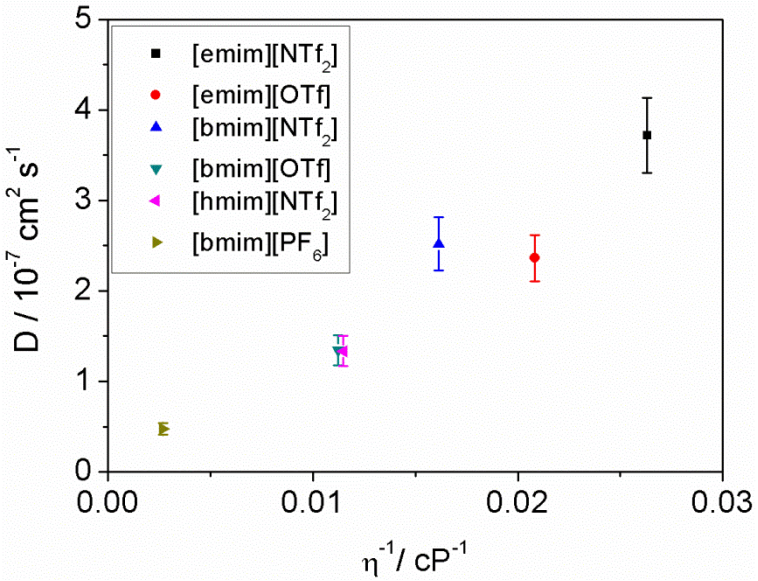

Figure 5.46. Plots of D vs. η^{-1} for TEMPO in six ILs. Values of diffusion coefficients were obtained from CV.

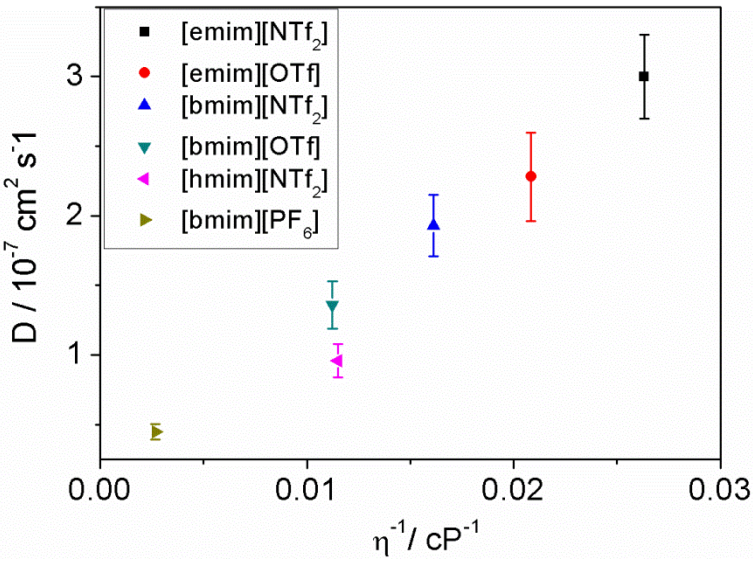

Figure 5.47. Plots of D vs. η^{-1} for TEMPOL in six ILs. Values of diffusion coefficients were obtained from CV.

In general, the diffusion coefficients are smallest in the highest viscosity ILs [bmim][PF_6] and largest in the lowest viscosity ILs [emim][NTf_2]. Viscosity is the most important factor in the investigation of the movements of molecules in liquids but there are many other factors which must be considered. Indeed, the solvents also play an important role through the interactions with solute (as mentioned in section 5.1.4 and 5.1.5). Diffusion coefficient of TTF in [emim][NTf_2] (39 cP, 293 K, T/η = 7.5 K cP^{-1}) is (3.1 ± 0.4) × 10^{-7} cm^2 s^{-1}, while in [hmim][NTf_2] (39 cP, 313 K, T/η = 8.0 K cP^{-1}) it is (4.5 ± 0.6) × 10^{-7} cm^2 s^{-1}. The difference once again confirms the important contribution of solvation in ILs.

The diffusion process of all diffusing particles in ILs seems to obey either the Stokes-Einstein or the Sutherland equation. However, before drawing any conclusions about this, one must be careful. It has been reported that there is no conformity between D and η in terms of the classical model mentioned above, but linear behaviour of D vs. η^{-1} was observed [15,16]. Another plot of the product D × η against η (Figs. 5.48– 5.52) should be considered. There are two boundary lines (b=4 and b=6), formed by calculation of the value of D × η when using an ellipsoid radius of 3.04 Å for TTF, obtained from theoretical calculations [127].

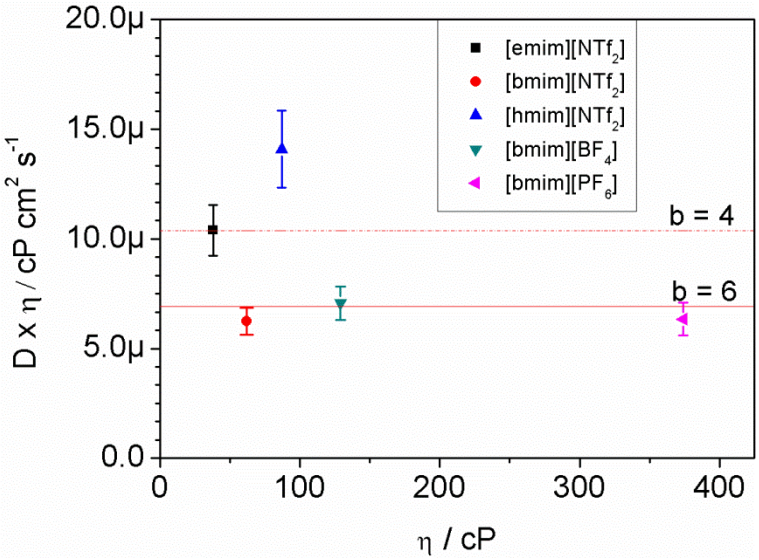

Figure 5.48. Plots of product D × η vs. η for TCNE. Two horizontal lines (b=4, b=6) show the value of D × η determined from Eq. 2.33 with the value of radius of TTF is 3.1 Å. Values of diffusion coefficients were obtained from CV.

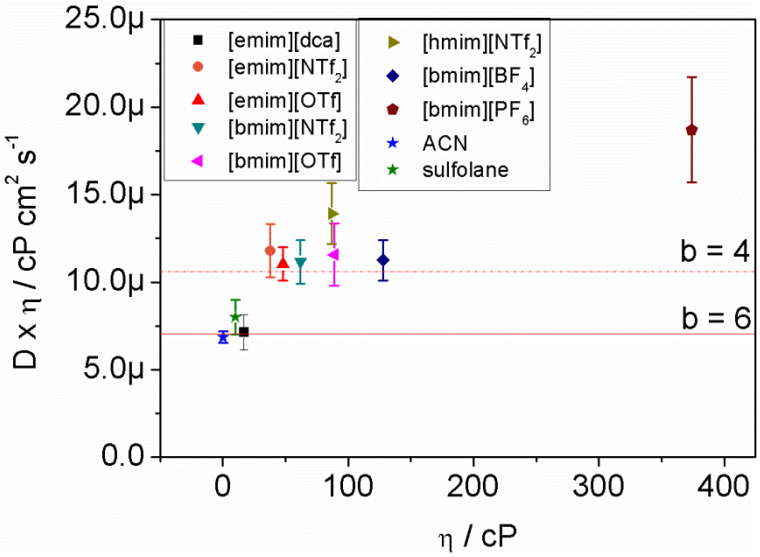

Figure 5.49. Plots of product D × η vs. η for TTF. Two horizontal lines (b=4, b=6) show the value of D × η determined from Eq. 2.33 with the value of radius of TTF is 3.04 Å. Values of diffusion coefficients were obtained from CV.

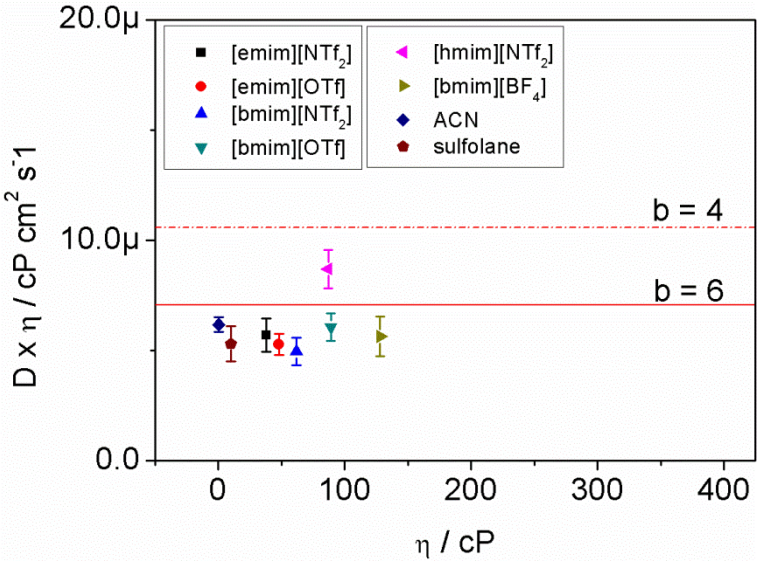

Figure 5.50. Plots of product D × η vs. η for $TTFClO_4$. Two horizontal lines (b=4, b=6) show the value of D × η determined from Eq. 2.33 with the value of radius of $TTF^{\cdot+}$ is 3.04 Å. Values of diffusion coefficients were obtained from CV.

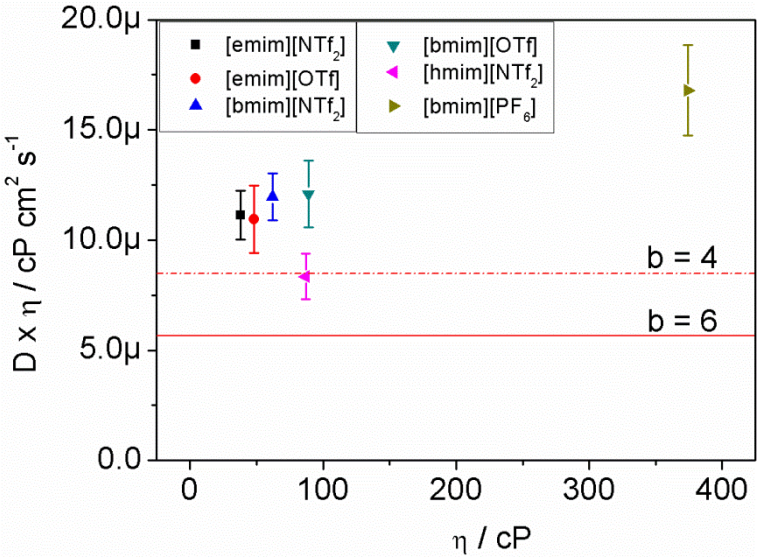

Figure 5.51. Plots of product D × η vs. η for TEMPO. Two horizontal lines (b=4, b=6) show the value of D × η determined from Eq. 2.33 with the value of radius of TEMPO is 3.73 Å. Values of diffusion coefficients were obtained from CV.

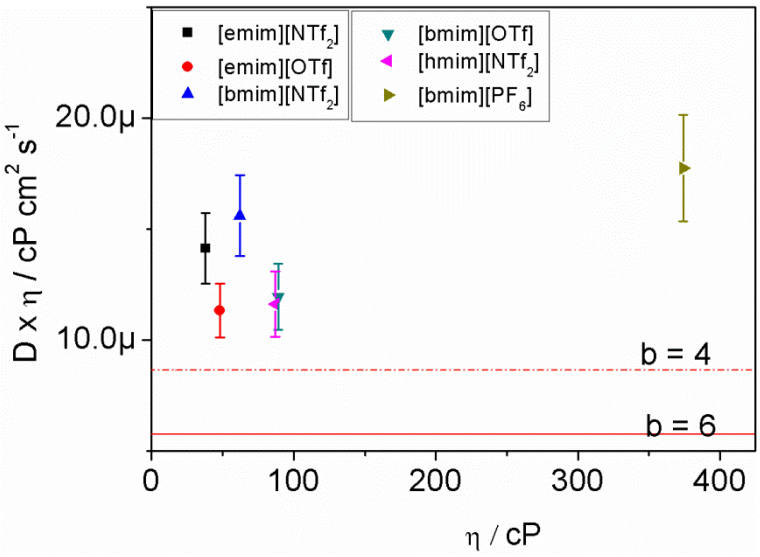

Figure 5.52. Plots of product D × η vs. η for TEMPOl. Two horizontal lines (b=4, b=6) show the value of D × η determined from Eq. 2.33 with the value of radius of TEMPO is 3.9 Å. Values of diffusion coefficients were obtained from CV.

For TTF the values of D × η in most ILs are close to the boundary condition b=4, except [emim][dca], where b is close to 6. Those of $TTF^{\cdot+}$ in ILs are close to the line b=6. However, there were no clear correlation observed in ILs: [hmim][NTf_2], [bmim][PF_6]. The results obtained can be explained by a weaker interaction between TTF and ILs compared with the stronger one of $TTF^{\cdot+}$. This leads to the slipping condition (b=4) in Eq. 2.33. Same results are reported by Vorotyntsev et al. on the diffusion of Fc in high viscosity ILs. In contrast, due to the electrostatic attraction of a positive charge in $TTF^{\cdot+}$ cation and anion of the ionic liquid, this ion sticks to the surface of the ionic liquid and diffuses following the Stokes-Einstein behaviour. This is also observed for TTF in [emim][dca] probably due to a strong interaction between TTF and the [dca] anion. In fact, a complex is formed when mixing $TTF^{\cdot+}$ and [emim][dca]. As expected, the product D × η for TTF and $TTF^{\cdot+}$ are both near b=6 in the case of ACN as solvent.

For TCNE, D × η is mainly close to b=6 which agrees well with the conclusion given above (section 5.1.5) for strong interactions between TCNE and IL.

For TEMPO and TEMPOL, there is no conformity between the experiment data with the sticking or slipping model in spite of a good liner relationship between D and η^{-1}.

5.1.6.2. Hole theory

Hole theory is used to explain the non-correlation of D in terms of classical model for the case of TCNE in [nmim][NTf_2], TTF in [hmim][NTf_2] and [bmim][PF_6], TEMPO and TEMPOL in all given ILs. The size of holes, r_{hole}, in each IL at a given temperature was calculated using Eq. 2.34. The value of hydrodynamic radius determined from Eq. 2.31. is called r_{SE}. The values of r_H and r_{SE} are listed in Tables 5.11 -5.13. For TEMPO and TEMPO there is a good conformity of r_{SE} and r_{hole} in low-viscous ILs. The results above leads to the applicability of using hole theory in explaining diffusion mechanisms of TEMPO and TEMPOL in ILs. However, the differences between the two values of radii become larger in high-viscous ILs. This is similar for TCNE and TTF in ILs at high viscosity. The reason for that may arise from the values of hole radii which are smaller or larger than the true value.

Table 5.11. The hydrodynamic radii r_{SE} (Å) and hole radii r_{hole} (Å) for TCNE and TTF in selected ILs.

TTF				TCNE	
[hmim][NTf_2]		[bmim][PF_6]		[hmim][NTf_2]	
r_{SE}	r_{hole}	r_{SE}	r_{hole}	r_{SE}	r_{hole}
1.5	1.8	1.2	1.5	1.5	1.8
1.3	1.8	1.4	1.6	1.5	1.8
1.4	1.9	1.4	1.6	1.5	1.9
1.6	1.9	1.3	1.6	1.4	1.9
1.6	1.9	1.4	1.7	1.5	1.9
1.7	2.0	1.5	1.7	1.6	2.0

Table 5.12. The hydrodynamic radii r_{SE} and hole radii r_{hole} for TEMPO in ILs.

TEMPO	[emim][NTf_2]		[emim][OTf]		[bmim][NTf_2]		[bmim][OTf]		[hmim][NTf_2]		[bmim][PF_6]	
T/ K	r_{SE}	r_{hole}	r_{SE}	r_{hole}	r_{SE}	r_{hole}	r_{SE}	r_{hole}	r_{SE}	r_{hole}	r_{SE}	r_{hole}
293	1.5	1.6	1.9	1.6	1.3	1.8	1.8	1.8	1.9	1.8	1.2	1.5
303	1.4	1.7	1.8	1.6	1.3	1.9	1.7	1.8	1.8	1.8	1.2	1.6
313	1.5	1.7	1.8	1.7	1.4	1.9	1.8	1.9	1.8	1.9	1.1	1.6
323	1.5	1.8	1.9	1.7	1.3	2.0		1.9	1.8	1.9	1.2	1.6
333	1.5	1.8	1.8	1.7	1.4	2.0		1.9	1.8	1.9	1.2	1.7
343	1.7	1.8	1.9	1.8	1.5	2.1		2.0	1.8	2.0	1.2	1.7

Table 5.13. The hydrodynamic radii r_{SE} and hole radii r_{hole} for TEMPOL in ILs.

TEMPOL	[emim][NTf_2]		[emim][OTf]		[bmim][NTf_2]		[bmim][OTf]		[hmim][NTf_2]		[bmim][PF_6]	
T/ K	r_{SE}	r_{hole}	r_{SE}	r_{hole}	r_{SE}	r_{hole}	r_{SE}	r_{hole}	r_{SE}	r_{hole}	r_{SE}	r_{hole}
293	1.8	1.6	1.9	1.6	1.8	1.8	1.8	1.8	2.6	1.8	1.3	1.5
303	1.8	1.7	1.9	1.6	1.7	1.9	1.6	1.8	2.4	1.8	1.3	1.6
313	1.8	1.7	2.1	1.7	1.8	1.9	1.5	1.9	2.4	1.9	1.3	1.6
323	2.0	1.8		1.7	1.8	2.0	1.6	1.9	2.5	1.9	1.3	1.6
333	1.9	1.8		1.7	1.8	2.0	1.8	1.9	2.5	1.9	1.3	1.7
343	1.9	1.8		1.8	1.9	2.1	1.6	2.0	2.5	2.0	1.3	1.7

5.2. Heterogeneous electron transfer rate constants k_{het}

5.2.1. Determining k_{het} using cyclic voltammetry

There are several approaches in determining k_{het} from cyclic voltammograms.

The first well- known method which calculate k_{het} from the separation of the anodic and cathodic potentials as a function of scan rate ν was published by Nicholson [138]:

$$k_{het} = \frac{\Psi}{\gamma^{\alpha}} \sqrt{\frac{\pi D_o n \nu F}{RT}} \tag{5.2}$$

where α is charge transfer coefficient, Ψ is a dimensionless parameter which can be calculated from the peak potential difference. γ is given by $(D_o/D_R)^{1/2}$ with D_o, D_R are diffusion coefficients of oxidant and reductant, respectively, for electron transfer reaction O + ne = R.

The second approach was suggested by Klinger and Kochi [139]:

$$k_{het} = 2.8 \left(\frac{D\beta nF\nu}{RT}\right)^{1/2} \exp\left[\frac{\beta^2 nF}{RT} (E_p^a - E_p^c)\right] \tag{5.3}$$

Good agreement between two methods is achieved.

A third approach was given by Gileadi in which the peak potential difference ΔE_p is plotted vs. log(ν) [140]. For lower scan rate, the horizontal curve is observed while at higher scan rate, a linear one was formed.

$$\log k_{het} = -0.48\,\alpha + 0.52 + \tfrac{1}{2} \log (nFD\alpha\nu_c/2.3\,RT) \tag{5.4}$$

Where ν_c is the critical scan rate obtained by extrapolating the linear curve.

In this work, Nicholson's method was used to calculate the k_{het}. There are several ways to calculate Ψ. Nicholson first tabulated the value of Ψ for the ΔE_p in the range of 60 -200 mV which is from reversible to irreversible process. However, this method does not work well for systems with very fast k_{het} or close to totally reversible mechanism.

The other empirical equation was introduced by Magno [141]:

$$\Psi = (-0.6288 + 0.0021\ X)/\ (1-0.017\ X) \tag{5.5}$$

$$\text{Where } X = \Delta E_p \times n$$

To the best of our knowledge, the relation between Ψ and ΔE_p was well described by Rüssel and this equation was used for all the calculation in this work [142]:

$$\Delta E_p = A + B\ \Psi^{-1} + C\ \Psi^{-2} + D\ \Psi^{-3} \tag{5.6}$$

$$\text{With } A = 81.34;\ B = -3.06\ ;\ C = 149;\ D = -145.5\ \text{mV}$$

Ohmic drop causes a considerable difference of ΔE_p between the values with and without iR correction. This leads a deviation in Ψ (table 5.14, 5.15) and finally in k_{het}. Therefore, when using cyclic voltamograms to determine k_{het}, the iR drop must be taken into account.

Table 5.14. Values of the dimensionless parameter Ψ for TEMPO in [bmim][NTf_2] at scan rate 500 mV/s with and without Ohmic drop correction.

T/K	ΔEp /mV	Ψ	ΔE / mV (iR correction)	Ψ (iR correction)
293	90.5	0.7	70	1.88
303	82.5	1.0	71	1.9
313	88	0.8	76	1.4
323	89	0.8	78	1.2
333	90	0.7	80	1.1
343	91	0.7	82	1.0

ΔE_p at different temperature can be computed using the experimental ΔE_p at room temperature by the following equation [143]:

$$\Delta E_p^T = \Delta E_p^{298} \times \frac{T}{298} \tag{5.7}$$

However, ΔE_p from the experiments shows the increase with temperature only for TCNE and TTF (Table 5.14). In contrast, for TEMPO and TEMPOL, ΔE_p

decreases with the increasing temperature (Table 5.15). Thus, in this work, the k_{het} of all the redox couples in ILs were calculated at different temperature using the experimental value of ΔE_p with iR correction. The values of k_{het} for TCNE, TTF, TEMPO, and TEMPOL in selected ILs are listed in Tables 5.16 - 5.18.

Table 5.15. Values of the dimensionless parameter Ψ for TEMPO in [bmim][NTf_2] at scan rate 500 mV/s with and without Ohmic drop correction.

T / K	ΔE_p /mV	Ψ	ΔE_p / mV (iR correction)	Ψ (iR correction)
293	148	0.207	99	0.55
303	136	0.2502	90	0.73
313	125	0.305	85	0.863
323	119	0.343	81	1.035
333	114	0.404	80	1.085
343	111	0.407	79	1.145

Table 5.16. k_{het} (cm/s) for TCNE in ILs at a range temperature of 293 -343 K.

T / K	[emim][NTf_2]	[bmim][NTf_2]	[hmim][NTf_2]	[bmim][BF_4]	[bmim][PF_6]
293	0.0082	0.0043	0.0024	0.0024	0.0006
303	0.0091	0.0049	0.0036	0.0030	0.0010
313	0.0098	0.0054	0.0049	0.0033	0.0014
323	0.0105	0.0060	0.0068	0.0039	0.0017
333	0.0114	0.0068	0.0089	0.0047	0.0024
343	0.0120	0.0073	0.0120	0.0053	0.0032

Table 5.17. k_{het} (cm/s) for TTF in ILs at a range temperature of 293 -343 K.

T / K	[bmim][NTf_2]	[hmim][NTf_2]	[bmim][BF_4]	[bmim][PF_6]
293	0.0083	0.0044	0.0045	0.0021
303	0.0088	0.0061	0.0048	0.0025
313	0.0094	0.0074	0.0053	0.0028
323	0.0101	0.0095	0.0059	0.0032
333	0.0107	0.0109	0.0063	0.0033
343	0.0113	0.0121	0.0068	0.0039

Table 5.18. k_{het} (cm/s) for TEMPO in ILs at a range temperature of 293 -343 K.

T / K	[emim][NTf_2]	emim][OTf]	[bmim][NTf_2]	[bmim][OTf]	[hmim][NTf_2]	[bmim][PF_6]
293	0.0075	0.0047	0.0037	0.0011	0.0017	0.0005
303	0.0089	0.0060	0.0049	0.0016	0.0027	0.0008
313	0.0112	0.0074	0.0065	0.0023	0.0042	0.0013
323	0.0141	0.0090	0.0094		0.0061	0.0020
333	0.0171	0.0107	0.0125		0.0080	0.0027
343	0.0202	0.0133	0.0156		0.0103	0.0038

Table 5.19. k_{het} (cm/s) for TEMPOL in ILs at a range temperature of 293 -343 K.

T / K	[emim][NTf_2]	[emim][OTf]	[bmim][NTf_2]	[bmim][OTf]	[hmim][NTf_2]	[bmim][PF_6]
293	0.0040	0.0038	0.0028	0.0017	0.0017	0.0006
303	0.0052	0.0052	0.0040	0.0024	0.0029	0.0011
313	0.0068	0.0068	0.0054	0.0033	0.0040	0.0014
323	0.0091		0.0079	0.0044	0.0060	0.0023
333	0.0133		0.0102	0.0053	0.0080	0.0036
343	0.0171		0.0126	0.0071	0.0101	0.0054

5.2.2. Failure to determine k_{het} by using steady-state voltammogram

In an attempt to apply an easy and precise method to evaluate k_{het} in ILs, steady-state voltammetry was tested.

Kinetic parameters can be easily calculated by using the potential differences $E_{1/4}$-$E_{1/2}$ and $E_{1/2}$-$E_{3/4}$ where $E_{1/2}$, $E_{1/4}$, $E_{3/4}$ are potentials corresponding to the current $i_{ss}/2$; $i_{ss}/4$; $3\times i_{ss}/4$. The kinetic parameters are tabulated by a method from Mirkin and Bard depending on geometry of electrochemical systems [144].

However, for the investigated system, the precision of $\Delta E_{1/4}$ and $\Delta E_{3/4}$ is higher than 0.5 mV which leads to the difficulty in using the method above. In some cases, the values $\Delta E_{1/4}$ and $\Delta E_{3/4}$ reach the lower limit causing high uncertainties in value of k_{het}. The upper limit for k_{het} for this method is around 0.05 cm/s.

5.2.3. Heterogeneous electron transfer rate constant and viscosity

Electron transfer in organic solvent is much faster than in IL. For example, k_{het} of TTF in ACN is 2.2 cm/s [127] which is 2 -3 orders of magnitude higher than that in ILs. The high k_{het} was also observed for low-viscous IL (Table 5.16 -5.18). To find out whether k_{het} is dependent on viscosity, the following equation was used:

$$k_{het} \propto \eta^{-\beta} \tag{5.9}$$

with β is an empirical parameter ($0 < \beta \leq 1$) and 1 for solvent friction limit.

Plots of $\ln(k_{het})$ vs. $\ln 1/\eta$ for TCNE, TTF, TEMPO and TEMPOL are shown in Fig. 5.53. It can be easily seen that the value of k_{het} is smallest in highest-viscous IL, [bmim][PF_6] and largest in lowest-viscous IL, [emim][NTf_2]. In general, k_{het} is proportional to the inverse of viscosity which indicates the effect of solvent dynamic on the electron transfer rate constant.

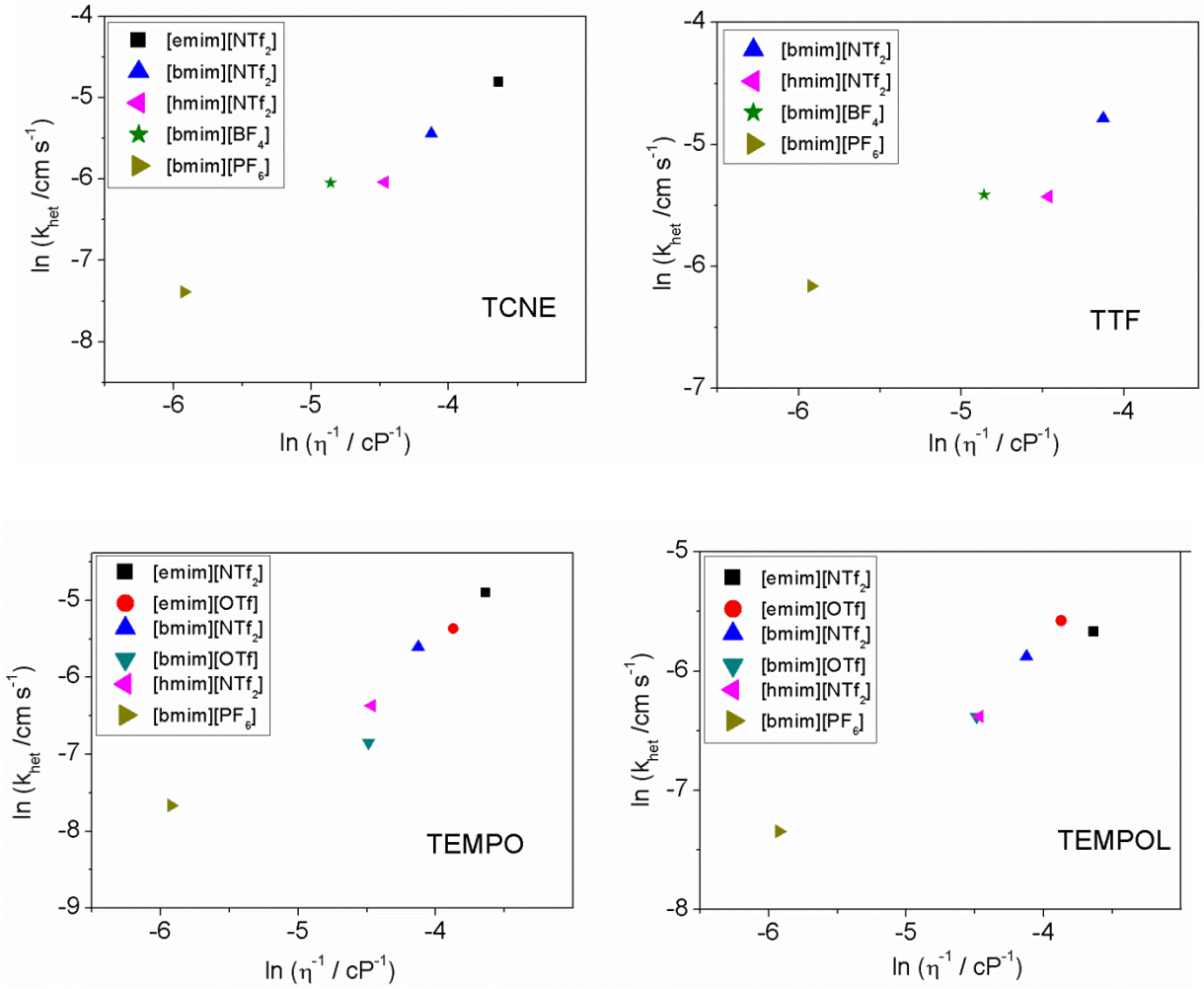

Figure 5.53. Plots of $\ln k_{het}$ vs. $\ln 1/\eta$ for TCNE, TTF, TEMPO and TEMPOL in ILs at 293 K.

5.2.4. Does Marcus theory work in ionic liquids?

In Marcus theory, the rate constant, khet, can be described by:

$$k_{het} = \kappa_{el} Z_{het} \exp\left(\frac{-\Delta G^*}{RT}\right) \tag{5.10}$$

where Z_{het} is the collision number at the electrode wich is described in the previous section in Eq. 2.17.

$$Z_{het} = \sqrt{\frac{kT}{2\pi M}} \tag{5.11}$$

From Eqs. 5.10 and 5.11, activation energy can be extracted in the following equation:

$$\frac{k_{het}}{\sqrt{T}} = \sqrt{\frac{k}{2\pi M}}\,\kappa_{el}\,\exp\left(\frac{-\Delta G^*}{RT}\right) \qquad (5.12)$$

ΔG^* was then calculated from the plots of ln ($k_{het}T^{-1/2}$) vs. T^{-1}.

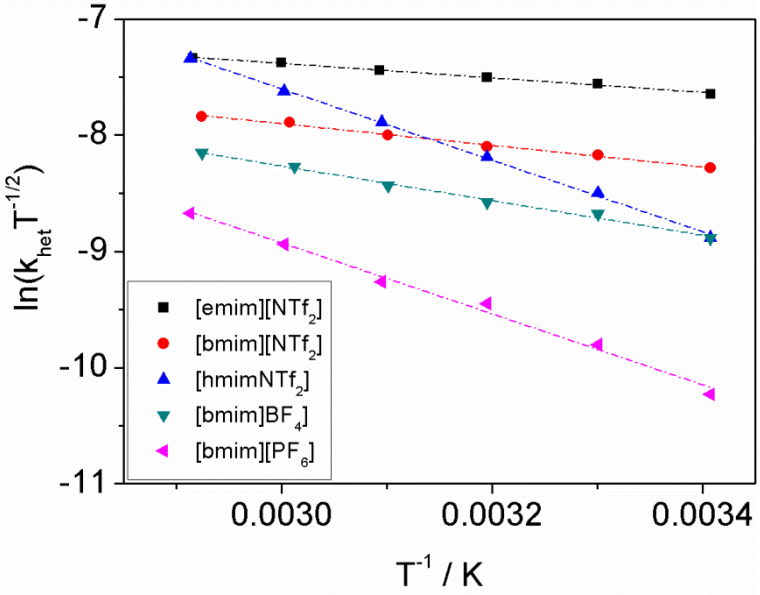

Figure 5.54. Plots of ln($k_{het}T^{-1/2}$) vs. T^{-1} for TCNE in selected ILs.

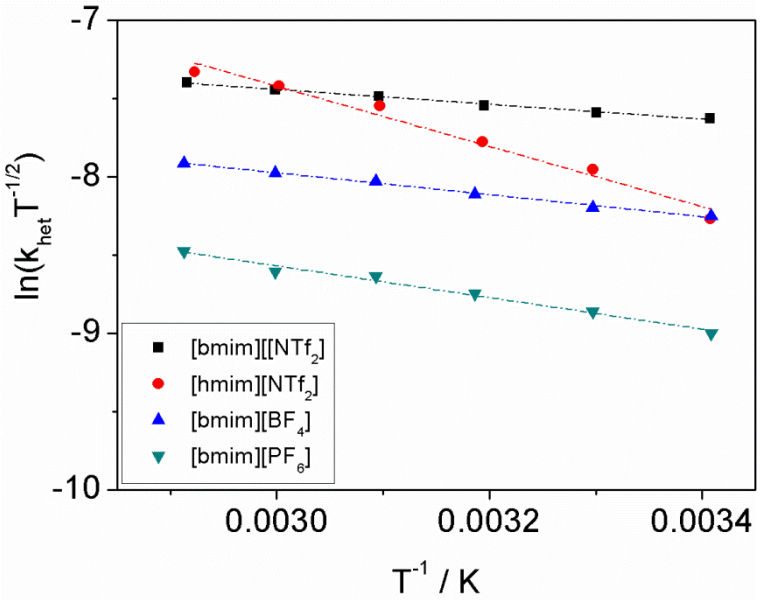

Figure 5.55. Plots of ln($k_{het}T^{-1/2}$) vs. T^{-1} for TTF in selected ILs.

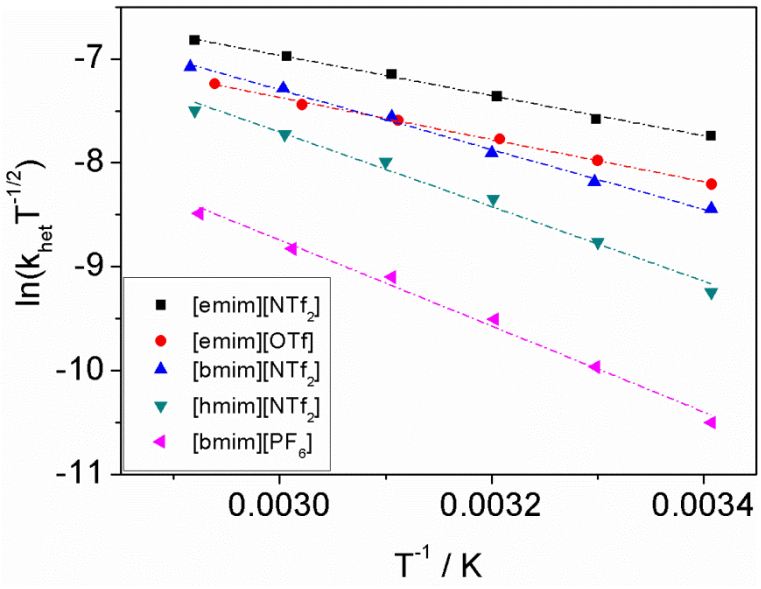

Figure 5.56. Plots of $\ln(k_{het}T^{-1/2})$ vs. T^{-1} for TEMPO in selected ILs.

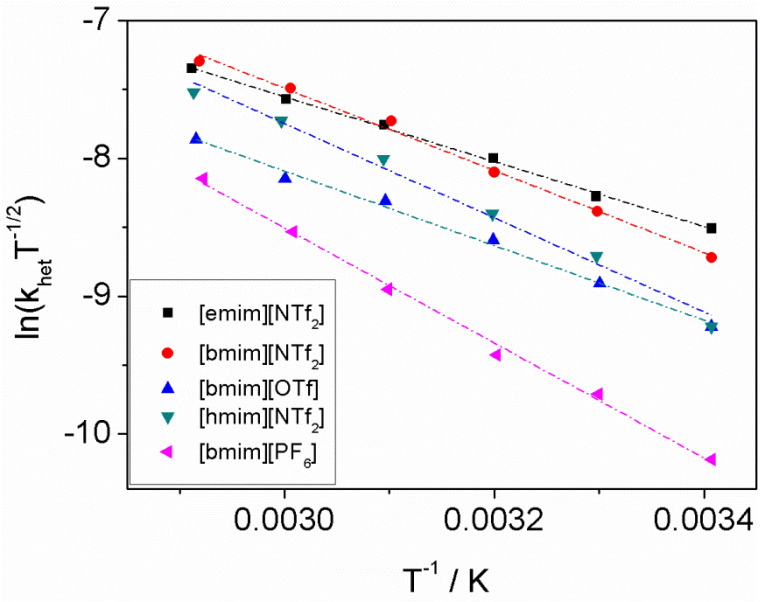

Figure 5.57. Plots of $\ln(k_{het}T^{-1/2})$ vs. T^{-1} for TEMPOL in selected ILs.

Figs. 5.54 - 5.57 present the relationship between ln $(k_{het}T^{-1/2})$ and T^{-1} for TCNE, TTF, TEMPO and TEMPOL in ILs. The slopes of these lines increase with the increase in viscosity of ILs except for TCNE and TTF in [hmim][NTf_2]. From the slope of those lines, ΔG^*_{exp} of electron transfer of all the compounds were caculated and listed in Tables 5.20 - 5.23. In the same IL, ΔG^*_{exp} is in the following order: TTF < TCNE < TEMPO ~ TEMPOL which agrees well with the

order of inner sphere reorganization energy λ_i. Using the value of ΔG^*_{exp}, the differences in the value of k_{het} of different substances in the same IL can be easily explained. For example, from Table 5.24. the order of k_{het} in [bmim][NTf_2] is in the range of TEMPOL < TEMPO < TCNE < TTF which is comparable to the reverse of ΔG^*_{exp} (Eq. 2.7) with TEMPOL (24.8 ± 0.9 > TEMPO (23.9 ± 0.8) > TCNE (7.8 ± 0.3) > TTF (3.9 ± 0.2).

Table 5.20. Values of ΔG^*_{exp}, λ_i, λ_o (calculated) of electron transfer reaction of TCNE in ILs in kJ/mol.

Ils	ΔG^*_{exp}	$\lambda_i/4$	$\lambda_o/4$ Marcus[a]	$\lambda_o/4$ Hush[b]	λ_{IL}	Eη
[emim][NTf_2]	5.2±0.2	1.6	11.5	23.0	3.6	24.7±0.4[c]
[bmim][NTf_2]	7.8±0.3	1.6	11.8	23.5	6.2	27.9±0.7[c]
[hmim][NTf_2]	26±1	1.6	11.5	23.0	24.4	32.2±0.6[c]
[bmim][BF_4]	12.4±0.5	1.6	12.0	23.9	10.8	38±2[c]
[bmim][PF_6]	25±1	1.6	12.4	24.7	23.4	40±1 [c]

[a] calculated from Eq. 2.15 with $d_{het} = 2r$
[b] calculated from Eq. 2.15 with $d_{het} = \infty$
[c] from our measurements

Table 5.21. Values of ΔG*, λi, λo (calculated) of electron transfer reaction of TTF in ILs in kJ/mol.

Ils	ΔG^*_{exp}	λi/4	$\lambda_o/4$ Marcus	$\lambda_o/4$ Hush	λ_{IL}	Eη
[bmim][NTf_2]	3.9±0.2	1.6	12.0	24.0	2.3	27.9±0.7
[hmim][NTf_2]	16±1	1.6	11.7	23.5	14.4	32.2±0.6
[bmim][BF_4]	5.8±0.2	1.6	12.2	24.4	4.2	38±2
[bmim][PF_6]	8.4±0.5	1.6	12.6	25.2	6.8	40±1

Table 5.22. Values of ΔG*, λi, λo (calculated) of electron transfer reaction of TEMPO in ILs in kJ/mol.

Ils	ΔG^*_{exp}	$\lambda_i/4$	$\lambda_o/4$ Marcus	$\lambda_o/4$ Hush	λ_{IL}	E_η
[emim][NTf_2]	16.1±0.5	5.8	9.6	19.1	10.3	24.7±0.4
[emim][OTf]	16.9±0.4	5.8	9.9	19.8	11.1	24.1±0.9[126]
[bmim][NTf_2]	23.9±0.8	5.8	9.8	19.5	18.1	27.9±0.7
[bmim][OTf]	28.9±0.6	5.8	9.5	18.9	23.1	29.5±0.8[84]
[hmim][NTf_2]	29±1	5.8	9.6	19.1	23.6	32.2±0.6
[bmim][PF_6]	34 ±2	5.8	10.3	20.6		40±1

Table 5.23. Values of ΔG*, λi, λo (calculated) of electron transfer reaction of TEMPOL in ILs in kJ/mol.

Ils	ΔG^*_{exp}	$\lambda_i/4$	$\lambda_o/4$ Marcus	$\lambda_o/4$ Hush	λ_{IL}	E_η
[emim][NTf_2]	19.6±0.4	5.7	9.1	18.3	13.9	24.7±0.4
[emim][OTf]	22±0.4	5.7	9.5	19.0	16.3	24.1±0.9[126]
[bmim][NTf_2]	24.8±0.9	5.7	9.3	18.7	19.1	27.9±0.7
[bmim][OTf]	22.5±0.8	5.7	9.0	18.1	16.8	29.5±0.8[84]
[hmim][NTf_2]	28 ±1	5.7	9.2	18.3	22.7	32.2±0.6
[bmim][PF_6]	35±1	5.7	9.8	19.7	29.3	40±1

Table 5.24. Values of k_{het} of TCNE, TTF, TEMPO, TEMPOL in selected ILs in kJ/mol.

	k_{het} / cm s^{-1}			
ILs	TCNE	TTF	TEMPO	TEMPOL
[bmim][NTf_2]	0.0043	0.0083	0.0037	0.0028
[hmim][NTf_2]	0.0024	0.0044	0.0017	0.0017
[bmim][PF_6]	0.0006	0.0021	0.0005	0.0006

The inner sphere organization energy λ_i was taken from Ref. [145]. Unfortunately, the outer sphere organization energy λ_o in ILs can not be calculated using the continuum model in section 2.1.4.2. This model in fact considers the solvent reorganization based on polarization of solvent molecules which is not suitable for ILs (Fig. 5.58). Indeed, there is no correlation between ΔG^*_{exp} and $(\lambda_i + \lambda_o)/4$ where λ_o was calculated by Eq. 2.15 by using Marcus and Hush models using the values of n_D, ε_s from literature (Tables 5.20 - 5.23). The value of ΔG^*_{exp} is so much smaller than $(\lambda_i + \lambda_o)/4$ in all ILs.

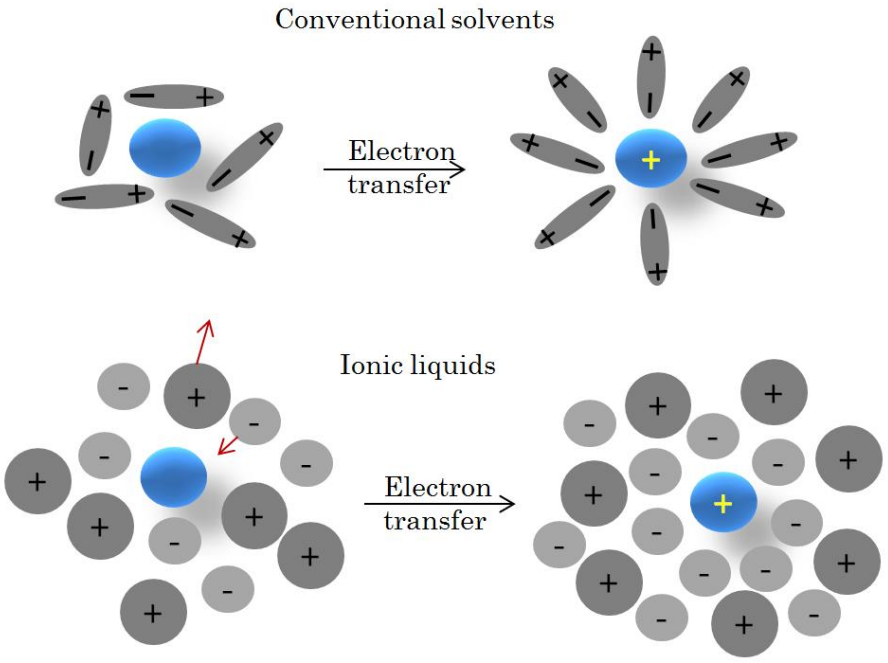

Figure 5.58. Reorientations of solvent molecules during electron transfer in conventional solvents in comparison to ILs.

Table 5.25. Values of refractive index n_D and dielectric constant ε_s of ILs at 298 K.

ILs	[emim][NTf_2]	[emim][OTf]	[bmim][NTf_2]	[bmim][OTf]	[hmim][NTf_2]	[bmim][BF_4]	[bmim][PF_6]
n_D	1.423[80]	1.433[80]	1.427[80]	1.438[80]	1.429[146]	1.42[147]	1.409[147]
ε_s	12[148]	16.5[148]	14[148]	12.9[148]	12.7[149]	14.6[149]	16.1[149]

Composing entirely ions, ILs has no reorientation in dipole moment during electron transfer (Fig. 5.58). Thus, the term 'relaxation' does not exist for electron transfer in IL. The activation energy in this case may include energy in changing bond length and angle of reactant; energy for diffusing cation and anion, the

energy difference between the interaction between reactant ILs before and after electron transfer. Therefore, to understand more the relation between ΔG^{*}_{exp} and the other components beside λ_i, another term λ_{IL} was defined in the following equation:

$$\Delta G^{*}_{exp} = \lambda_i/4 + \lambda_{IL} \qquad (5.13)$$

λ_{IL} was calculated and listed in Tables 5.20 - 5.23. λ_{IL} in all cases increase with the increase in activation energy of viscosity E_η. Plots of λ_{IL} vs. E_η were used to confirm this relationship (Fig. 5.59). In general, for TCNE, TEMPO and TEMPOL, λ_{IL} increases with the increase of E_η which suggest the effect of solvent dynamic on the electron transfer. The higher viscosity cause higher activation energy for diffusing ions leading to a larger activation energy of electron transfer.

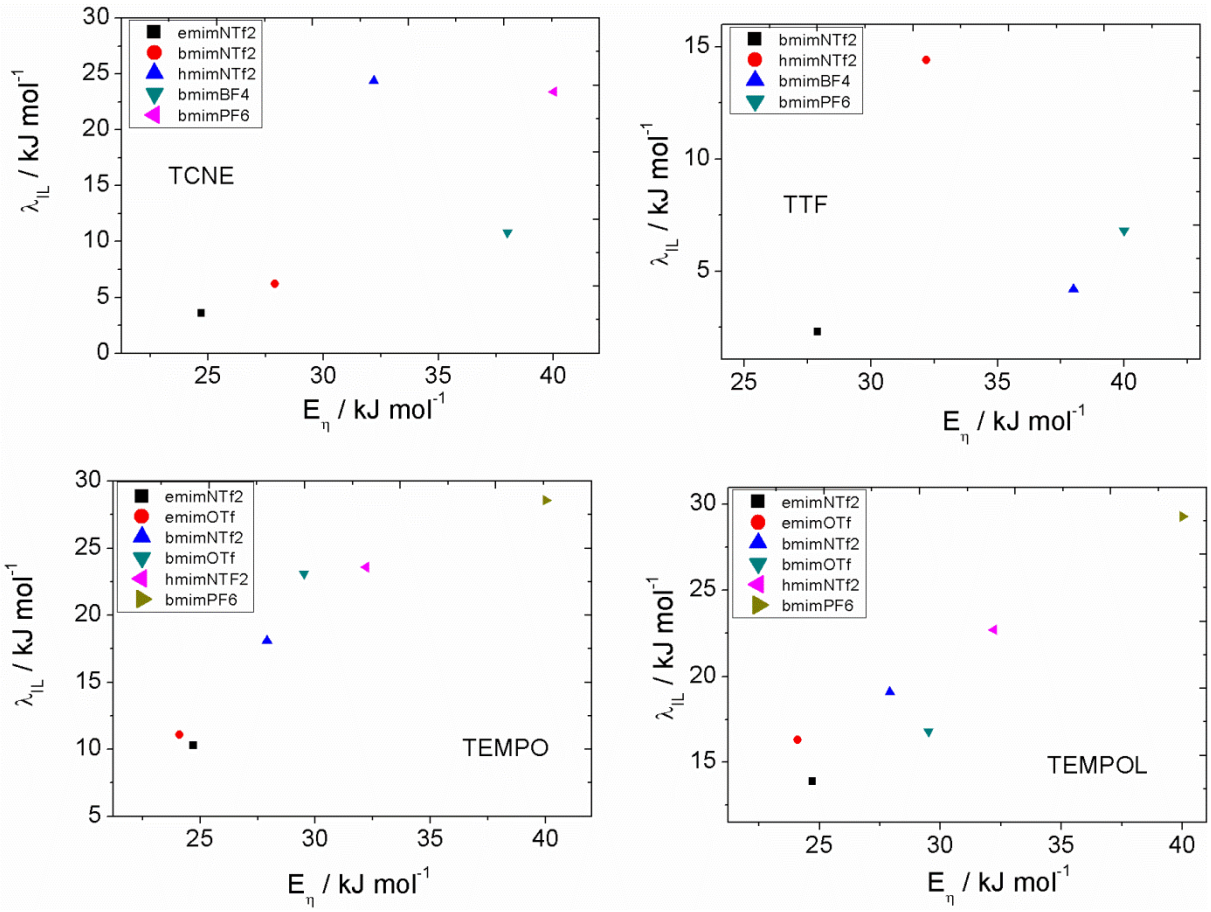

Figure 5.59. Plots of λ_{IL} vs. E_η for all compounds in ILs.

6. Conclusions and Outlook

6.1. Conclusions

The aim of this work is to get insight into the diffusion and electron transfer of redox species in eight different imidazolium-based ionic liquids which contain following cations: 1-ethyl-3-methylimidazolium [emim], 1-butyl-3-methylimidazolium [bmim], and 1-hexyl-3-methylimidazolium [hmim] and anions: bis(trifluoromethylsulfonyl)imide [NTf_2], tetrafluoroborate [BF_4], hexafluorophosphate [PF_6], trifluoromethanesulfonate [OTf] and dicyanamine [dca]. The electrochemical probes were chosen include acceptors and donors such as: tetracyanoethylene (TCNE), tetrathiafulvalene (TTF) and its radical cation ($TTF^{\cdot+}$), and 2,2,6,6-tetramethylpiperidine-1-oxyl (TEMPO) and 4-hydroxy-2,2,6,6-tetramethylpiperidine-1-oxyl (TEMPOL).

Impurities in ILs may react with the compounds leading to deviations in the true concentration. This is the case for TCNE with ILs from commercial company without any purification. Non-miscible ILs were purified to remove 1-methyimimdazole before making any solution of TCNE. Solutions of TCNE in purified-ILs give no change colour. The other impurity which causes most difficulties when using IL is water. ILs were dried under high vacuum diffusion pump with the pressure 2-6 105 at 323 K for 24h. The temperature during drying must be lower than 323 K for the [BF_4] and [PF_6] containg ILs due to the hydrolysis of those anions in the presence of water at high temperature. The water content was checked by NIR spectroscopy. The density and viscosity of some ILs were measured and the results compare well with the values from literature.

The organic substances were dissolved directly in ILs by magnetic stirring for 1-2h. The evaporation method of solutions in organic solvents was not used due to the evaporation of compounds under vacuum, especially for TEMPO and TEMPOL which have low volatile pressures. Because of high viscosities of ILs, only the weights were used to calculate the concentration instead of the volume. The sustances concentrations were checked by using UV-Vis spectroscopy. In

addition, the results also show that identity of molecule are similar in both ILs and organic solvents.

Electrochemical measurements were done using two different self-constructed temperature-controlled cells useable for small volumes. The first cell was used for measuring cyclic voltammetry (CV) at millimeter diameter working electrode. Steady-state voltammetry (SSV) was done using the second cell contruction for micrometer –working electrodes. Ohmic drop is a big challenge when using CV. IR drop of all ILs at were measured different temperatures using impedance method. The remaining resistance was used later in correcting all the CV before doing any further analysis. Choosing the optimal scan rate for CV and SSV measurements also were considered in detail. For CV, the scan rates were chosen in the range of 100-1100 mV/s to avoid any aggregation of products on the surface of electrode due to the viscous solvent. For SSV, the scan rates were chosen carefully due to the sluggish mass transfer in ILs. In order to get a good signal/noise ratio the concentration of redox species in ILs were larger than 5mM.

Diffusion coefficients of TCNE, TTF and its radical cation $TTF^{\cdot+}$, TEMPO and TEMPOL were investigated over a range of temperature in eight ILs using cyclic and steady-state voltammetry (the latter only for TTF and TEMPO). The diffusions of TTF and $TTF^{\cdot+}$ were also studied in the organic solvents, acetonitrile and sulfolane. SSV in ILs must be done under long-time measuring conditions. That can cause convection effects. The values of D from the two methods give similar results. For TTF, the values from SSV are slightly larger which may attributed to the convection. For TEMPO, the values from SSV are equal or a bit smaller due to a tiny evaporation of TEMPO at high temperature at long-time scale. Diffusion coefficients of all substances in ILs were then analyzed under the effects of concentration, temperature, nature of species, and viscosity. Diffusion coefficients are independent on concentration. In fact, measurements of CV of TTF and $TTF^{\cdot+}$ at different concentration showed a good linear between the peak currents and concentration. Thus, it is possible to get the value of diffusion coefficients at one concentration. The dependence of the diffusion coefficients on temperature were in in agreement with Arrhenius-type relationship in the range

of temperature used. The activation energies of diffusion of TCNE, TTF, $TTF^{\cdot+}$, TEMPO, and TEMPOL in each IL as well as the activation energy of the relevant IL, are similar indicating the same kind of movement of those species in ILs. In the same IL, the diffusion coefficients is in the order: TCNE < TTF ≈ TEMPO < TEMPOL. Size and weight of diffusing molecule have no significant effect on the diffusion in ILs. The interaction between solute and ILs plays an important role in diffusion in ILs. Indeed, having a smallest radius and lightest weight in the four given compounds, TCNE has the lowest value of D. Especially in the case of TTF and its radical cation $TTF^{\cdot+}$, the values of the diffusion coefficients of $TTF^{\cdot+}$ were found to be half as big as those of TTF in five ILs. The ratio of $TTF^{\cdot+}$ and TTF values at 293 K is 0.43-0.62 in five different ILs, as compared to 0.90 in acetonitrile and 0.67 in a viscous organic solvent, sulfolane. The differences of these two values in ILs were observed to be higher than in acetonitrile, reflecting the important role of solvation in ILs. Therefore, the approximation of equal diffusion of TTF and $TTF^{\cdot+}$ in ILs in further calculations must be considered carefully. Finally, diffusion was analyzed in terms of Stokes-Einstein and Sutherland equations. The traditional plots of D vs η^{-1} of all the substances gave a good linear relationship. In order to get any conclusion about the agreement between experimental results and classical model, another plots of $D \times \eta$ vs. η were made. For the case of TTF and $TTF^{\cdot+}$, diffusion of TTF follows 'slip condition' while $TTF^{\cdot+}$ obeys 'stick condition' in most ILs. However, there was no clear correlation for TCNE, TEMPO and TEMPOL. In attempt to explain the observed results, hole theory was used. In most cases, a good agreement between the hole radius and hydrodynamic radius is observed. In high –viscous ILs, the discrepancies of those values become larger.

Heterogeneous rate constants (k_{het}) of electron transfer of TCNE, TTF, TEMPO and TEMPOL were determined using cyclic voltammetry. As mentioned before, iR drop must be compensated especially in calculating k_{het} due to the large deviation of the potential differences between with and without Ohmic correction. k_{het} depends on viscosity of ILs. k_{het} is small in a viscous IL. The value of k_{het} in organic solvents is 2-3 order of magnitudes larger than that in ILs. Activation energies of

electron transfer reactions are then calculated from the slope of $\ln(k_{het}/T^{-1/2})$ vs. T^{-1}. The values of reorganization energies calculated from Marcus theory give no relation to the experimental activation energies. The activation energies are correlated to the activation energies of viscous flow of ILs. Therefore, Marcus theory for outer-sphere reorganization energy breaks down in ILs.

6.2. Outlook

The assumption of equal values of diffusion coefficient of the neutral form and its radical ions has been used widely in many equations for the conventional solvents. It seems not to be wise in ILs. The differences are confirmed as described in the literature. However, the investigation limits in radical cation because of the unstability of radical anion. In this work, another effort in measuring D of a neutral form and its radical anion of other substances was made for TCNE. Unfortunately, $TCNE^{\cdot-}$ forms dimer in ILs. Therefore, it is necessary to find out more systems to study the effect of nature of substances in diffusion ILs.

The diffusion of some substances obey either the classical model or hole theory. To answer these questions, more diffusion coefficients must be investigated in a number of redox compounds and in a wide variety of ILs as well as of high viscous organic solvents. In parallel, theoretical studies based on interactions of solute and ILs also give a better understanding of diffusion in ILs.

In addition, methods for measuring fast electron transfer reaction is also required.

The outer-sphere reorganization energy of electron transfer in ILs is still a big problem. How do the ILs reorganize during electron transfer? Is viscosity the major factor that effects on activation energy of this process?. More theoretical and experimental studies on dielectric constant of ILs and reorganization energy of electron transfer in ILs are necessary.

7. References

[1] D.R. MacFarlane, M. Forsyth, P.C. Howlett, J.M. Pringle, J. Sun, G. Annat, et al., Ionic liquids in electrochemical devices and processes: managing interfacial electrochemistry., Acc. Chem. Res. 40 (2007) 1165–1173. doi:10.1021/ar7000952.

[2] N. V Plechkova, K.R. Seddon, Applications of ionic liquids in the chemical industry., Chem. Soc. Rev. 37 (2008) 123–150. doi:10.1039/b006677j.

[3] J.P. Hallett, T. Welton, Room-temperature ionic liquids: solvents for synthesis and catalysis. 2., Chem. Rev. 111 (2011) 3508–3576. doi:10.1021/cr1003248.

[4] R.G. Evans, O. V Klymenko, P.D. Price, S.G. Davies, C. Hardacre, R.G. Compton, A comparative electrochemical study of diffusion in room temperature ionic liquid solvents versus acetonitrile., Chemphyschem. 6 (2005) 526–533. doi:10.1002/cphc.200400549.

[5] M.J.A. Shiddiky, A.A.J. Torriero, C. Zhao, I. Burgar, G. Kennedy, A.M. Bond, Nonadditivity of Faradaic currents and modification of capacitance currents in the voltammetry of mixtures of ferrocene and the cobaltocenium cation in protic and aprotic ionic liquids., J. Am. Chem. Soc. 131 (2009) 7976–7989. doi:10.1021/ja8092295.

[6] M.J.A. Shiddiky, A. a J. Torriero, J.M. Reyna-González, A.M. Bond, Nonadditivity of faradaic currents and modification of double layer capacitance in the voltammetry of mixtures of ferrocene and ferrocenium salts in ionic liquids., Anal. Chem. 82 (2010) 1680–1691. doi:10.1021/ac9020159.

[7] E.I. Rogers, D.S. Silvester, D.L. Poole, L. Aldous, C. Hardacre, R.G. Compton, Voltammetric Characterization of the Ferrocene|Ferrocenium and Cobaltocenium|Cobaltocene Redox Couples in RTILs, J. Phys. Chem. C. 112 (2008) 2729–2735. doi:10.1021/jp710134e.

[8] M. a Vorotyntsev, V. a Zinovyeva, D. V Konev, M. Picquet, L. Gaillon, C. Rizzi, Electrochemical and spectral properties of ferrocene (Fc) in ionic liquid: 1-butyl-3-methylimidazolium triflimide, [BMIM][NTf(2)]. Concentration effects., J. Phys. Chem. B. 113 (2009) 1085–1099. doi:10.1021/jp809095q.

[9] Y. Wang, E.I. Rogers, R.G. Compton, The measurement of the diffusion coefficients of ferrocene and ferrocenium and their temperature dependence in acetonitrile using double potential step microdisk electrode chronoamperometry, J. Electroanal. Chem. 648 (2010) 15–19. doi:10.1016/j.jelechem.2010.07.006.

[10] R.G. Evans, O. V. Klymenko, S.A. Saddoughi, C. Hardacre, R.G. Compton, Electroreduction of Oxygen in a Series of Room Temperature Ionic Liquids Composed of Group 15-Centered Cations and Anions, J. Phys. Chem. B. 108 (2004) 7878–7886. doi:10.1021/jp031309i.

[11] M. Matsumiya, M. Terazono, K. Tokuraku, Temperature dependence of kinetics and diffusion coefficients for ferrocene/ferricenium in ammonium-imide ionic liquids, Electrochim. Acta. 51 (2006) 1178–1183. doi:10.1016/j.electacta.2005.06.006.

[12] A.W. Taylor, F. Qiu, J. Hu, P. Licence, D.A. Walsh, Heterogeneous electron transfer kinetics at the ionic liquid/metal interface studied using cyclic voltammetry and scanning electrochemical microscopy., J. Phys. Chem. B. 112 (2008) 13292–13299. doi:10.1021/jp8024717.

[13] R.G. Evans, O. V. Klymenko, C. Hardacre, K.R. Seddon, R.G. Compton, Oxidation of N,N,N′,N′-tetraalkyl-para-phenylenediamines in a series of room temperature ionic liquids incorporating the bis(trifluoromethylsulfonyl)imide anion, J. Electroanal. Chem. 556 (2003) 179–188. doi:10.1016/S0022-0728(03)00343-7.

[14] M. Zistler, P. Wachter, P. Wasserscheid, D. Gerhard, a. Hinsch, R. Sastrawan, et al., Comparison of electrochemical methods for triiodide diffusion coefficient measurements and observation of non-Stokesian diffusion behaviour in binary mixtures of two ionic liquids, Electrochim. Acta. 52 (2006) 161–169. doi:10.1016/j.electacta.2006.04.050.

[15] A.W. Taylor, P. Licence, A.P. Abbott, Non-classical diffusion in ionic liquids., Phys. Chem. Chem. Phys. 13 (2011) 10147–10154. doi:10.1039/c1cp20373h.

[16] K.R.J. Lovelock, A. Ejigu, S.F. Loh, S. Men, P. Licence, D.A. Walsh, On the diffusion of ferrocenemethanol in room-temperature ionic liquids: an electrochemical study., Phys. Chem. Chem. Phys. 13 (2011) 10155–10164. doi:10.1039/c1cp20392d.

[17] S.R. Belding, N.V. Rees, L. Aldous, C. Hardacre, R.G. Compton, Behavior of the Heterogeneous Electron-Transfer Rate Constants of Arenes and Substituted Anthracenes in Room-Temperature Ionic Liquids, J. Phys. Chem. C. 112 (2008) 1650–1657. doi:10.1021/jp7103598.

[18] N. Fietkau, A.D. Clegg, R.G. Evans, C. Villagrán, C. Hardacre, R.G. Compton, Electrochemical rate constants in room temperature ionic liquids: the oxidation of a series of ferrocene derivatives., Chemphyschem. 7 (2006) 1041–1045. doi:10.1002/cphc.200500709.

[19] A.A. Kornyshev, Double-layer in ionic liquids: paradigm change?, J. Phys. Chem. B. 111 (2007) 5545–5557. doi:10.1021/jp067857o.

[20] W.F. Libby, Theory of Electron Exchange Reactions in Aqueous Solution, J. Phys. Chem. 56 (1952) 863–868. doi:10.1021/j150499a010.

[21] R.A. Marcus, Electrostatic Free Energy and Other Properties of States Having Nonequilibrium Polarization. I, J. Chem. Phys. 24 (1956) 979–989. doi:10.1063/1.1742724.

[22] R.A. Marcus, On the Theory of Oxidation-Reduction Reactions Involving Electron Transfer. I, J. Chem. Phys. 24 (1956) 966–978. doi:10.1063/1.1742723.

[23] R. a. Marcus, On the Theory of Oxidation-Reduction Reactions Involving Electron Transfer. II. Applications to Data on the Rates of Isotopic Exchange Reactions, J. Chem. Phys. 26 (1957) 867–871. doi:10.1063/1.1743423.

[24] R.A. Marcus, ON THE T HEORY OF ELECTROCHEMICAL AND CHEMICAL ELECTRON TRANSFER PROCESSES, Can. J. Chem. 37 (1959) 155–169.

[25] R.A. Marcus, Exchange reactions and electron transfer reactions including isotopic exchange. Theory of oxidation-reduction reactions involving electron transfer. Part 4.?A statistical-mechanical basis for treating contributions from solvent, ligands, and inert salt, Discuss. Faraday Soc. 29 (1960) 21 –31. doi:10.1039/df9602900021.

[26] N.S. Hush, Adiabatic theory of outer sphere electron-transfer reactions in solution, Trans. Faraday Soc. 57 (1961) 557–580. doi:10.1039/tf9615700557.

[27] R.A. Marcus, On the Theory of Electron-Transfer Reactions. VI. Unified Treatment for Homogeneous and Electrode Reactions, J. Chem. Phys. 43 (1965) 679–701. doi:10.1063/1.1696792.

[28] R.A. Marcus, Electron transfer reactions in chemistry . Theory and experiment, Pure Appl. Chem. 69 (1997) 13–29.

[29] B.S. Brunschwig, N. Sutin, Energy surfaces, reorganization energies, and coupling elements in electron transfer, Coord. Chem. Rev. 187 (1999) 233–254. doi:10.1016/S0010-8545(98)00255-0.

[30] L.D. Zusman, The theory of electron transfer reactions in solvents with two characteristic relaxation times l.d. zusman, Chem. Phys. 119 (1988) 51–61.

[31] M.J. Weaver, Dynamical Solvent Effects on Activated Electron-Transfer Reactions: Principles, Pitfalls, and Progresst, Chem. Rev. 92 (1992) 463–480.

[32] G.J. Kavarnos, Fundamentals of Photoinduced Electron Transfer, VCH, New York, 1993.

[33] M.J.W. and F.C. Anson, Distinguishing between Inner- and Outer-sphere electrode reactions. Reactivity patterns for some Chromium (III)-Chromium (II) electron-transfer reactions at mercury electrodes, Inorg. Chem. 15 (1976) 1871–1881.

[34] M.J.F.C.A. Weaver, Simple criteria for distinguishing between Inner- and Outer-Sphere electrode reaction mechanism, J. Am. Chem. Soc. (1975) 4403–4405.

[35] S. Tanimoto, A. Ichimura, Discrimination of Inner- and Outer-Sphere Electrode Reactions by Cyclic Voltammetry Experiments, J. Chem. Educ. 90 (2013) 778–781. doi:10.1021/ed200604m.

[36] S.F. Nelsen, M.D. Newton, Estimation of Electron Transfer Distances from AM1 Calculations, J. Phys. Chem. A. 104 (2000) 10023–10031. doi:10.1021/jp002211w.

[37] I. Rips, J. Jortner, Dynamic solvent effects on outer-sphere electron transfer, J. Chem. Phys. 87 (1987) 2090. doi:10.1063/1.453184.

[38] I. Rips, J. Jortner, Outer sphere electron transfer in polar solvents. Activationless and inverted regimes, J. Chem. Phys. 87 (1987) 6513. doi:10.1063/1.453434.

[39] M. Bixon, J. Jortner, Solvent relaxation dynamics and electron transfer, Chem. Phys. 176 (1993) 467–481. doi:10.1016/0301-0104(93)80255-8.

[40] H. Sumi, R. a. Marcus, Dynamical effects in electron transfer reactions, J. Chem. Phys. 84 (1986) 4894. doi:10.1063/1.449978.

[41] J.R. Miller, L.T. Calcaterra, G.L. Closs, Intramolecular long-distance electron transfer in radical anions. The effects of free energy and solvent on the reaction rates, J. Am. Chem. Soc. 106 (1984) 3047–3049. doi:10.1021/ja00322a058.

[42] G.L. Closs, L.T. Calcaterra, N.J. Green, K.W. Penfield, J.R. Miller, Distance, stereoelectronic effects, and the Marcus inverted region in intramolecular electron transfer in organic radical anions, J. Phys. Chem. 90 (1986) 3673–3683. doi:10.1021/j100407a039.

[43] R.M. Metzger, Unimolecular electronics, J. Mater. Chem. 18 (2008) 4364. doi:10.1039/b802804b.

[44] S. Eisele, M. Schwarz, B. Speiser, C. Tittel, Diffusion coefficient of ferrocene in 1-butyl-3-methylimidazolium tetrafluoroborate – concentration

dependence and solvent purity, Electrochim. Acta. 51 (2006) 5304–5306. doi:10.1016/j.electacta.2006.02.001.

[45] O. Fontaine, C. Lagrost, J. Ghilane, P. Martin, G. Trippé, C. Fave, et al., Mass transport and heterogeneous electron transfer of a ferrocene derivative in a room-temperature ionic liquid, J. Electroanal. Chem. 632 (2009) 88–96. doi:10.1016/j.jelechem.2009.04.001.

[46] D. Zigah, A. Wang, C. Lagrost, P. Hapiot, Diffusion of molecules in ionic liquids/organic solvent mixtures. Example of the reversible reduction of O2 to superoxide., J. Phys. Chem. B. 113 (2009) 2019–2023. doi:10.1021/jp8095314.

[47] G. Denuault, M. Sosna, K. Williams, 11. Classical Experiments, in: Z. C.G (Ed.), Handb. Electrochem., Elsevier B.V., 2007: pp. 431–469.

[48] J.E. Baur, 19. Diffusion Coefficients, in: C.G. Zoski (Ed.), Handb. Electrochem., 2007: pp. 829–848.

[49] L. Xiong, L. Aldous, M.C. Henstridge, R.G. Compton, Investigation of the optimal transient times for chronoamperometric analysis of diffusion coefficients and concentrations in non-aqueous solvents and ionic liquids, Anal. Methods. 4 (2012) 371–376. doi:10.1039/c1ay05667k.

[50] R.S. Nicholson, I. Shain, Theory of Stationary Electrode Polarography. Single Scan and Cyclic Methods Applied to Reversible, Irreversible, and Kinetic Systems., Anal. Chem. 36 (1964) 706–723. doi:10.1021/ac60210a007.

[51] Allen J. Bard; Larry R. Faulkner, Electrochemical Methods: Fundamentals and Applications, John Wiley & Sons, 1980.

[52] Richard G. Compton ; Craig E. Banks, Understanding Voltammetry, 2nd ed., Imperial College Press, 2010.

[53] H. Tokuda, K. Hayamizu, K. Ishii, M.A.B.H. Susan, M. Watanabe, Physicochemical Properties and Structures of Room Temperature Ionic Liquids. 1. Variation of Anionic Species, J. Phys. Chem. B. 108 (2004) 16593–16600. doi:10.1021/jp047480r.

[54] H. Tokuda, K. Hayamizu, K. Ishii, M.A.B.H. Susan, M. Watanabe, Physicochemical properties and structures of room temperature ionic liquids. 2. Variation of alkyl chain length in imidazolium cation., J. Phys. Chem. B. 109 (2005) 6103–6110. doi:10.1021/jp044626d.

[55] H. Tokuda, K. Ishii, M.A.B.H. Susan, S. Tsuzuki, K. Hayamizu, M. Watanabe, Physicochemical properties and structures of room-temperature

ionic liquids. 3. Variation of cationic structures., J. Phys. Chem. B. 110 (2006) 2833–2839. doi:10.1021/jp053396f.

[56] A. Einstein, Uber die von der rnolekularkinetischem Theorie der Warme geforderte Bewegumg von in ruhenden Flussigkeiten suspendierten Teilchen, Ann. Phys. 17 (1905) 549–560.

[57] S.H. Chung, R. Lopato, S.G. Greenbaum, H. Shirota, E.W. Castner, J.F. Wishart, Nuclear magnetic resonance study of the dynamics of imidazolium ionic liquids with -CH2Si(CH3)3 vs -CH2C(CH3)3 substituents., J. Phys. Chem. B. 111 (2007) 4885–4893. doi:10.1021/jp071755w.

[58] K.L. Ngai, On enhanced translational diffusion or the fractional Stokes-Einstein relation observed in a supercooled ionic liquid., J. Phys. Chem. B. 110 (2006) 26211–26214. doi:10.1021/jp065601c.

[59] W. Hyk, A. Nowicka, Z. Stojek, Direct determination of diffusion coefficients of substrate and product by chronoamperometric techniques at microelectrodes for any level of ionic support., Anal. Chem. 74 (2002) 149–157.

[60] R.D. Martin, P.R. Unwin, Theory and Experiment for the Substrate Generation/Tip Collection Mode of the Scanning Electrochemical Microscope: Application as an Approach for Measuring the Diffusion Coefficient Ratio of a Redox Couple, Anal. Chem. 70 (1998) 276–284. doi:10.1021/ac970681p.

[61] R.D. Martin, P.R. Unwin, Scanning electrochemical microscopy: theory and experiment for the positive feedback mode with unequal diffusion coefficients of the redox mediator couple, J. Electroanal. Chem. 439 (1997) 123–136. doi:0022-0728/97.

[62] C. a. Brooks, A.P. Doherty, Concentration-dependent diffusion in room temperature ionic liquids: a microelectrode study, Electrochem. Commun. 6 (2004) 867–871. doi:10.1016/j.elecom.2004.06.012.

[63] L. Nagy, G. Gyetvai, L. Kollár, G. Nagy, Electrochemical behavior of ferrocene in ionic liquid media., J. Biochem. Biophys. Methods. 69 (2006) 121–132. doi:10.1016/j.jbbm.2006.03.005.

[64] C. Lagrost, D. Carrié,, M. Vaultier, P. Hapiot, Reactivities of Some Electrogenerated Organic Cation Radicals in Room-Temperature Ionic Liquids: Toward an Alternative to Volatile Organic Solvents?, J. Phys. Chem. A. 107 (2003) 745–752. doi:10.1021/jp026907w.

[65] L.E. Barrosse-Antle, L. Aldous, C. Hardacre, A.M. Bond, R.G. Compton, Dissolved Argon Changes the Rate of Diffusion in Room Temperature Ionic Liquids: Effect of the Presence and Absence of Argon and Nitrogen on the

Voltammetry of Ferrocene, J. Phys. Chem. C. 113 (2009) 7750–7754. doi:10.1021/jp9015849.

[66] W. Sutherland, Sutherland a dynamical theory of diffusion.pdf, Phil. Mag. S. 9 (1905) 781–785.

[67] M.A. Vorotyntsev, V.A. Zinovyeva, M. Picquet, Diffusional transport in ionic liquids: Stokes–Einstein relation or "sliding sphere" model? Ferrocene (Fc) in imidazolium liquids, Electrochim. Acta. 55 (2010) 5063–5070. doi:10.1016/j.electacta.2010.03.070.

[68] W. Hayduk, H. Laudie, Prediction of diffusion coefficients for nonelectrolytes in dilute aqueous solutions, AIChE J. 20 (1974) 611–615. doi:10.1002/aic.690200329.

[69] N. Umesi, R.P. Danner, Predicting Diffusion Coefficients in Nonpolar Solvents, Ind. Eng. Che. Process Des. Dev. 20 (1987) 662–665.

[70] M.A. Slddlqi, K. Lucas, F. Thermodynamik, U. Duisburg, Correlations for Prediction of Diffusion in Liquids, Can. J. Chem. Eng. 64 (1986) 839–843.

[71] C.R. Wilke, P. Chang, Correlation of diffusion coefficients in dilute solutions, AIChE J. 1 (1955) 264–270. doi:10.1002/aic.690010222.

[72] J.S. Wilkes, A short history of ionic liquids—from molten salts to neoteric solvents, Green Chem. 4 (2002) 73–80. doi:10.1039/b110838g.

[73] P. Kubisa, Application of ionic liquids as solvents for polymerization processes, Prog. Polym. Sci. 29 (2004) 3 –12. doi:10.1016/j.progpolymsci.2003.10.002.

[74] L.E. Barrosse-Antle, A.M. Bond, R.G. Compton, A.M. O'Mahony, E.I. Rogers, D.S. Silvester, Voltammetry in room temperature ionic liquids: comparisons and contrasts with conventional electrochemical solvents., Chem. Asian J. 5 (2010) 202–230. doi:10.1002/asia.200900191.

[75] J.A. Widegren, E.M. Saurer, K.N. Marsh, J.W. Magee, Electrolytic conductivity of four imidazolium-based room-temperature ionic liquids and the effect of a water impurity, J. Chem. Thermodyn. 37 (2005) 569–575. doi:10.1016/j.jct.2005.04.009.

[76] K.R. Seddon, A. Stark, M.-J. Torres, Influence of chloride, water, and organic solvents on the physical properties of ionic liquids, Pure Appl. Chem. 72 (2000) 2275–2287. doi:10.1351/pac200072122275.

[77] G. Tollin, Reactions of Triethylamine with Copper(1) and Copper(I1) Halides', Inorg. Chem. 2 (1962) 1210–1216.

[78] D.R. MacFarlane, K.R. Seddon, Ionic Liquids—Progress on the Fundamental Issues, Aust. J. Chem. 60 (2007) 3. doi:10.1071/CH06478.

[79] K. Dong, S. Zhang, D. Wang, X. Yao, Hydrogen bonds in imidazolium ionic liquids., J. Phys. Chem. A. 110 (2006) 9775–82. doi:10.1021/jp054054c.

[80] P. Bonhôte, A.-P. Dias, M. Armand, N. Papageorgiou, K. Kalyanasundaram, M. Grätzel, Hydrophobic, Highly Conductive Ambient-Temperature Molten Salts., Inorg. Chem. 35 (1996) 1168–1178.

[81] and D.R.M. Stewart A. Forsyth, Jennifer M. Pringle, Ionic liquids--an overview., Aust. J. Chem. 57 (2004) 113–119.

[82] H.L. Ngo, K. LeCompte, L. Hargens, A.B. McEwen, Thermal properties of imidazolium ionic liquids, Thermochim. Acta. 357-358 (2000) 97–102. doi:10.1016/S0040-6031(00)00373-7.

[83] J.G. Huddleston, A.E. Visser, W.M. Reichert, H.D. Willauer, G. a. Broker, R.D. Rogers, Characterization and comparison of hydrophilic and hydrophobic room temperature ionic liquids incorporating the imidazolium cation, Green Chem. 3 (2001) 156–164. doi:10.1039/b103275p.

[84] M. Shamsipur, A.A.M. Beigi, M. Teymouri, S.M. Pourmortazavi, M. Irandoust, Physical and electrochemical properties of ionic liquids 1-ethyl-3-methylimidazolium tetrafluoroborate, 1-butyl-3-methylimidazolium trifluoromethanesulfonate and 1-butyl-1-methylpyrrolidinium bis(trifluoromethylsulfonyl)imide, J. Mol. Liq. 157 (2010) 43–50. doi:10.1016/j.molliq.2010.08.005.

[85] C.P. Fredlake, J.M. Crosthwaite, D.G. Hert, S.N.V.K. Aki, J.F. Brennecke, Thermophysical Properties of Imidazolium-Based Ionic Liquids, J. Chem. Eng. Data. 49 (2004) 954–964. doi:10.1021/je034261a.

[86] M. Larriba, P. Navarro, J. García, F. Rodríguez, Liquid–Liquid Extraction of Toluene from Heptane Using [emim][DCA], [bmim][DCA], and [emim][TCM] Ionic Liquids, Ind. Eng. Chem. Res. 52 (2013) 2714–2720. doi:10.1021/ie303357s.

[87] J. Klomfar, M. Souc, Temperature Dependence Measurements of the Density at 0 . 1 MPa for 1-Alkyl-3-methylimidazolium-Based Ionic Liquids with the Trifluoromethanesulfonate and Tetrafluoroborate Anion, J. Chem. Eng. Data. 55 (2010) 4054–4057.

[88] U. Domańska, M. Królikowska, M. Królikowski, Phase behaviour and physico-chemical properties of the binary systems {1-ethyl-3-methylimidazolium thiocyanate, or 1-ethyl-3-methylimidazolium tosylate+water, or+an alcohol}, Fluid Phase Equilib. 294 (2010) 72–83. doi:10.1016/j.fluid.2010.01.020.

[89] Y. Yoshida, O. Baba, G. Saito, Ionic Liquids Based on Dicyanamide Anion : Influence of Structural Variations in Cationic, J. Phys. Chem. B. 111 (2007) 4742–4749.

[90] A. Stoppa, O. Zech, W. Kunz, R. Buchner, The Conductivity of Imidazolium-Based Ionic Liquids from (−35 to 195) °C. A. Variation of Cation's Alkyl Chain †, J. Chem. Eng. Data. 55 (2010) 1774–1778. doi:10.1021/je900789j.

[91] J. Leys, M. Wübbenhorst, C. Preethy Menon, R. Rajesh, J. Thoen, C. Glorieux, et al., Temperature dependence of the electrical conductivity of imidazolium ionic liquids., J. Chem. Phys. 128 (2008) 064509. doi:10.1063/1.2827462.

[92] M.S. Calado, J.C.F. Diogo, J.L. Correia da Mata, F.J.P. Caetano, Z.P. Visak, J.M.N. a. Fareleira, Electrolytic Conductivity of Four Imidazolium-Based Ionic Liquids, Int. J. Thermophys. 34 (2013) 1265–1279. doi:10.1007/s10765-013-1491-2.

[93] J. Vila, L.M. Varela, O. Cabeza, Cation and anion sizes influence in the temperature dependence of the electrical conductivity in nine imidazolium based ionic liquids, Electrochim. Acta. 52 (2007) 7413–7417. doi:10.1016/j.electacta.2007.06.044.

[94] J. Fuller, R.T. Carlin, R.A. Osteryoung, The Room Temperature Ionic Liquid Electrochemical Couples and Physical Properties, J. Electrochem. Soc. 144 (1997) 3881–3886.

[95] R.F. d. S. and J.D. P.A.Z.Suarez, S. Einloft, J.E.L.Dullius, Synthesis and physical-chemical properties of ionic liquids based on 1-butyl-3-methylimidazolium cation, J. Chim. Phys. 95 (1998) 1626–1639.

[96] H. Olivier-bourbigou, L. Magna, Ionic liquids : perspectives for organic and catalytic reactions, J. Mol. Catal. A. 182 - 183 (2002) 419–437.

[97] A. Stoppa, J. Hunger, R. Buchner, Conductivities of Binary Mixtures of Ionic Liquids with Polar Solvents †, J. Chem. Eng. Data. 54 (2009) 472–479. doi:10.1021/je800468h.

[98] R. Gilliam, J. Graydon, D. Kirk, S. Thorpe, A review of specific conductivities of potassium hydroxide solutions for various concentrations and temperatures, Int. J. Hydrogen Energy. 32 (2007) 359–364. doi:10.1016/j.ijhydene.2006.10.062.

[99] M. Wakihara, Recent developments in lithium ion batteries, Mater. Sci. Eng. 33 (2001).

[100] M. Kosmulski, J. Gustafsson, J.B. Rosenholm, Thermal stability of low temperature ionic liquids revisited, Thermochim. Acta. 412 (2004) 47–53. doi:10.1016/j.tca.2003.08.022.

[101] A. Noda, M. Watanabe, Highly conductive polymer electrolytes prepared by in situ polymerization of vinyl monomers in room temperature molten salts, Electrochim. Acta. 45 (2000) 1265–1270. doi:10.1016/S0013-4686(99)00330-8.

[102] a. Lewandowski, I. St?pniak, Relative molar Gibbs energies of cation transfer from a molecular liquid to ionic liquids at 298.15 K, Phys. Chem. Chem. Phys. 5 (2003) 4215. doi:10.1039/b305734h.

[103] T. Nishida, Y. Tashiro, M. Yamamoto, Physical and electrochemical properties of 1-alkyl-3-methylimidazolium tetrafluoroborate for electrolyte, J. Fluor. Chem. 120 (2003) 135–141. doi:10.1016/S0022-1139(02)00322-6.

[104] P. a. Z. Suarez, V.M. Selbach, J.E.L. Dullius, S. Einloft, C.M.S. Piatnicki, D.S. Azambuja, et al., Enlarged electrochemical window in dialkyl-imidazolium cation based room-temperature air and water-stable molten salts, Electrochim. Acta. 42 (1997) 2533–2535. doi:10.1016/S0013-4686(96)00444-6.

[105] J. Barisci, Investigation of ionic liquids as electrolytes for carbon nanotube electrodes, Electrochem. Commun. 6 (2004) 22–27. doi:10.1016/j.elecom.2003.09.015.

[106] A.M. O'Mahony, D.S. Silvester, L. Aldous, C. Hardacre, R.G. Compton, Effect of Water on the Electrochemical Window and Potential Limits of Room-Temperature Ionic Liquids, J. Chem. Eng. Data. 53 (2008) 2884–2891. doi:10.1021/je800678e.

[107] S. V Dzyuba, R.A. Bartsch, Influence of Structural Variations in Hexafluorophosphates and Bis (trifluoromethyl- sulfonyl) imides on Physical Properties of the Ionic Liquids **, Chemphyschem. 3 (2002) 161–166.

[108] C. Kolbeck, J. Lehmann, K.R.J. Lovelock, T. Cremer, N. Paape, P. Wasserscheid, et al., Density and surface tension of ionic liquids., J. Phys. Chem. B. 114 (2010) 17025–36. doi:10.1021/jp1068413.

[109] A. Deyko, K.R.J. Lovelock, J.-A. Corfield, A.W. Taylor, P.N. Gooden, I.J. Villar-Garcia, et al., Measuring and predicting Delta(vap)H298 values of ionic liquids., Phys. Chem. Chem. Phys. 11 (2009) 8544–55. doi:10.1039/b908209c.

[110] J. Klomfar, M. Sou, Temperature Dependence of the Surface Tension and Density at 0 . 1 MPa for 1-Ethyl- and 1-Butyl-3-methylimidazolium Dicyanamide, (2011) 3454–3462.

[111] P. Kilaru, G.A. Baker, P. Scovazzo, Density and Surface Tension Measurements of Imidazolium-, Quaternary Phosphonium-, and Ammonium-Based Room-Temperature Ionic Liquids: Data and Correlations, J. Chem. Eng. Data. 52 (2007) 2306–2314. doi:10.1021/je7003098.

[112] M.G. Freire, P.J. Carvalho, A.M. Fernandes, I.M. Marrucho, A.J. Queimada, J. a P. Coutinho, Surface tensions of imidazolium based ionic liquids: anion, cation, temperature and water effect., J. Colloid Interface Sci. 314 (2007) 621–30. doi:10.1016/j.jcis.2007.06.003.

[113] L.G. Sánchez, J.R. Espel, F. Onink, G.W. Meindersma, A.B. de Haan, Density, Viscosity, and Surface Tension of Synthesis Grade Imidazolium, Pyridinium, and Pyrrolidinium Based Room Temperature Ionic Liquids, J. Chem. Eng. Data. 54 (2009) 2803–2812. doi:10.1021/je800710p.

[114] M.G. Freire, L.M.N.B.F. Santos, A.M. Fernandes, J. a. P. Coutinho, I.M. Marrucho, An overview of the mutual solubilities of water–imidazolium-based ionic liquids systems, Fluid Phase Equilib. 261 (2007) 449–454. doi:10.1016/j.fluid.2007.07.033.

[115] N. Yaghini, L. Nordstierna, A. Martinelli, Effect of water on the transport properties of protic and aprotic imidazolium ionic liquids - an analysis of self-diffusivity, conductivity, and proton exchange mechanism., Phys. Chem. Chem. Phys. 16 (2014) 9266–75. doi:10.1039/c4cp00527a.

[116] M.J. Earle, C.M. Gordon, N. V Plechkova, K.R. Seddon, T. Welton, Decolorization of ionic liquids for spectroscopy., Anal. Chem. 79 (2007) 758–64. doi:10.1021/ac061481t.

[117] J.F. Brennecke, N. Dame, E. Section, Temperature and Composition Dependence of the Density and Viscosity of Binary Mixtures of Water + Ionic Liquid, J. Chem. Eng. Data. 51 (2006) 2145–2155.

[118] C. Villagrán, C.E. Banks, C. Hardacre, R.G. Compton, Electroanalytical determination of trace chloride in room-temperature ionic liquids., Anal. Chem. 76 (2004) 1998–2003. doi:10.1021/ac030375d.

[119] P.J. Scammells, J.L. Scott, R.D. Singer, Ionic Liquids: The Neglected Issues, Aust. J. Chem. 58 (2005) 155. doi:10.1071/CH04272.

[120] J.A. Riddick, W.B. Bunger, T.K. Sakano, Organic solvents physical properties and methods of purificaton, Fourth, John Wiley & Sons, 1986.

[121] C.D. Tran, S.H. De Paoli Lacerda, D. Oliveira, Absorption of water by room-temperature ionic liquids: effect of anions on concentration and state of water., Appl. Spectrosc. 57 (2003) 152–7. doi:10.1366/000370203321535051.

[122] V. Ganesan, S. V Rosokha, J.K. Kochi, Isolation of the latent precursor complex in electron-transfer dynamics. Intermolecular association and self-exchange with acceptor anion radicals., J. Am. Chem. Soc. 125 (2003) 2559–71. doi:10.1021/ja0211611.

[123] L.A. Chem, S. Hiinig, G. Kiejlich, H. Quast, Tetrathio-athylene und ihre hoheren Oxidationsstufen, Liebigs Ann. Chem. 32 (1973) 310–323.

[124] and P.E.S. J. B. Torrance, B.A. Scott, B.Welber, F. B. Kaufman, Optical properties of the radical cation tetrathiafulvalenium (TTF+) in its mixed-valence and monovalence halide salts, Phys. Rev. B. 19 (1979) 730–741. doi:http://dx.doi.org/10.1103/PhysRevB.19.730.

[125] W. Oelßner, F. Berthold, U. Guth, The iR drop – well-known but often underestimated in electrochemical polarization measurements and corrosion testing, Mater. Corros. 57 (2006) 455–466. doi:10.1002/maco.200603982.

[126] H. Rodríguez, J.F. Brennecke, Temperature and Composition Dependence of the Density and Viscosity of Binary Mixtures of Water + Ionic Liquid, J. Chem. Eng. Data. 51 (2006) 2145–2155. doi:10.1021/je0602824.

[127] and W.J. G. Grampp, A. Kapturkiewicz, Homogeneous and heterogeneous electron transfer rates of tetrathiafulvalens-system, Ber. Bunsenges. Phys. Chem. 94 (1990) 439–447. doi:0005-9021/90/0404-0439.

[128] T. Kondo, M. Okamura, K. Uosaki, Anion effect on the electrochemical characteristics of a gold electrode modified with a self-assembled monolayer of ferrocenylhexanethiol in aqueous and dichloromethane solutions, J. Organomet. Chem. 637-639 (2001) 841–844. doi:10.1016/S0022-328X(01)00985-8.

[129] R.P. Held, E. Luksha, H.J.M. Denessen, M. Alfenar, S.J.P. Singla, P. Neruia, et al., Electron Exchange between Ferrocene and Ferrocenium Ion. Effects of Solvent and of Ring Substitution on the Rateli2, J. Phys. Chem. 84 (1980) 3094–3099.

[130] J.S. Miller, Tetracyanoethylene (TCNE): the characteristic geometries and vibrational absorptions of its numerous structures., Angew. Chem. Int. Ed. Engl. 45 (2006) 2508–25. doi:10.1002/anie.200503277.

[131] I. Hargittai, J. Brunvollb, M. Kolonitc, V. Khodorkovskyd, Tetrathiafulvalene: gas-phase molecular structure from electron diffraction, J. Mol. Struct. 317 (1994) 273 –277.

[132] C. Katan, First-Principles Study of the Structures and Vibrational Frequencies for Tetrathiafulvalene TTF and TTF- d 4 in Different Oxidation States, J. Phys. Chem. A. 103 (1999) 1407–1413. doi:10.1021/jp983941v.

[133] B.Y. Mladenova, D.R. Kattnig, G. Grampp, Room-temperature ionic liquids discerned via nitroxyl spin probe dynamics., J. Phys. Chem. B. 115 (2011) 8183–98. doi:10.1021/jp201703c.

[134] V. Strehmel, S. Berdzinski, H. Rexhausen, Interactions between ionic liquids and radicals, J. Mol. Liq. 192 (2014) 153–170. doi:10.1016/j.molliq.2013.12.007.

[135] I. Introduction, T H E CHEMISTRY OF TETRACYANOETHYLENE, (1967).

[136] V. Strehmel, A. Laschewsky, R. Stoesser, A. Zehl, W. Herrmann, Mobility of spin probes in ionic liquids, J. Phys. Org. Chem. 19 (2006) 318–325. doi:10.1002/poc.1072.

[137] W.J. G. Grampp, Kinetics of diabatic and adiabatic electron exchange in organic systems. Comparison of theory and experiment, Ber. Bunsenges. Phys. Chem. 95 (1991) 904–927. doi:10.1016/j.jelechem.2010.05.018.

[138] R.S. Nicholson, Theory and Application of Cyclic Voltammetry f m Measurement of Electrode Reaction Kinetics, J. Anal. Chem. 37 (1965) 1351–1355.

[139] R.J. Klilngler, J.K. Kochi, Electron-Transfer Kinetics from cyclic voltammetry. Quantitative description of electrochemical reversibility, J. Phys. Chem. 85 (1981) 1731–1741.

[140] U. Eisner, E. Gileadi, Anodic oxidation of hydrazine and its derivatives, J. Electroanal. Chem. Interfacial Electrochem. 28 (1970) 81–92. doi:10.1016/S0022-0728(70)80284-4.

[141] I. Lavagnini, R. Antiochia, F. Magno, An Extended Method for the Practical Evaluation of the Standard Rate Constant from Cyclic Voltammetric Data, Electroanalysis. 16 (2004) 505–506. doi:10.1002/elan.200302851.

[142] C. Rüssel, Der Einfluß des Leitsalzes und der Polarität aprotischer Lösungsmittel auf die Austauschstromdichter bei Reduktion von Chinonen, University of Erlangen, 1984.

[143] E.F. Meyer, Temperature-Dependent Determination of the Standard Heterogeneous Rate Constant with Cyclic Voltammetry, Am. Chem. Soc. 54 (1982) 1879–1880.

[144] M. V Mirkin, A.J. Bard, Simple Analysis of Quasi-Reversible Steady-State Voltammograms, Anal. Chem. 64 (1992) 2293–2302.

[145] N. Siraj, Noureen Siraj Heterogeneous Electron Transfer Rates of Organic Redox Systems Measured in Ionic Liquids, 2011.

[146] S. Lago, H. Rodríguez, A. Soto, A. Arce, Deterpenation of Citrus Essential Oil by Liquid−Liquid Extraction with 1-Alkyl-3-methylimidazolium Bis(trifluoromethylsulfonyl)amide Ionic Liquids, J. Chem. Eng. Data. 56 (2011) 1273–1281. doi:10.1021/je1011339.

[147] H. Jin, B. O'Hare, J. Dong, S. Arzhantsev, G. a Baker, J.F. Wishart, et al., Physical properties of ionic liquids consisting of the 1-butyl-3-methylimidazolium cation with various anions and the bis(trifluoromethylsulfonyl)imide anion with various cations., J. Phys. Chem. B. 112 (2008) 81–92. doi:10.1021/jp076462h.

[148] M. Huang, Y. Jiang, P. Sasisanker, G.W. Driver, H. Weingärtner, Static Relative Dielectric Permittivities of Ionic Liquids at 25 °C, J. Chem. Eng. Data. 56 (2011) 1494–1499. doi:10.1021/je101184s.

[149] J. Hunger, A. Stoppa, S. Schrçdle, G. Hefter, R. Buchner, Temperature Dependence of the Dielectric Properties and Dynamics of Ionic Liquids, Chemphyschem. 6150 (2009) 723–733. doi:10.1002/cphc.200800483.